# Experimental studies of nuclear shapes and collectivity

Magda Zielińska, CEA Saclay

- Nuclei can take a variety of shapes (spherical, prolate, oblate, octupole etc.) that emerge as a consequence of the complicated nucleon-nucleon interaction.
- The nuclear shape is not an observable, but we can deduce it from multiple experimental probes.

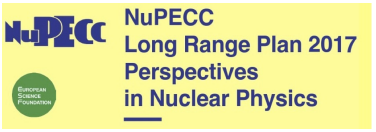


identified among key questions in nuclear structure:

- How does nuclear structure evolve across the nuclear landscape and what shapes can nuclei adopt?
- How complex are nuclear excitations?

# Nuclear shapes

- general description of a shape:

  $R(\theta,\phi) = R_0\left[1 + \sum_{\lambda=0}^{\infty}\sum_{\mu=-\lambda}^{\lambda} a_{\lambda,\mu} Y_{\lambda\mu}(\theta,\phi)\right]$

- important nuclear shapes:
  - $a_{2,\mu}$ quadrupole deformation (triaxial ellipsoid)
  - $a_{3,\mu}$ octupole deformation (pear shape)
- in the principal axes frame $a_{2,1} = a_{2,-1} = 0$ and only two parameters are enough to describe all possible quadrupole shapes:

  $a_{2,0} = \beta\cos\gamma$

  $a_{2,2} = a_{2,-2} = \frac{\beta\sin\gamma}{\sqrt{2}}$

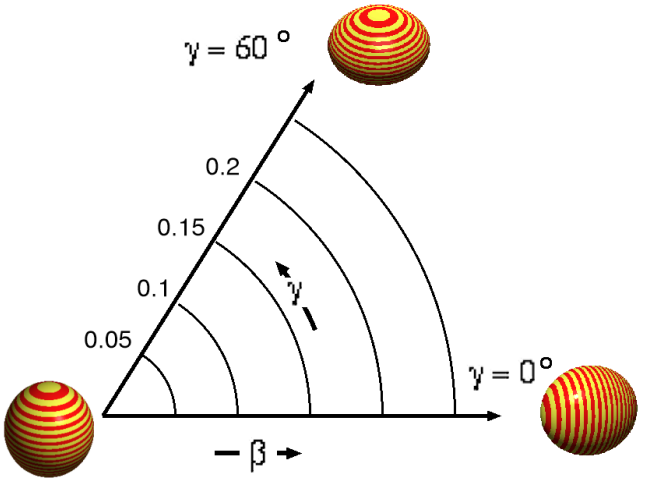


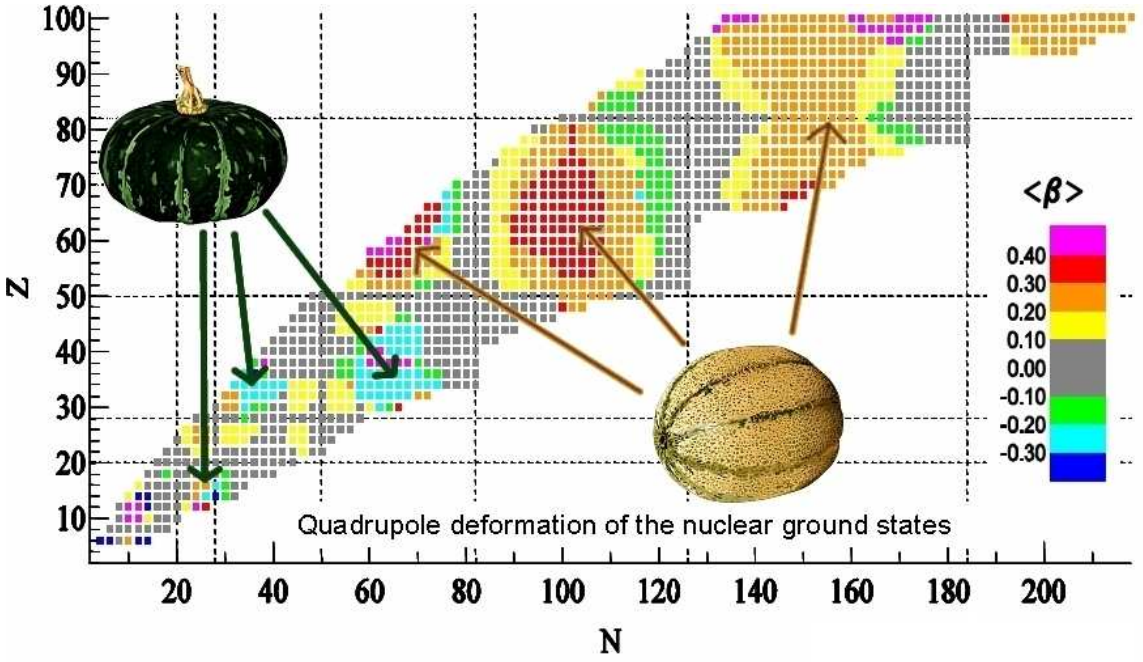

# Quadrupole collectivity: rotational bands

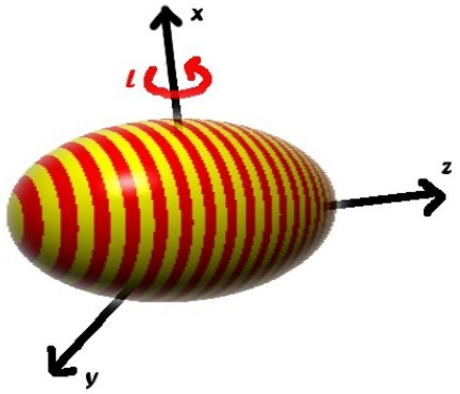


kinetic energy $E_{rot} = \frac{\hat{I}^2}{2\mathcal{J}}$

($\mathcal{J}$ – moment of intertia)

rotational band: $E(I) = \frac{I(I+1)}{2\mathcal{J}}$

at high spin: $\frac{\mathcal{J}^{(1)}}{\hbar^2} \approx \frac{2I-1}{E_\gamma}$

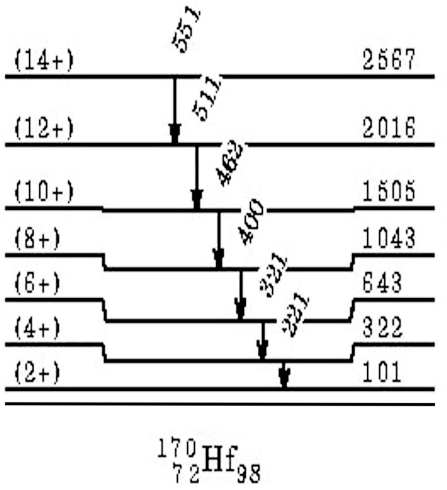


for rotational states:

$B(E2; I_i \rightarrow I_f) = \frac{\langle KI_f || \mathcal{M}(E2) || KI_i \rangle^2}{2I_i+1}$

$= \frac{5}{16\pi} (I_i, K, 2, 0 | I_f, K)^2 \, eQ_t^2$

$Q_t$ – transitional quadrupole moment

spectroscopic quadrupole moments expected to follow the same relation

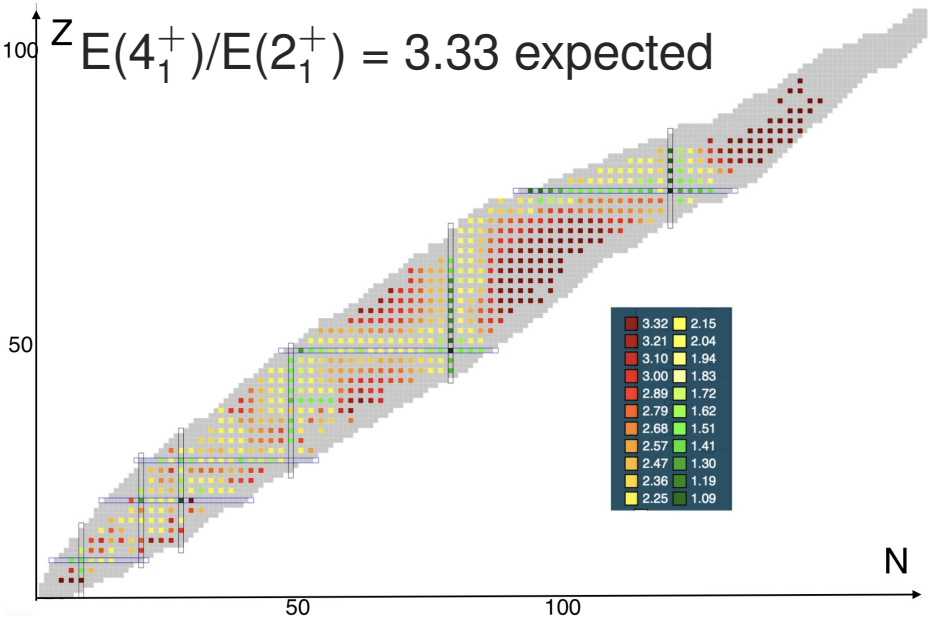

# Quadrupole collectivity: surface vibrations

$$R(\theta,\phi) = R_0\left[1 + \sum_\mu a_{2,\mu} Y_{2\mu}(\theta,\phi) + \sum_\mu a_{3,\mu} Y_{3\mu}(\theta,\phi)\right]$$

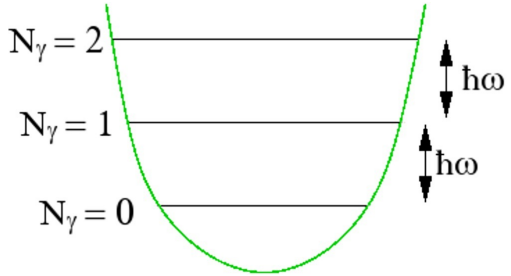


imagining the nucleus as a liquid drop, we can write the hamiltonian for the surface vibrations: $H_{osc} = \frac{1}{2}B_\lambda|\frac{da_{\lambda,\mu}}{dt}|^2 + \frac{1}{2}C_\lambda|a_{\lambda,\mu}|^2$ ($\lambda$ = 2,3)

its solution is a series of states characterised by phonon number N, spaced by $\hbar\omega$, where $\omega = \sqrt{C_\lambda/B_\lambda}$ → expected $E(4_1^+)/E(2_1^+) = 2$

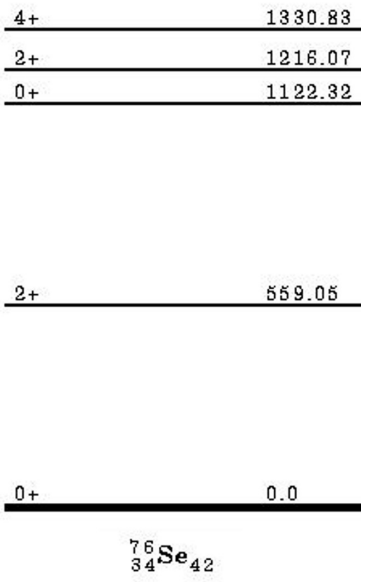


spin of each phonon: $\lambda$, parity $(-1)^\lambda$

B(E2; N=2 → N=1) = 2 B(E2; N=1 → N=0); transitions between states differing by N>1 forbidden

spectroscopic quadrupole moments equal to zero

energy levels for many nuclei closely resemble the vibrational pattern, but no complete set of two-phonon states known that fulfills the selection rules

# Quadrupole collectivity: gamma softness and triaxiality

appearance of a K=2 band at energy close to the $4_1^+$ state

expected $E(4_1^+)/E(2_1^+) = 2$

spectroscopic quadrupole moments equal to zero

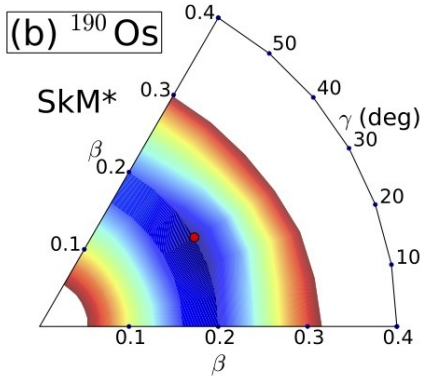


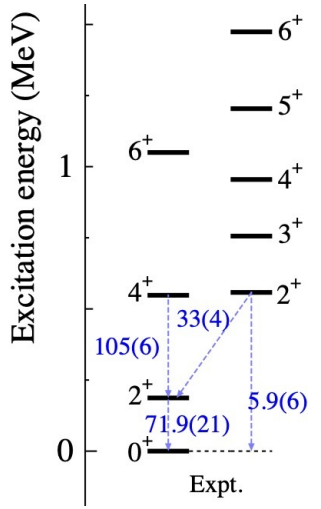


K. Nomura et al, PRL 108, 132501 (2012)

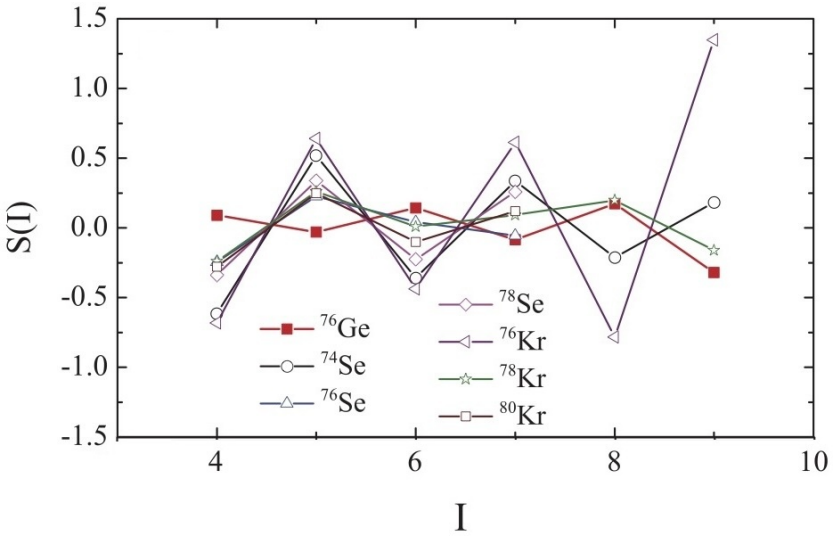


Y. Toh et al, PRC 87, 041304(R) (2013)

similar K=2 structure expected to appear as a result of collective rotation of a triaxial nucleus

attempts to distinguish between the two scenarios based on energy staggering in the K=2 band:

$$S(I) = \frac{[E(I)-E(I-1)]-[E(I-1)-E(I-2)]}{E(2_1^+)}$$

## What observables are related to nuclear shapes?

- differences in root mean square charge radii (determined for ground and isomeric states, usually via laser spectroscopy)
- level energies
  - energy of the first $2^+$ state: the simplest measure of collectivity
- transition probabilities: $B(E2; 0^+ \rightarrow 2^+) = ((3/4\pi)eZR_0^2)^2 \ \beta_2{}^2$
- quadrupole moments: measure of the charge distribution in a given state (always zero for spin 0 and 1/2, even if there is non-zero intrinsic deformation)
  - laser spectroscopy for long-lived states
  - reorientation effect in Coulomb excitation for short-lived states: influence of the quadrupole moment of an excited state on its excitation cross section
- deformation lengths from inelastic scattering: need for accurate potentials to describe the nuclear interaction between collision partners
- complete sets of E2 matrix elements:
  possibility to determine quadrupole invariants and level mixing
- monopole transition strengths: enhancements observed for shape coexistence with strong mixing

## "Classic" $\gamma$-ray spectroscopy: level energies and relative transition intensities

- level energies have to be put in some context – neighbouring isotopes, other states; we also need to have an idea about their spin-parities to make any structure conclusions
- can be used to conclude on nuclear shapes if other data not available (e.g. for very exotic nuclei)
- usually guidance from model calculations is needed

Main methods to populate excited states:

- fusion-evaporation reactions (limited to neutron-deficient nuclei)
- deep-inelastic reactions (mostly yrast states but practical for neutron-rich nuclei)
- beta decay (limitation on level spins related to the spin of the parent nucleus)
- fission (neutron-rich nuclei with A$\sim$100 and A$\sim$130)

# $\gamma$-$\gamma$ angular correlations

• angular distribution of $\gamma$ rays: probability of $\gamma$-ray emission as a function of direction; requires orientation of initial spins

• angular correlations – possible also for reactions that do not lead to spin orientation; the orientation of the system is given by the direction of the first $\gamma$ ray in a cascade, and we study the intensity of the following $\gamma$ ray as a function of the angle between them:

$W(\theta) = A_{00}\,[1 + a_2 P_2(\cos\theta) + a_4 P_4(\cos\theta)]$

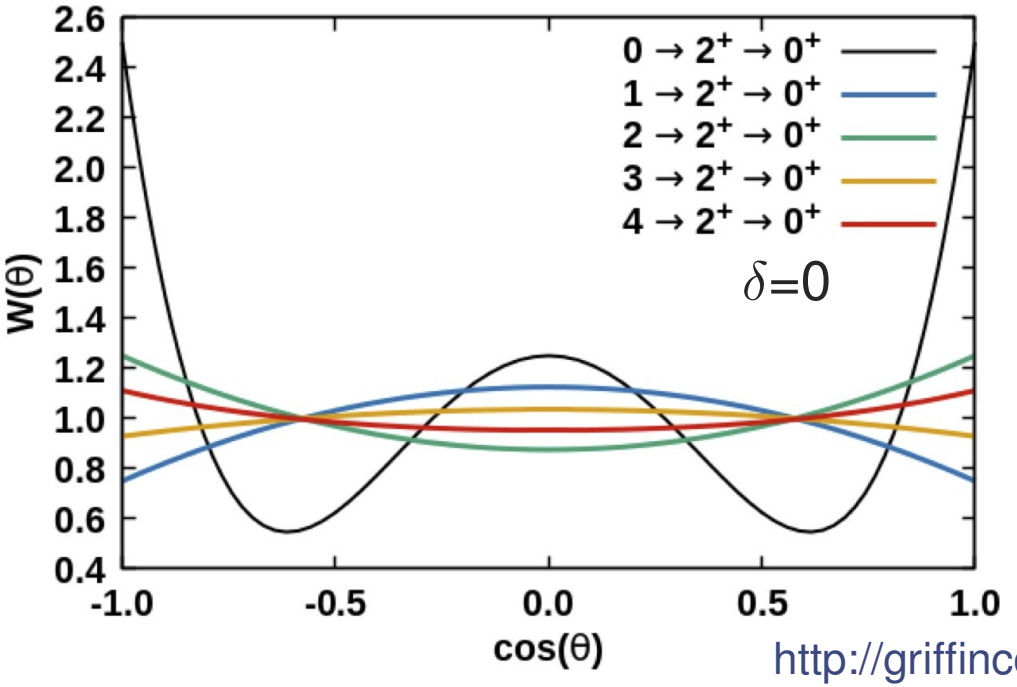


Assuming $\delta$=0:

| Cascade | $a_2$ | $a_4$ |
|---|---|---|
| $0 \to 2^+ \to 0^+$ | 0.357 | 1.143 |
| $1 \to 2^+ \to 0^+$ | -0.25 | 0 |
| $2 \to 2^+ \to 0^+$ | 0.25 | 0 |
| $3 \to 2^+ \to 0^+$ | -0.071 | 0 |
| $4 \to 2^+ \to 0^+$ | 0.102 | 0.009 |

• no sensitivity to level parity

http://griffincollaboration.github.io/AngularCorrelationUtility/

# Spin assignments from $\gamma$-$\gamma$ coincidences: example of $^{74}$Zn

M. Rocchini et al, PRL 130, 122502 (2023)

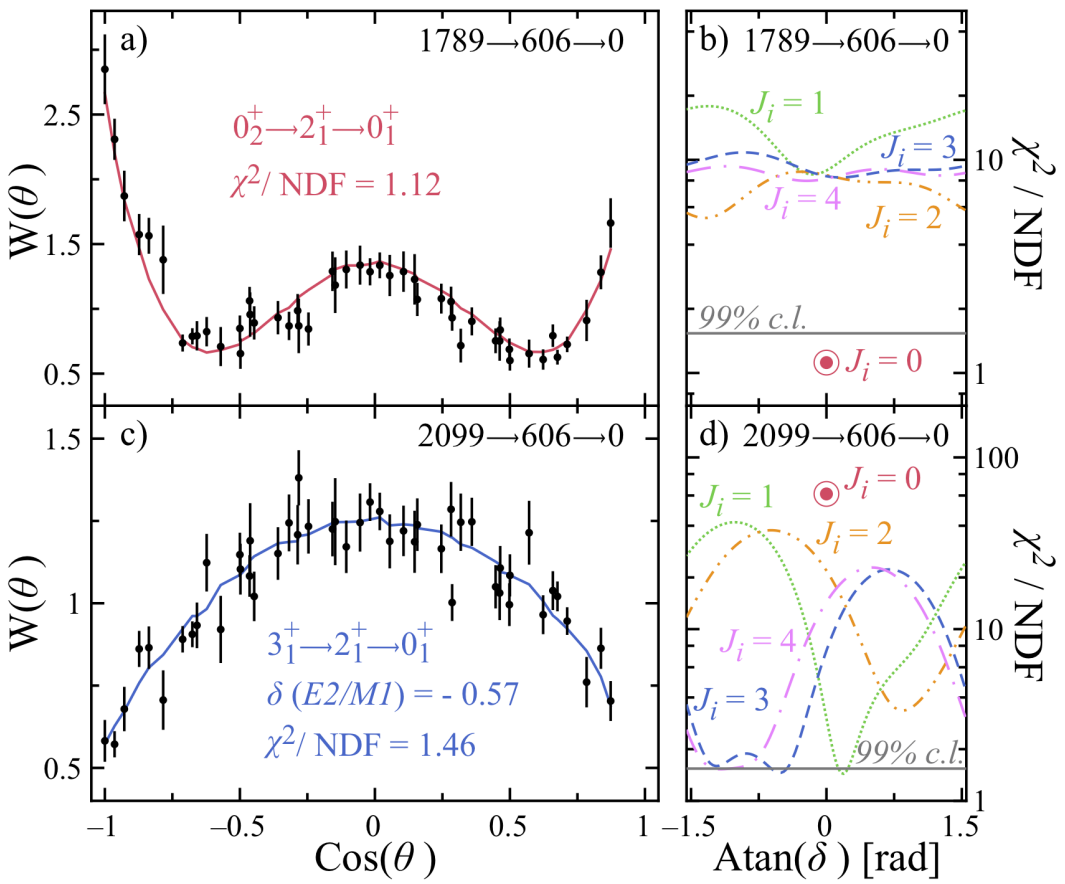


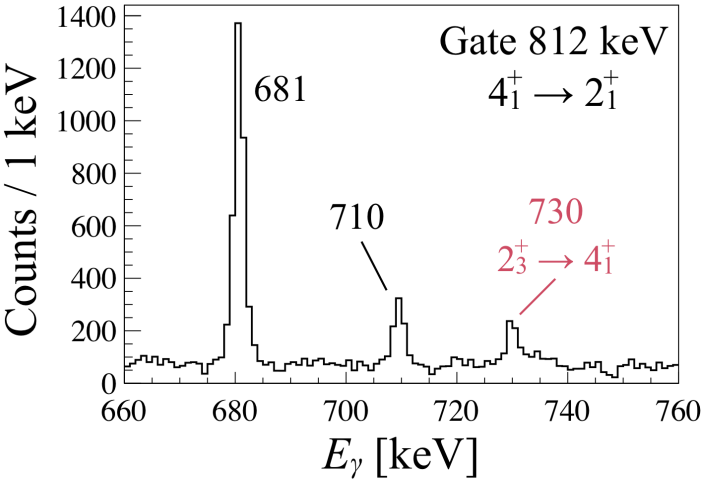


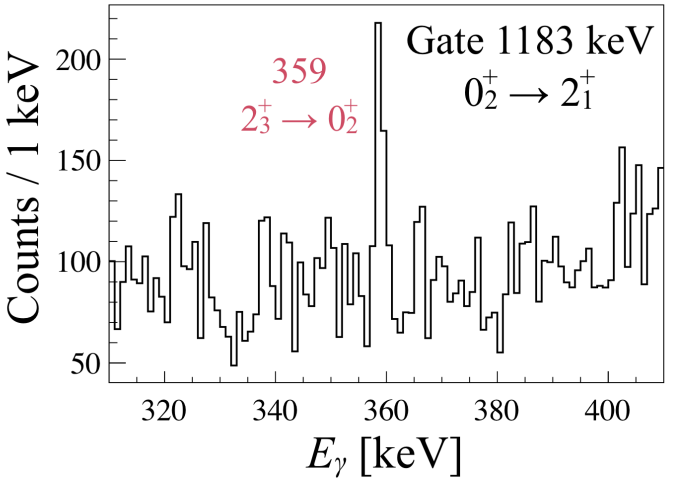


- unambiguous spin assignment for $0_2^+$, $2_2^+$, $2_3^+$, $3_1^+$ states
- new transitions observed: $2_3^+ \to 4_1^+$, $2_3^+ \to 0_1^+$

# Spin assignments from $\gamma$-$\gamma$ coincidences: example of $^{74}$Zn

M. Rocchini et al, PRL 130, 122502 (2023)

- unambiguous spin assignment for $0_2^+$, $2_2^+$, $2_3^+$, $3_1^+$ states in $^{74}$Zn
- new transitions observed: $2_3^+ \rightarrow 4_1^+$, $2_3^+ \rightarrow 0_1^+$
- relative B(E2) values deduced

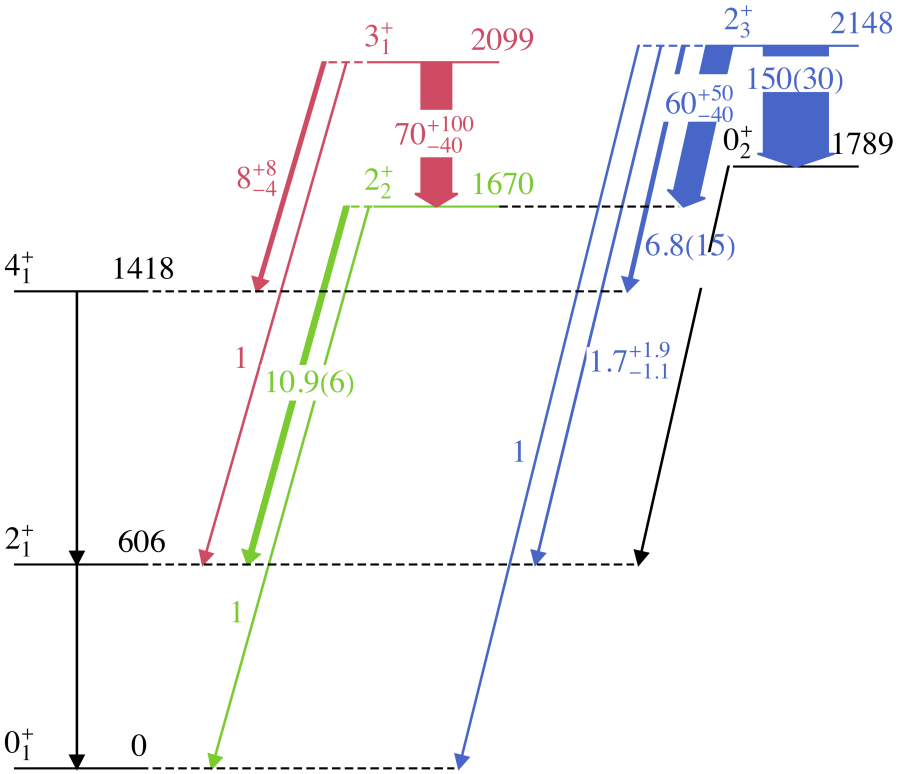


- first identification of a low-lying K=2 band in heavy Zn nuclei – triaxial degree of freedom important
- appearance of a K=0 band with a smaller energy spacing than gsb suggests shape coexistence

# Spin assignments from $\gamma$-$\gamma$ coincidences: example of $^{74}$Zn

M. Rocchini et al, PRL 130, 122502 (2023)

- unambiguous spin assignment for $0_2^+$, $2_2^+$, $2_3^+$, $3_1^+$ states in $^{74}$Zn
- new transitions observed: $2_3^+ \rightarrow 4_1^+$, $2_3^+ \rightarrow 0_1^+$
- relative B(E2) values deduced

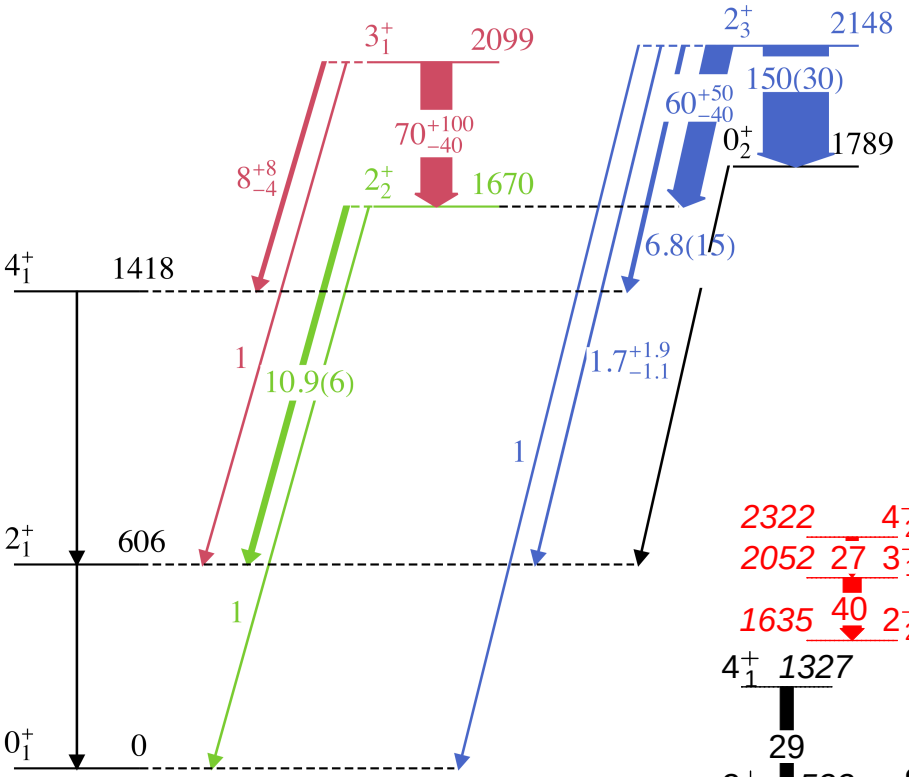


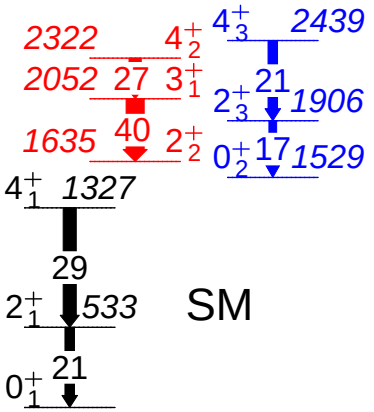


- first identification of a low-lying K=2 band in heavy Zn nuclei – triaxial degree of freedom important
- appearance of a K=0 band with a smaller energy spacing than gsb suggests shape coexistence
- state-of-the-art shell-model calculations reproduce very well the level scheme, but suggest instead very similar shapes of $0_1^+$ and $0_2^+$

# Heavy nuclei – possible E0 contributions to the decay

A.D. MacLean, PhD thesis, University of Guelph

combination of $\gamma$-$\gamma$ and $\gamma$-electron data in $\beta$ decay into $^{188}$Hg (TRIUMF)

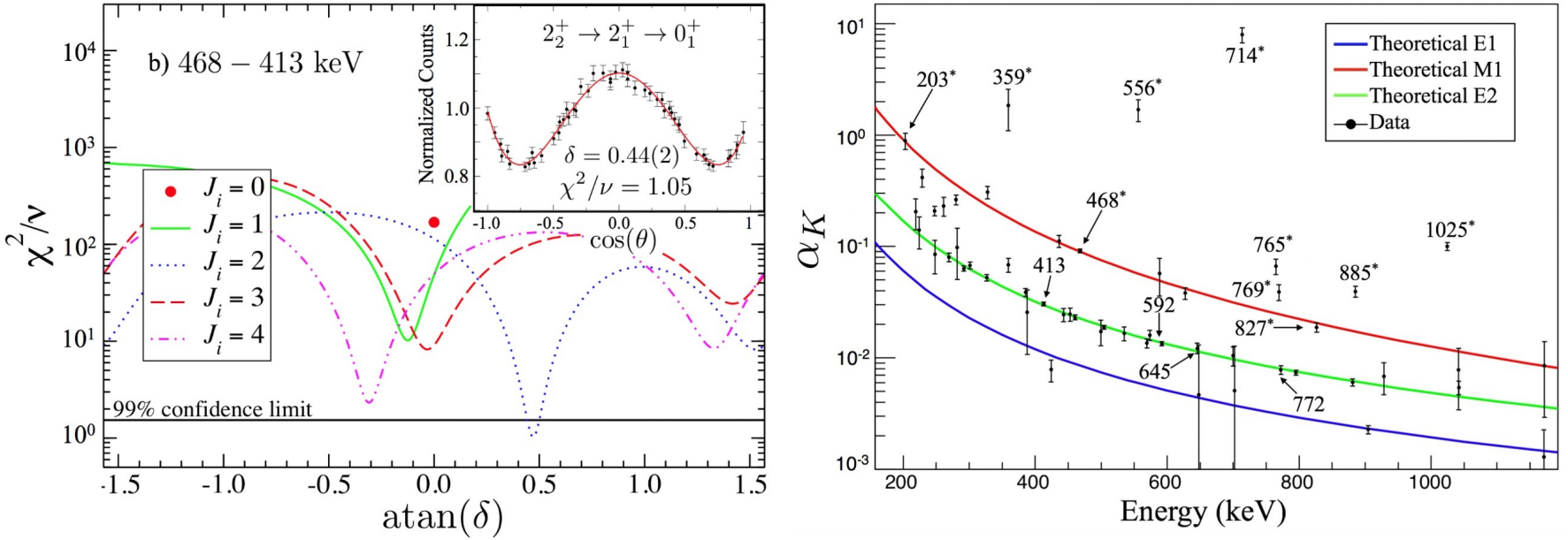


- any $\alpha_K$ larger than the $\alpha_K$(M1) value immediately indicates an E0 component
- consider the 468-keV transition: $\alpha_K$ would imply a pure M1 transition, but $\gamma$-$\gamma$ angular correlation determines E2/M1 mixing ratio $\delta$=0.44(2)
- angular correlations are vital to reliably extract J $\to$ J E0 components

# Lifetime measurements: direct timing

- fast scintillator array (typically $LaBr_3$) used in combination with a HPGe spectrometer
- gate on the high-resolution HPGe spectrum used to select the cascade of interest
- direct measurement of a time difference between “START” (feeding) and “STOP” (depopulating) transitions
- for lifetimes of a few hundreds picoseconds, exponential tail of the distribution observed, related to the lifetime

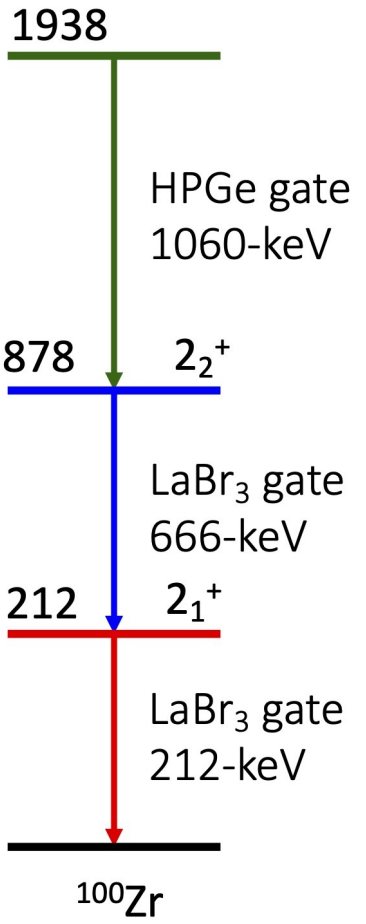


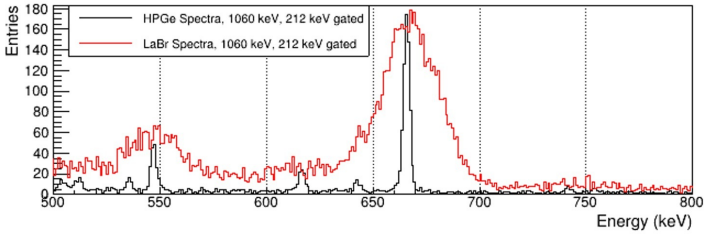


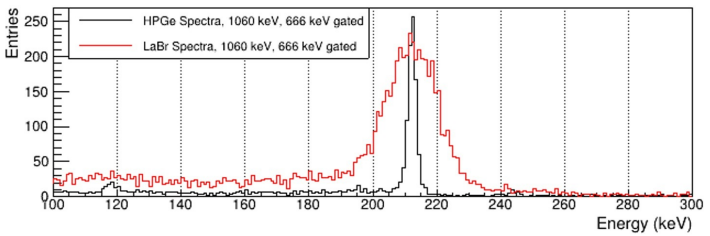


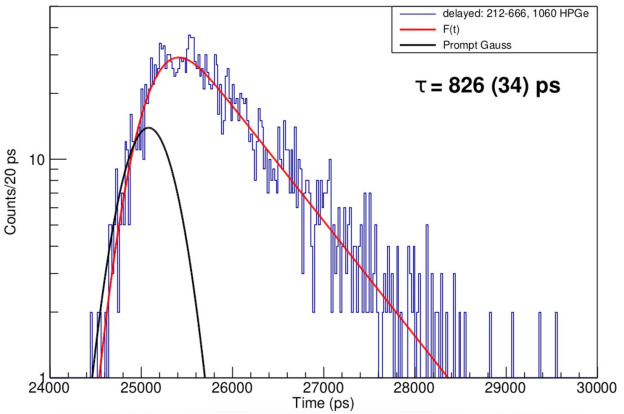


Example: $2_1^+$ state in $^{100}$Zr, H. Bidaman, PhD thesis, Uni Guelph (2023)

# Lifetime measurements: direct timing

Data from UWS: M.M.R. Chishti et al, Nature Physics 16, 853 (2020)

- $\tau$ below few hundred ps (depending on detector size) – Gaussian shape of the TAC distribution $\rightarrow$ mirror-symmetric centroid difference method
- corrections for the time-walk effect in the CFD modules needed: prompt response differences (PRD) curve

$\tau = (\Delta C - \Delta PRD)/2$

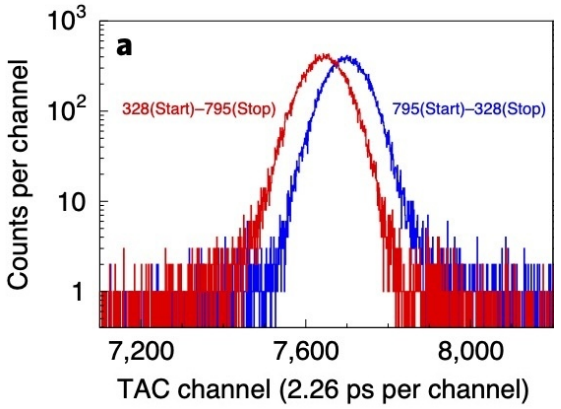


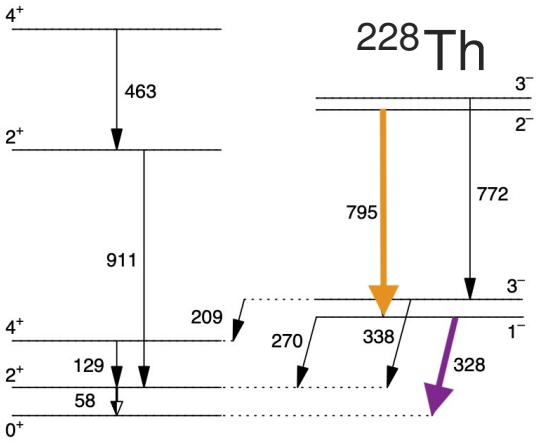


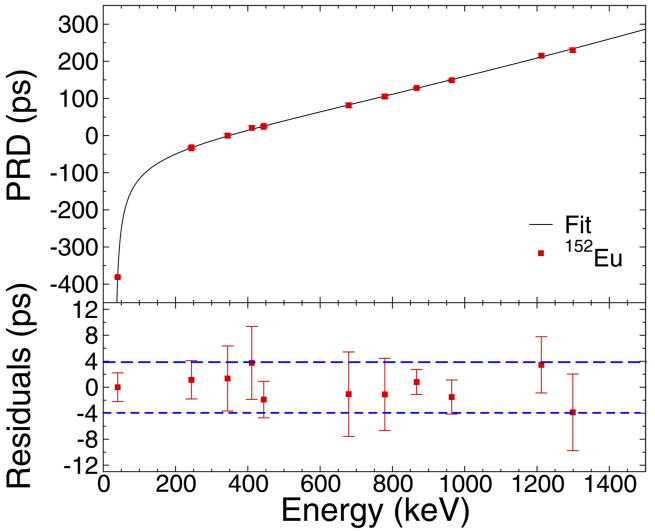


$\Delta$PRD: difference between PRD values for the energies of the “START” and “STOP” transitions
$\Delta$C: difference between centroids of the delayed and antidelayed distributions

- lifetimes down to a few picoseconds can be determined ($>$ 10 ps in typical in-beam conditions)

description of the method: J.-M. Régis et al, NIM A 622, 83 (2010)

# Lifetime measurements: Recoil Distance Doppler Shift

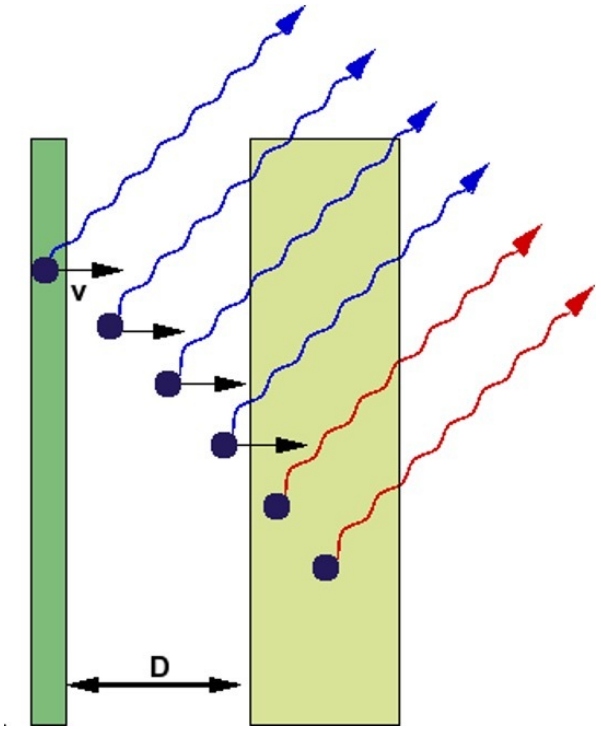


time of flight between the two foils separated by a distance D: $t_D = D/v$

number of $\gamma$ rays emitted after stopping in the second foil:

$$I_s = N_0 \exp\left(-\frac{t_D}{\tau}\right) = N_0 \exp\left(-\frac{D}{v\tau}\right)$$

number of $\gamma$ rays emitted between the two foils:

$$I_f = N_0 - I_s = N_0 \left(1 - \exp\left(-\frac{D}{v\tau}\right)\right)$$

$$\rightarrow \text{intensity ratio } \frac{I_s}{I_s + I_f} = \exp\left(-\frac{D}{v\tau}\right)$$

“plunger” device to control D;
instead of a stopper foil,
a degrader can be used
(enables identification of recoils)

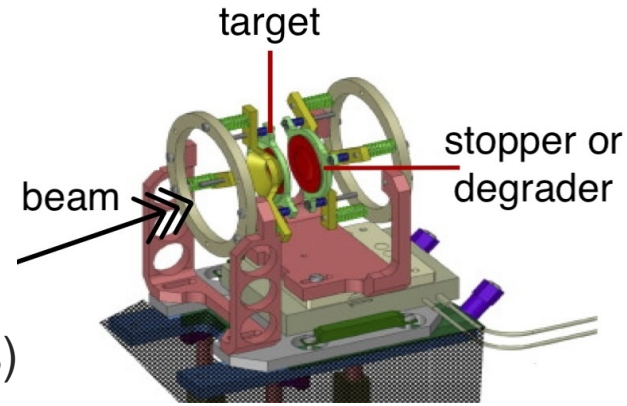

# Lifetime measurements: RDDS

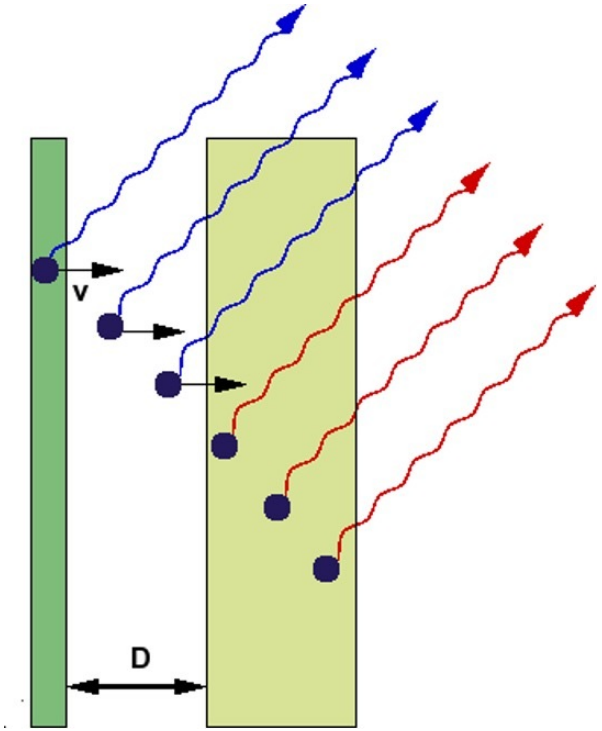


time of flight between the two foils separated by a distance D: $t_D = D/v$

number of $\gamma$ rays emitted after stopping in the second foil:

$$I_s = N_0 \exp\left(-\frac{t_D}{\tau}\right) = N_0 \exp\left(-\frac{D}{v\tau}\right)$$

number of $\gamma$ rays emitted between the two foils:

$$I_f = N_0 - I_s = N_0 \left(1 - \exp\left(-\frac{D}{v\tau}\right)\right)$$

$$\rightarrow \text{intensity ratio } \frac{I_s}{I_s + I_f} = \exp\left(-\frac{D}{v\tau}\right)$$

“plunger” device to control D;
instead of a stopper foil,
a degrader can be used
(enables identification of recoils)

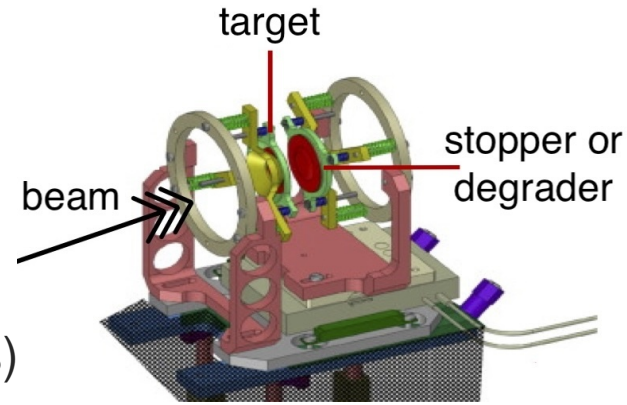

# Lifetime measurements: RDDS

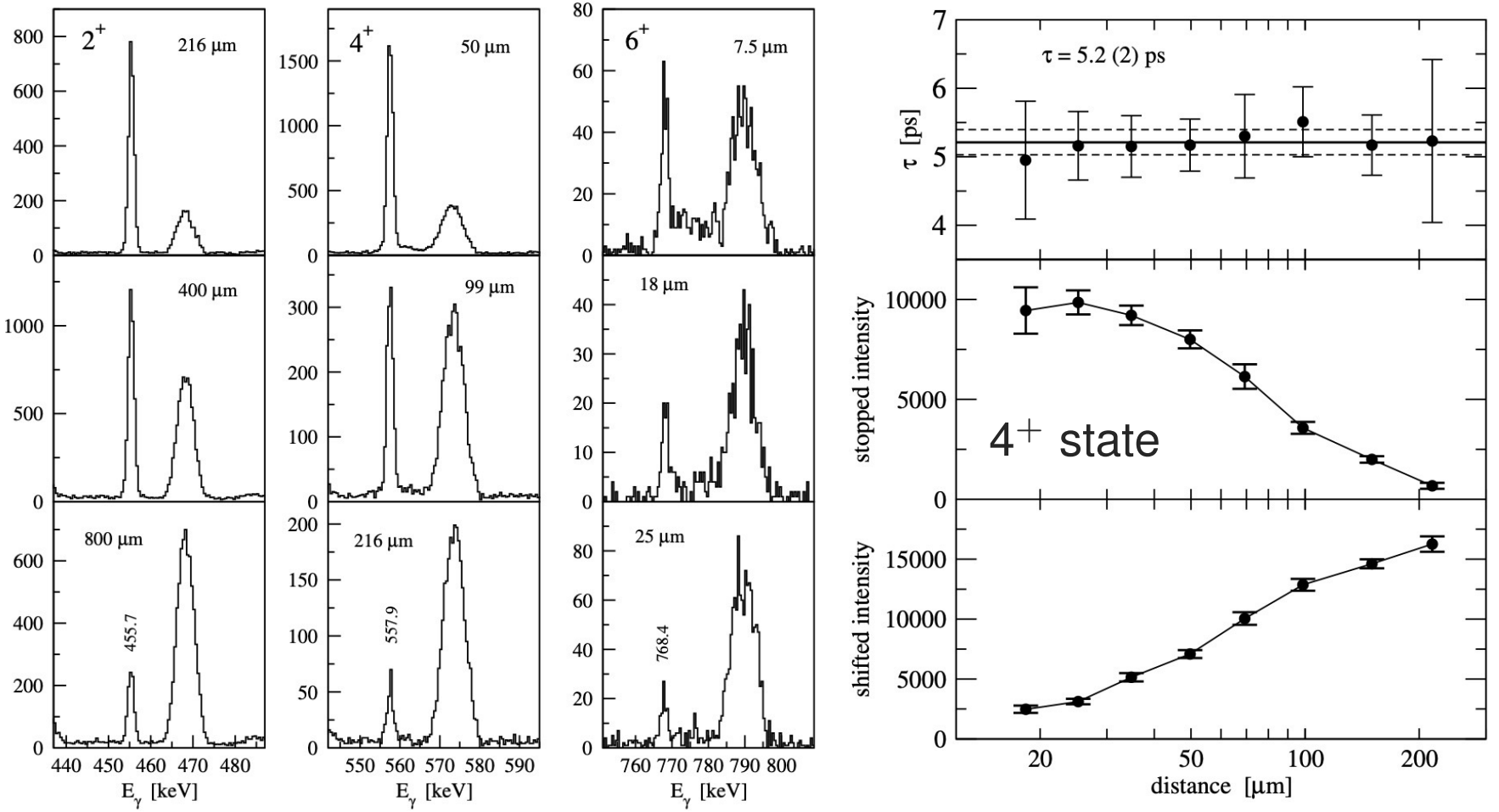


Example of $2^+$, $4^+$, $6^+$ decay in $^{74}$Kr: A. Görgen et al, Eur. Phys. J. A 26, 153 (2005)

# Lifetime measurements: RDDS

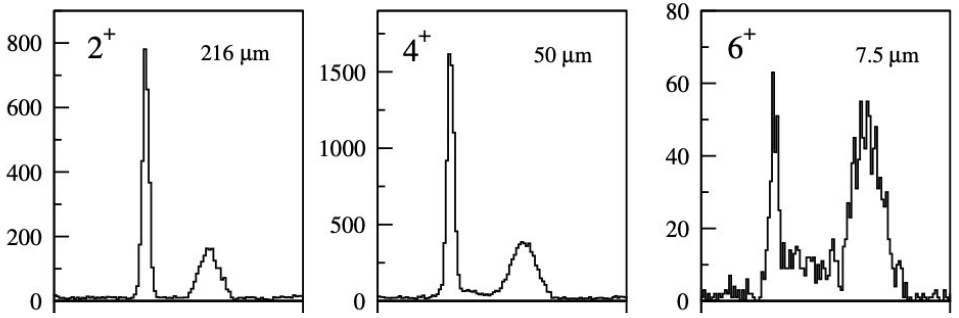


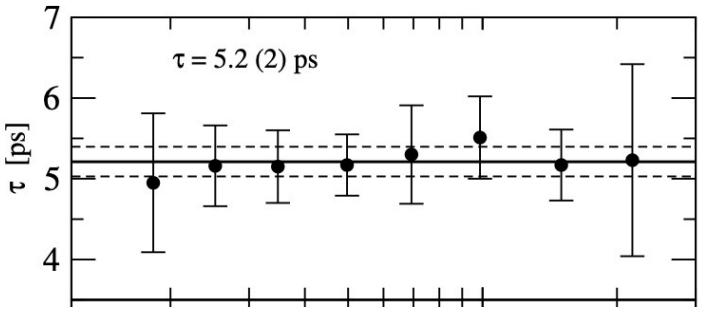


Example of $4^+$ decay in $^{100}$Zr: G. Pasqualato et al, Eur. Phys. J. A 59, 276 (2023)

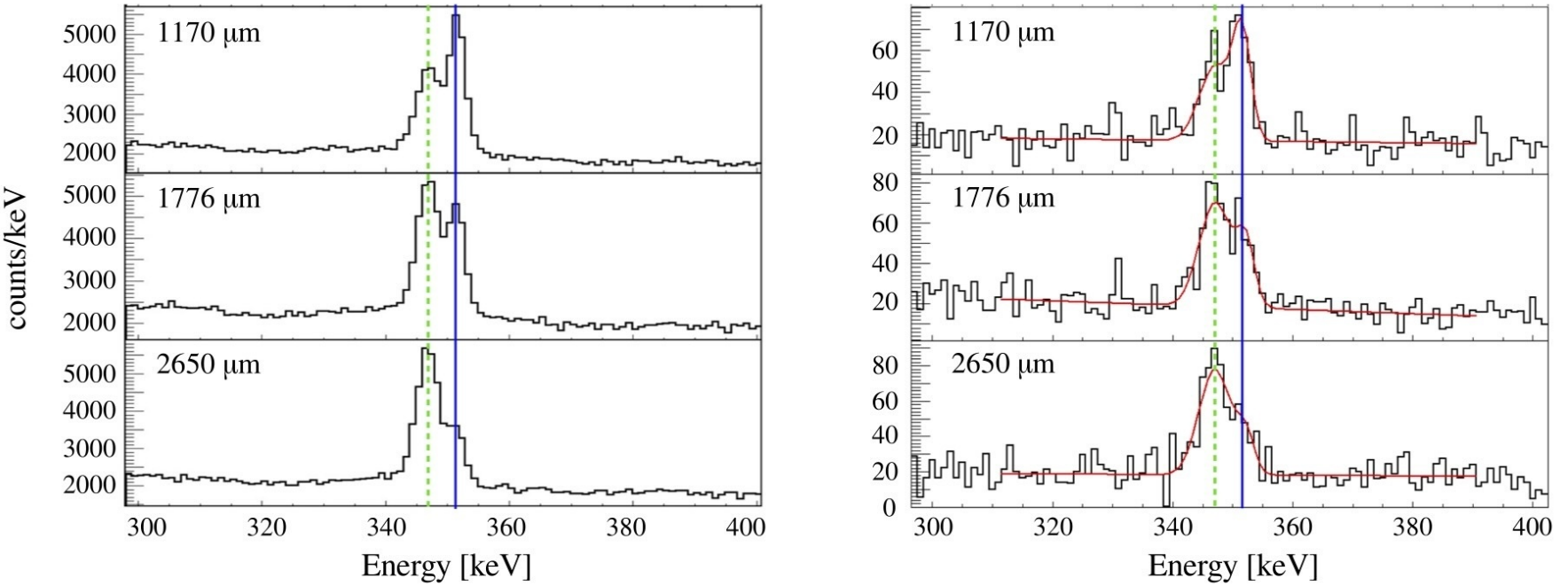


- use of a degrader brings the two components much closer together
- gating from above (on the shifted component) may modify their relative intensities

# Lifetime measurements: Doppler Shift Attenuation (DSAM)

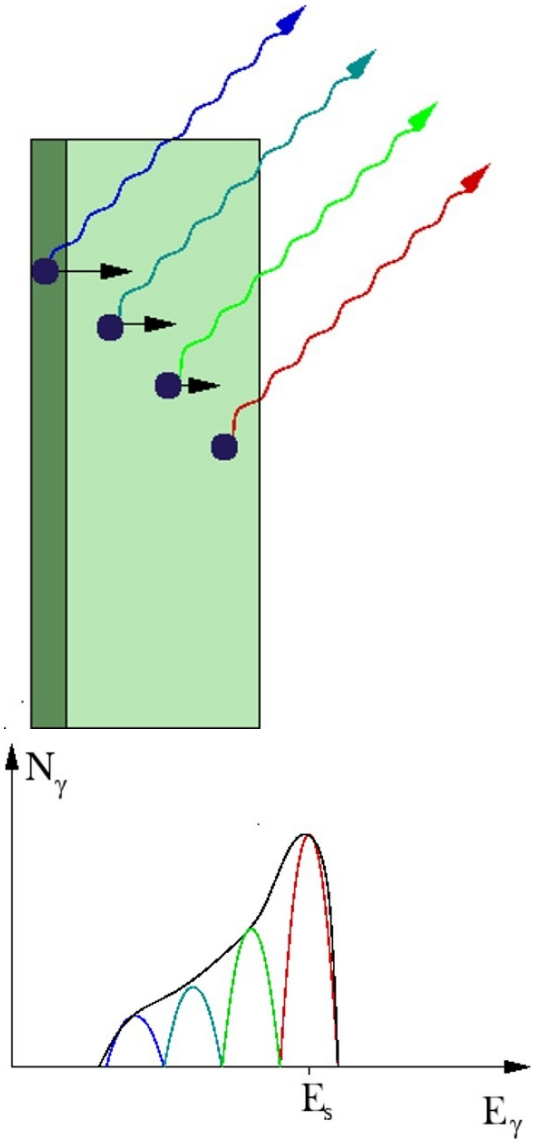


- $\gamma$-ray emission occurs while reaction products gradually slow down in a thick target backing
- instead of a target with a backing, a uniform thick target can be used (velocity profile of the incident beam is then included in the simulation)
- reaction products may also be allowed to leave the target (in order e.g. to have them identified in a mass spectrometer)
  - in this case it is important to know precisely the transition energy

Example: $4^-$ decay in $^{18}$N S. Ziliani et al, PRC 104, L041301 (2021)

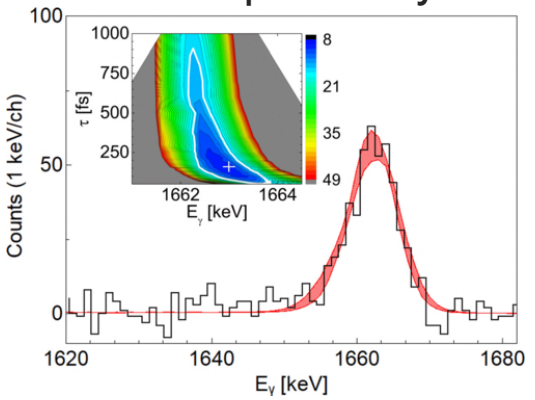


- at the same recoil velocity, gives access to shorter lifetimes than RDDS (typically used for lifetimes below 1 ps)

# Coulomb excitation

- population of excited states via purely electromagnetic interaction between the collision partners in the process of quasi-elastic scattering

- we observe gamma-ray decay of Coulomb-excited states in coincidence with scattered beam ions or target recoils

- the decay intensities, measured as a function of particle scattering angle, are related to reduced transition probabilities and spectroscopic quadrupole moments determined via a multi-dimensional fit of the measured particle-$\gamma$ coincidence yields that is usually constrained by literature data (branching and mixing ratios, lifetimes...)

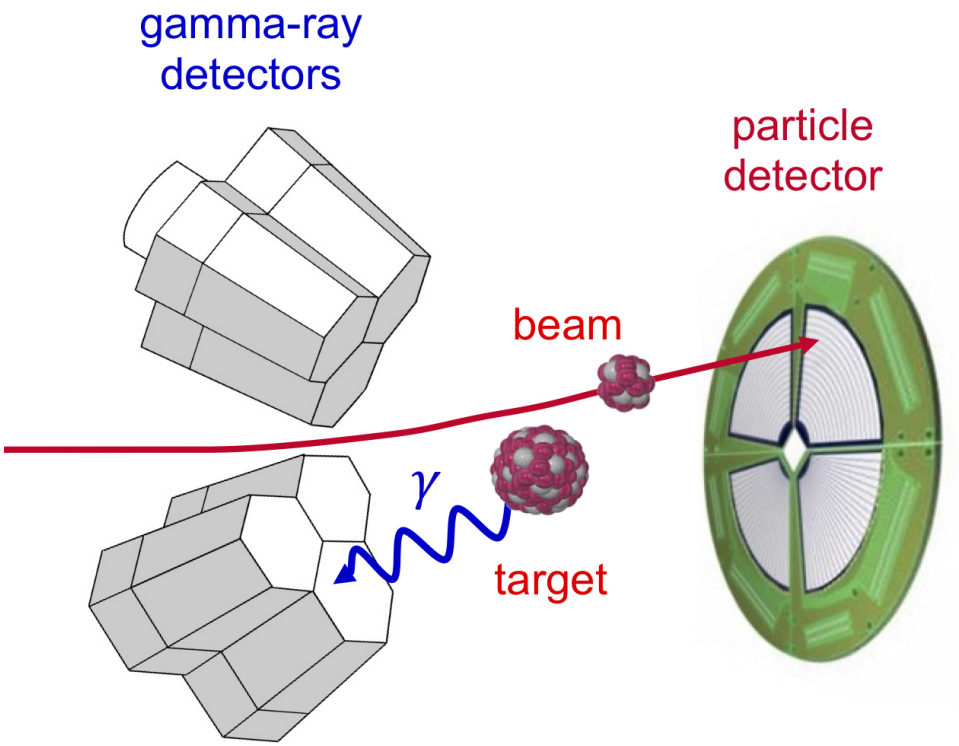


more about the method: MZ, Lecture Notes in Physics 1005 (2022), chapter 2

# Florence School on Coulomb Excitation

January 27 – 30, 2025

organised by INFN Firenze (A. Nannini, M. Rocchini, N. Marchini)

# Multi-step excitation and coupled equations

we expand the interaction potential between the two nuclei in a multipole series:

$V(r(t)) = Z_T Z_P e^2/r$ monopole-monopole (Rutherford) term

$+\sum_{\lambda\mu} V_P(\hat{E}\lambda,\mu) + \sum_{\lambda\mu} V_T(\hat{E}\lambda,\mu)$ electric multipole-monopole excitation,

$+\sum_{\lambda\mu} V_P(\hat{M}\lambda,\mu) + \sum_{\lambda\mu} V_T(\hat{M}\lambda,\mu)$ magnetic excitation (small at low v/c)

+ multipole-multipole terms (neglected – estimated at $\sim 0.5$ %)

$$i\hbar\frac{da_n(t)}{dt} = \sum_{m,\lambda}\langle\phi_n||\hat{E}\lambda||\phi_m\rangle\exp(i(E_n - E_m)/\hbar)a_m(t)$$

- in heavy-ion induced Coulomb excitation the interaction strength gives rise to multiple excitation
- excitation probability of an individual state may depend on many matrix elements involved in different excitation paths

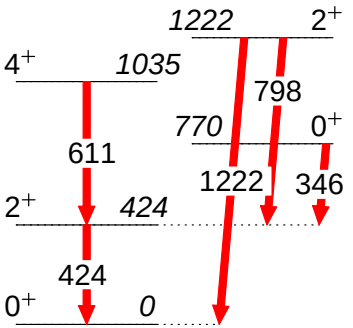


- high number of coupled equations for excitation amplitudes $a_n(t)$ – dedicated data analysis codes needed

(excitation cross sections $\sigma$ are Rutherford cross sections multiplied by the excitation probability $|a_n|^2$)

## Safe energy

D. Cline, Ann. Rev. Nucl. Part. Sci. 36, 683 (1986)

- Cline's "safe energy" criterion: contribution to the excitation cross sections from Coulomb-nuclear interference is below 0.5% if the distance between nuclear surfaces is greater than 5 fm:

$$D_{min} = 1.25 \cdot (A_p^{1/3} + A_t^{1/3}) + 5.0 \quad [\text{fm}]$$

- empirical criterion based on systematic studies of inelastic and transfer cross sections at beam energies of few MeV/A

- if one of the reaction partners is light (A<30), separation of 6 fm or more, depending on the mass, is suggested

- other criteria established for high-energy Coulomb excitation

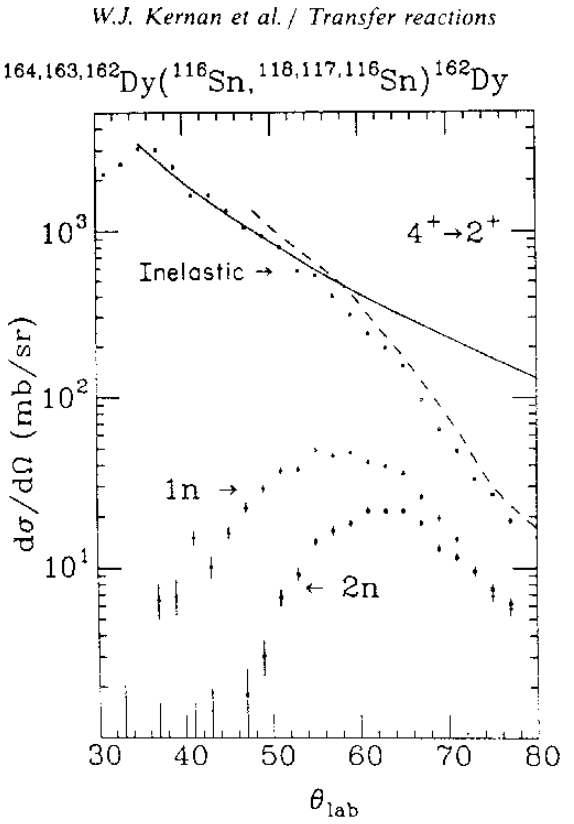


- this criterion does not mean that we will observe no transitions arising from one-neutron transfer; weak lines may appear, but we can nonetheless reliably link the measured Coulomb-excitation cross sections to structure parameters

## “Safe-energy” requirement

...is related to the condition that $D_{min}$ has to be sufficiently large.
But it is not the only way to ensure it!

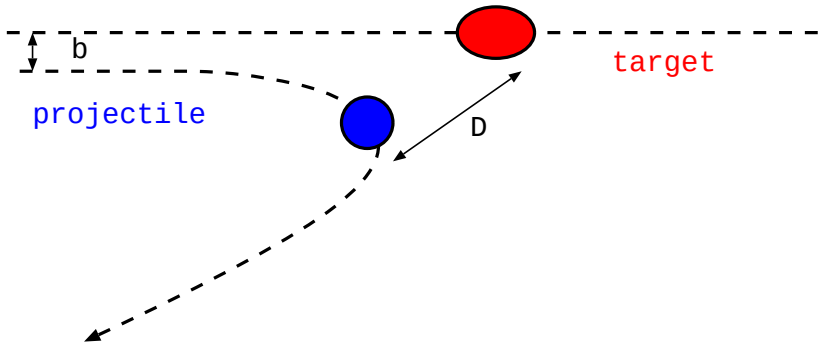


$$E(\theta_{CM}) = 0.72 \frac{Z_P Z_T}{D_{min}} \cdot \frac{A_P + A_T}{A_T} \left(1 + \frac{1}{\sin\left(\frac{\theta_{CM}}{2}\right)}\right) \qquad [\text{MeV}]$$

Two experimental possibilities:

- choose adequate beam energy ($D > D_{min}$ for all $\theta$)
  low-energy Coulomb excitation
- limit scattering angle, i.e. select impact parameter b ($E_b$, $\theta$) > $D_{min}$
  high-energy Coulomb excitation

# Dependence of cross sections on energy

$^{74}$Zn on $^{208}$Pb

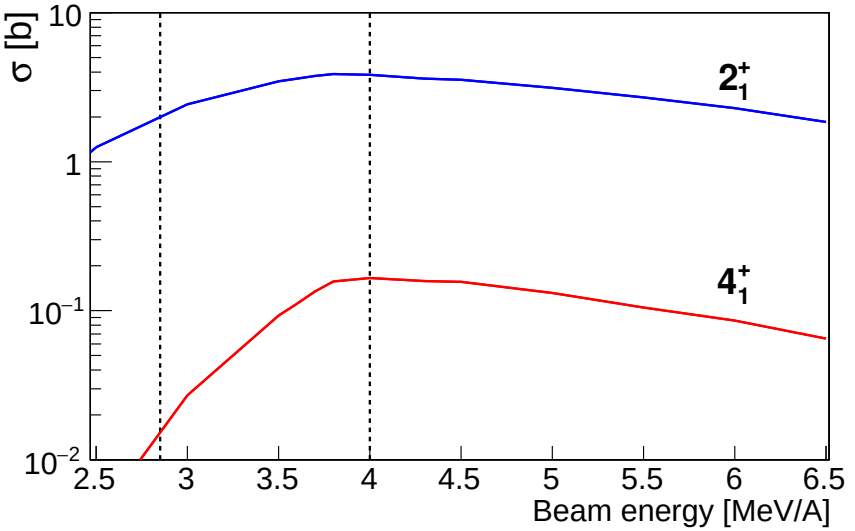


A. Illana *et al.*, PRC 108, 044305 (2023)

$^{40}$S on $^{197}$Au

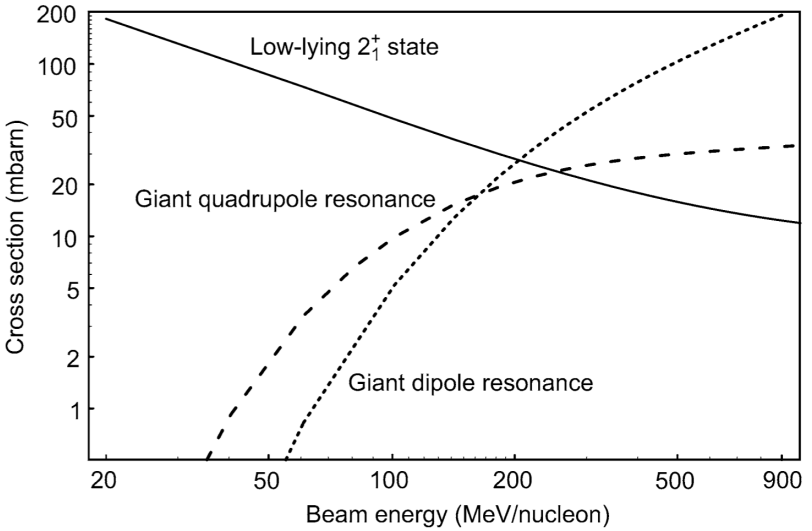


T. Glasmacher, NPA 693 (2001) 90

- low-energy Coulomb excitation: maximum cross section for single- and multi-step excitation at ∼4-5 MeV/A
  - stronger dependence of multi-step excitation cross sections on energy
- only single-step excitation important for energies of tens or hundreds MeV/A; slow decrease of cross section with energy
  - possibility to use very thick targets (g/cm$^2$) to compensate for that

# Measuring quadrupole moments of excited states

- reorientation effect: influence of the quadrupole moment on the excitation cross section

$^{76}$Zn, HIE-ISOLDE data from: A. Illana, MZ *et al.*, PRC 108, 044305 (2023)

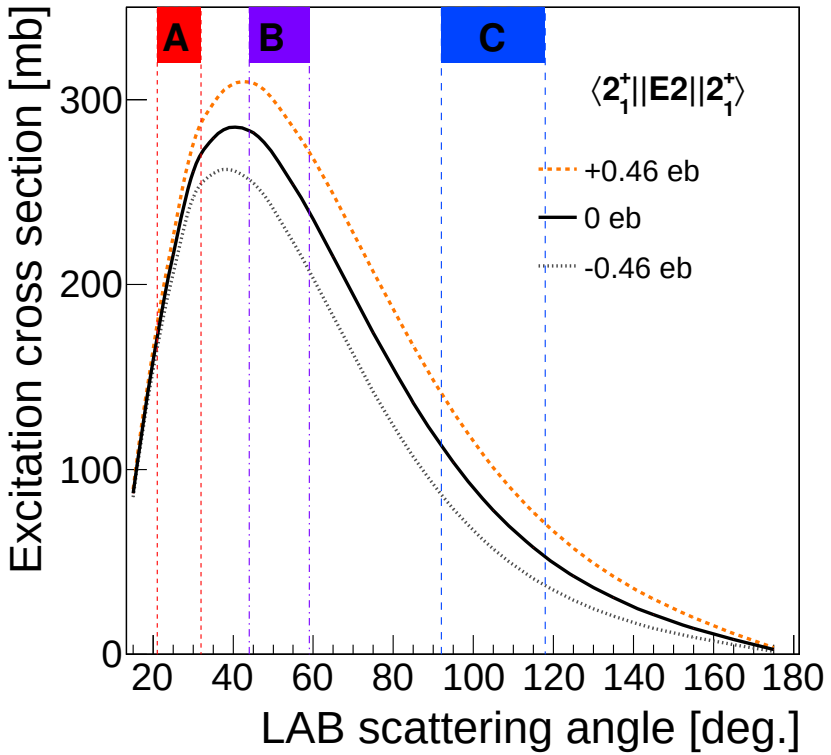


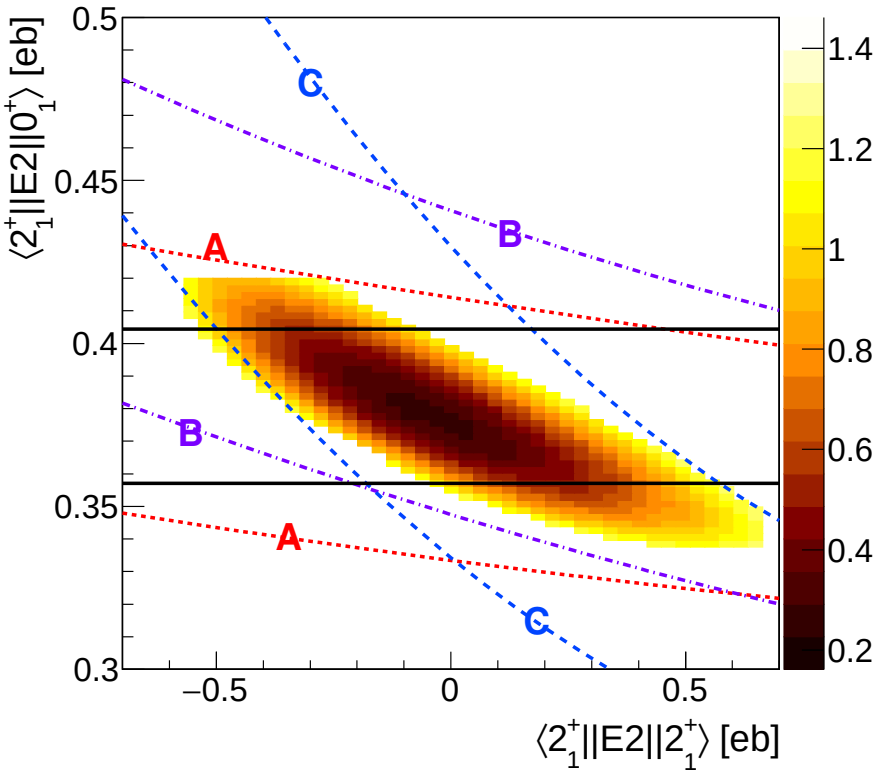


- $\chi^2$ comparison of measured cross sections with calculated ones
- independent lifetime measurements increase precision of extracted quadrupole moments
- possible at $\sim 10^4$ pps (statistics of at least 1000 counts needed)

# Measuring quadrupole moments of excited states

- integral cross-section measurements combined with lifetimes: possible at $\sim 10^3$ pps (statistics of 100-500 counts needed)

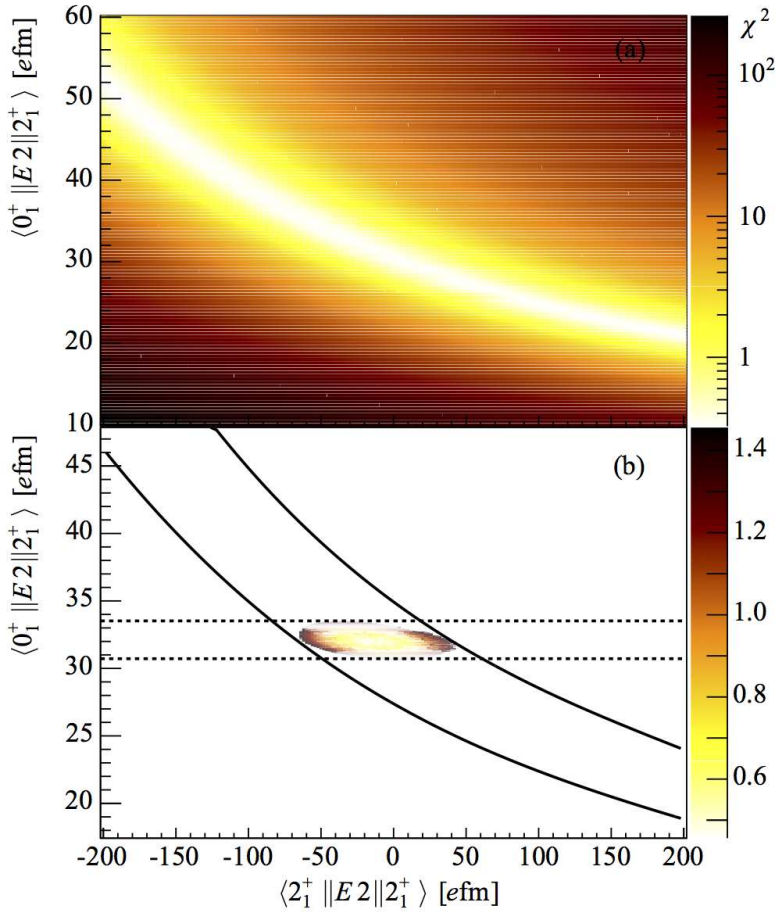


$^{62}$Fe, ISOLDE

L. Gaffney *et al.* EPJA 51, 136 (2015)

Coulomb excitation of $^{70}$Se, ISOLDE

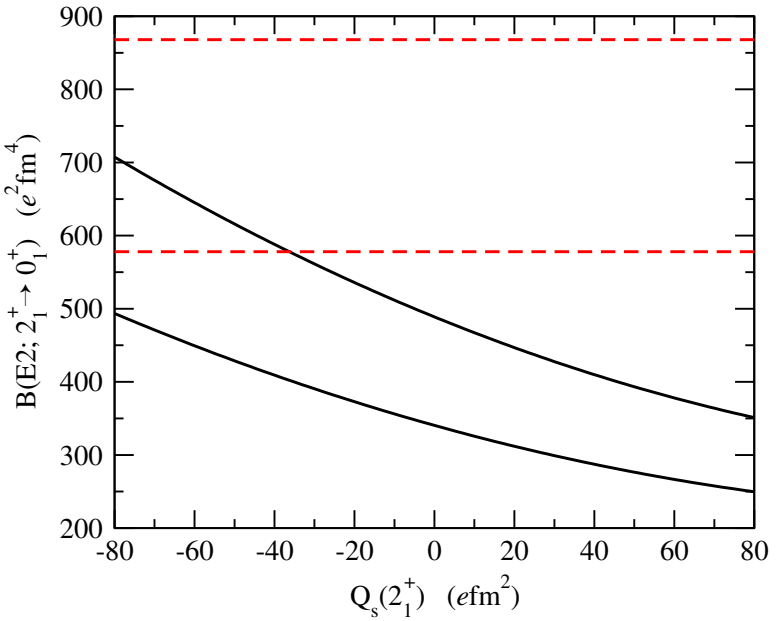


A.M. Hurst *et al.*,
Phys. Rev. Lett. 98, 072501 (2007)

# Measuring quadrupole moments of excited states

- integral cross section measurements combined with lifetimes: possible at $\sim 10^3$ pps (statistics of 100-500 counts needed)

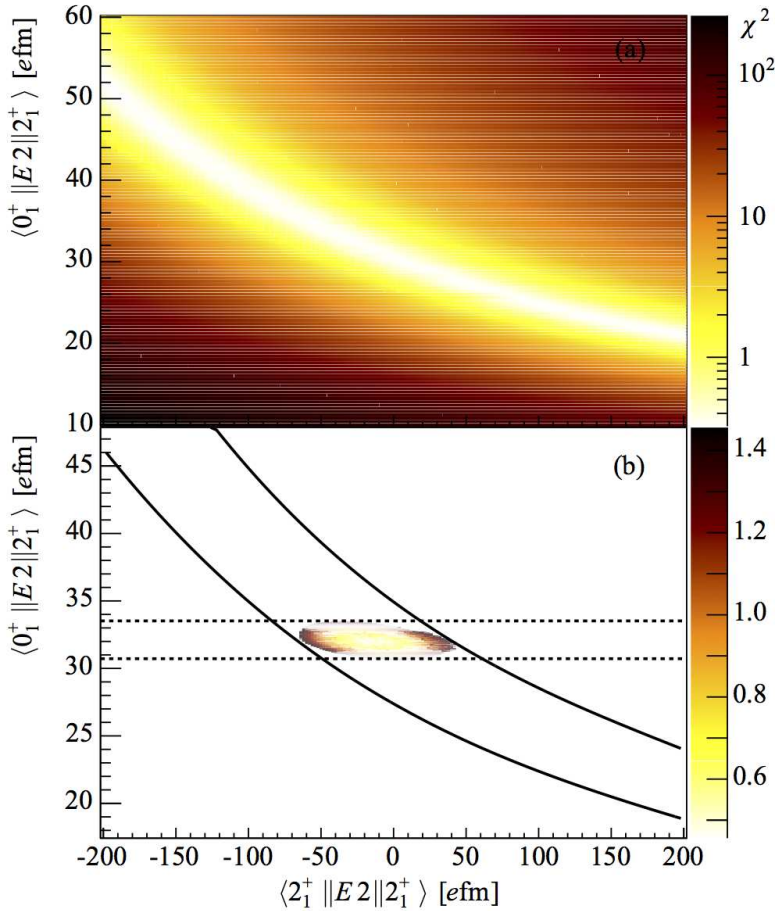


$^{62}$Fe, ISOLDE

L. Gaffney *et al.* EPJA 51, 136 (2015)

Coulomb excitation of $^{70}$Se, ISOLDE

+ new lifetime

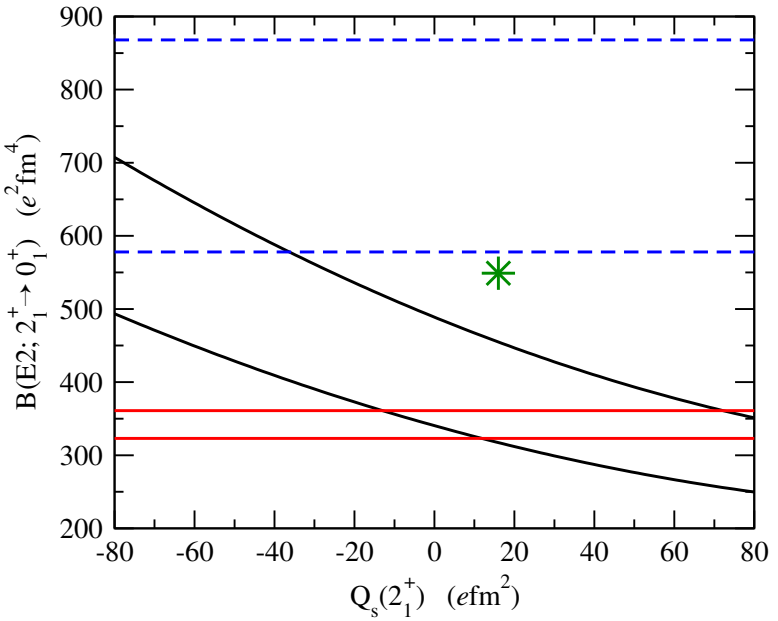


J. Ljungvall *et al.*,

Phys. Rev. Lett. 100, 102502 (2008)

reliable lifetimes needed!

## Quadrupole sum rules

D. Cline, Ann. Rev. Nucl. Part. Sci. 36 (1986) 683
K. Kumar, PRL 28 (1972) 249

• electromagnetic multipole operators are spherical tensors – products of such operators coupled to angular momentum 0 are rotationally invariant

• in the intrinsic frame of the nucleus, the E2 operator may be expressed using two parameters Q and $\delta$ related to charge distribution:

$$\begin{aligned} E(2,0) &= Q\cos\delta \\ E(2,2) = E(2,-2) &= \frac{Q}{\sqrt{2}}\sin\delta \\ E(2,1) = E(2,-1) &= 0 \end{aligned}$$

$$\frac{\langle Q^2\rangle}{\sqrt{5}} = \langle i|\,[E2\times E2]^0\,|i\rangle = \frac{1}{\sqrt{(2I_i+1)}}\sum_t \langle i||E2||t\rangle\langle t||E2||i\rangle \begin{Bmatrix} 2 & 2 & 0 \\ I_i & I_i & I_t \end{Bmatrix}$$

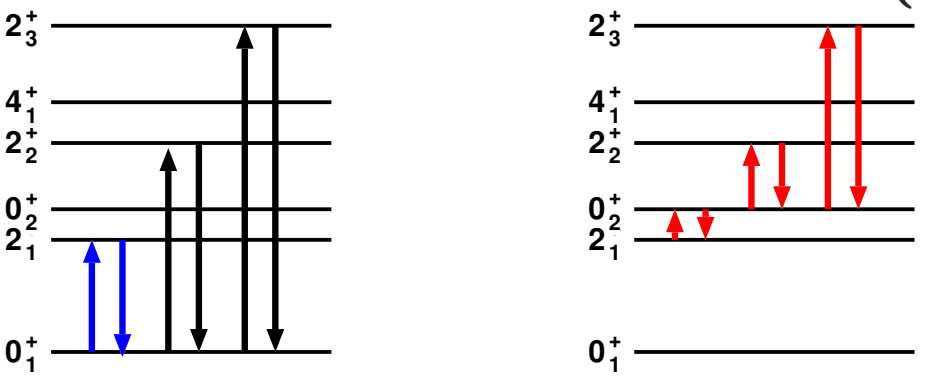


$\langle Q^2\rangle$: measure of the overall deformation;
for the ground state – extension of $B(E2; 0^+ \rightarrow 2^+) = ((3/4\pi)eZR_0^2)^2\ \beta_2{}^2$

Contributions to $\langle Q^2\rangle$ in $^{100}$Mo: K. Wrzosek-Lipska *et al.*, PRC 86 (2012) 064305

# Determination of $\langle Q^2 \rangle$: example of $^{100}$Mo

K. Wrzosek-Lipska et al, PRC 86 (2012) 064305

| state | loop | contribution to $\langle Q^2 \rangle$ [e2b2] |
|---|---|---|
| $0_1^+$ | $\langle 0_1^+ \|\|E2\|\| 2_1^+ \rangle \langle 2_1^+ \|\|E2\|\| 0_1^+ \rangle$ | 0.46 |
| | $\langle 0_1^+ \|\|E2\|\| 2_2^+ \rangle \langle 2_2^+ \|\|E2\|\| 0_1^+ \rangle$ | 0.01 |
| | $\langle 0_1^+ \|\|E2\|\| 2_3^+ \rangle \langle 2_3^+ \|\|E2\|\| 0_1^+ \rangle$ | 0.0002 |
| | Total | 0.48 |
| $0_2^+$ | $\langle 0_2^+ \|\|E2\|\| 2_1^+ \rangle \langle 2_1^+ \|\|E2\|\| 0_2^+ \rangle$ | 0.26 |
| | $\langle 0_1^+ \|\|E2\|\| 2_2^+ \rangle \langle 2_2^+ \|\|E2\|\| 0_2^+ \rangle$ | 0.10 |
| | $\langle 0_2^+ \|\|E2\|\| 2_3^+ \rangle \langle 2_3^+ \|\|E2\|\| 0_2^+ \rangle$ | 0.25 |
| | Total | 0.62 |

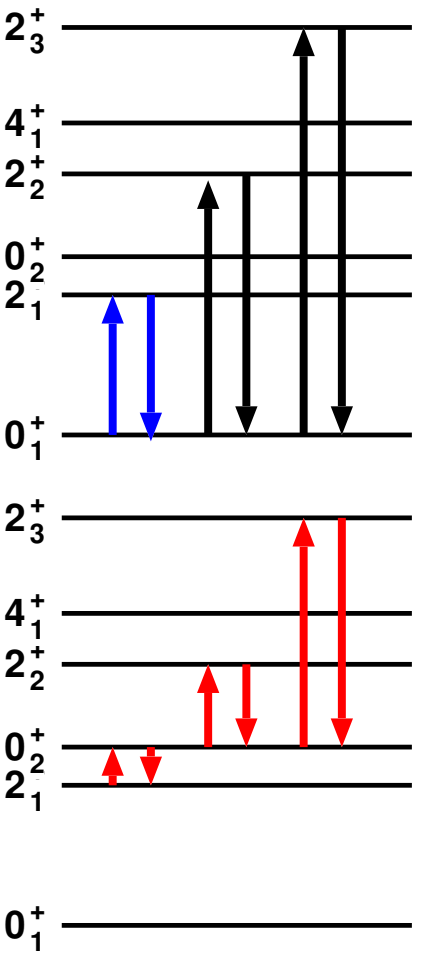

# Quadrupole sum rules: triaxiality

D. Cline, Ann. Rev. Nucl. Part. Sci. 36 (1986) 683

K. Kumar, PRL 28 (1972) 249

$$\sqrt{\frac{2}{35}}\langle Q^3\cos 3\delta\rangle = \langle i|\{[E2\times E2]^2\times E2\}^0|i\rangle$$
$$= \frac{1}{(2I_i+1)}\sum_{t,u}\langle i||E2||u\rangle\langle u||E2||t\rangle\langle t||E2||i\rangle \begin{Bmatrix} 2 & 2 & 2 \\ I_i & I_t & I_u \end{Bmatrix}$$

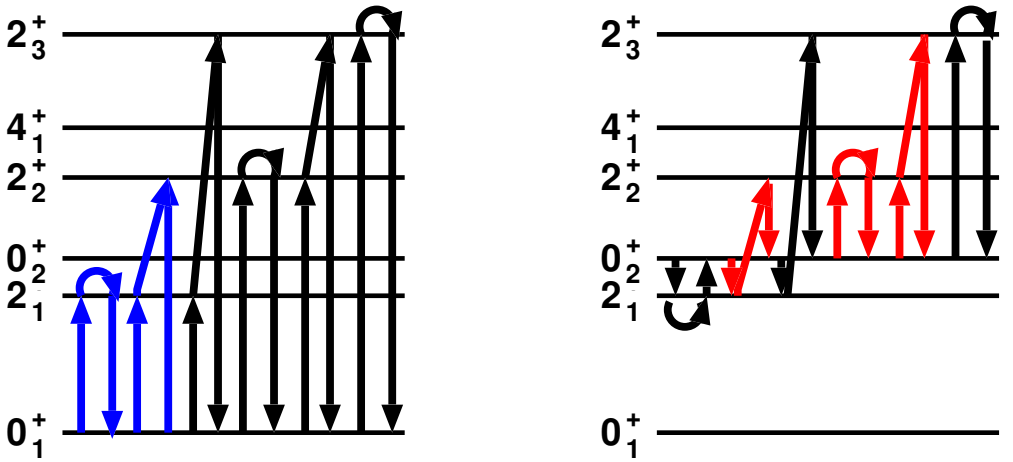


$\langle\cos 3\delta\rangle$: measure of triaxiality

- relative signs of E2 matrix elements are needed: can we get them experimentally?

Contributions to $\langle Q^3\cos 3\delta\rangle$ in $^{100}$Mo: K. Wrzosek-Lipska *et al.*, PRC 86 (2012) 064305

# Relative signs of E2 matrix elements

- Coulomb-excitation cross section are sensitive to relative signs of MEs: result of interference between single-step and multi-step amplitudes

- excitation amplitude of state A: $a_A \sim \langle A||E2||g.s.\rangle + \langle B||E2||g.s.\rangle\langle A||E2||B\rangle$

- excitation probability ($\sim a_A^2$) contains interference terms $\langle A||E2||g.s.\rangle\langle B||E2||g.s.\rangle\langle A||E2||B\rangle$

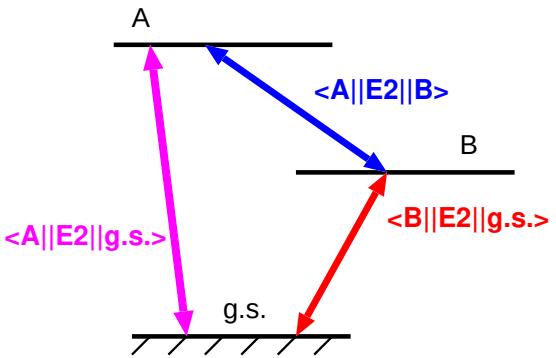


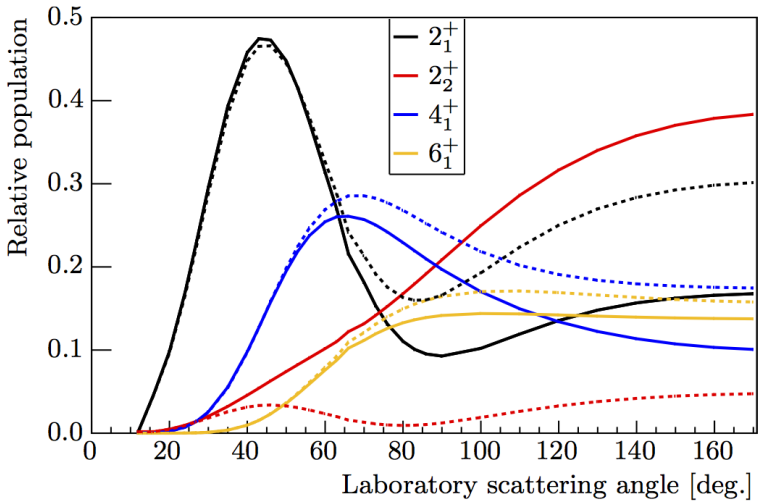


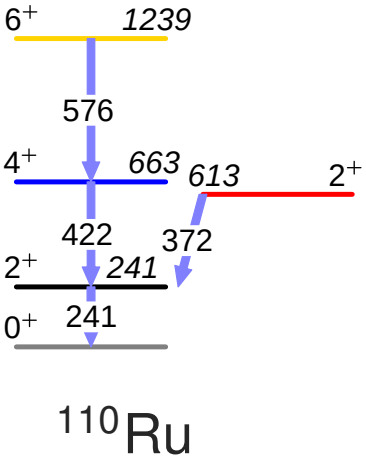


$^{110}$Ru

- negative $\langle 2_1^+||E2||2_2^+\rangle$ (solid lines): much higher population of $2_2^+$ at high CM angles

- sign of a product of matrix elements is an observable

# Sensitivity to relative signs of matrix elements

MZ, EPJ Web Conf 178 (2018) 02014

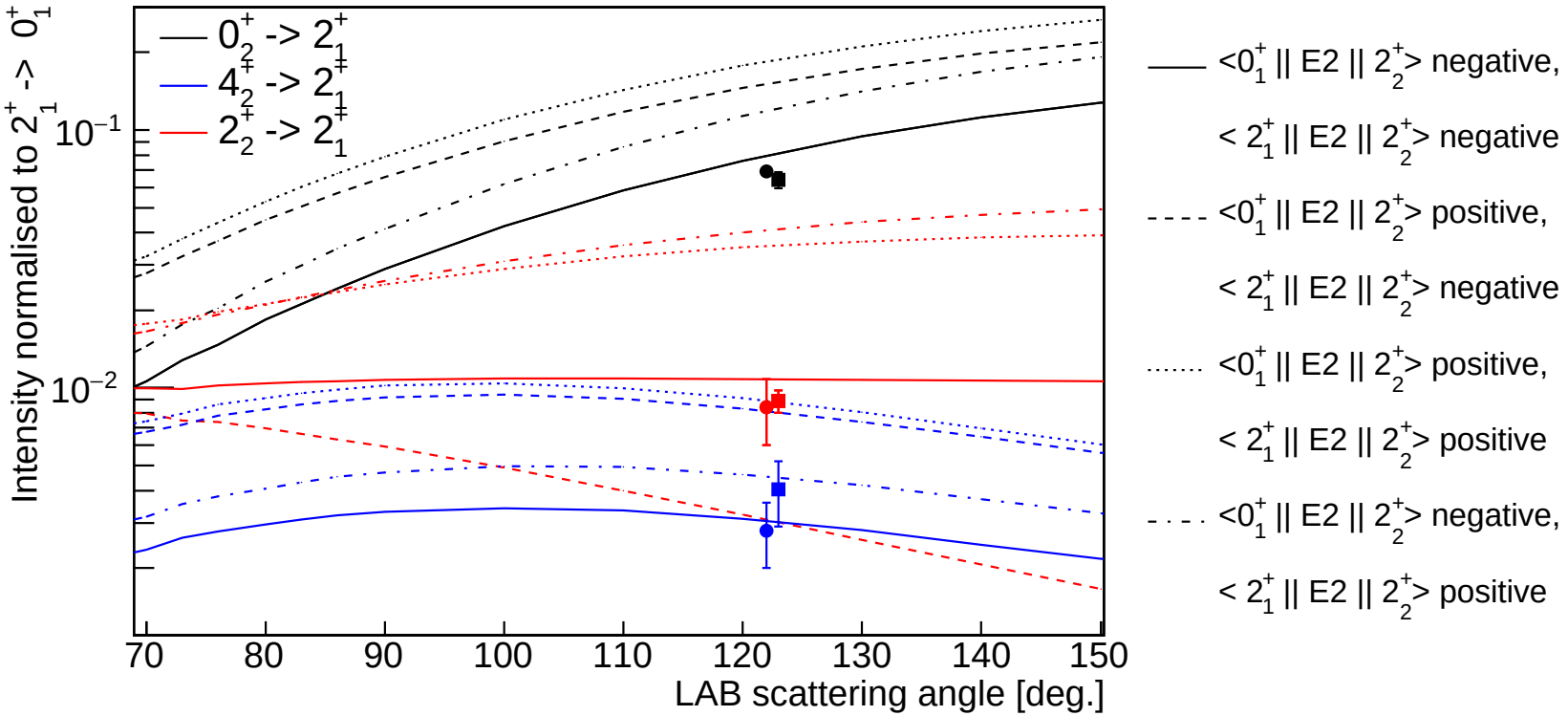


- solid: final set of matrix elements, dashed: other combinations of signs
- different combinations of signs lead to changes in population of the states of a factor of two or more
- precision of the lifetimes: 2% - 20%

# Determination of $\langle \cos 3\delta \rangle$: example of $^{100}$Mo

| state | loop | contribution to $\langle Q^3 \cos 3\delta \rangle$ |
|---|---|---|
| $0_1^+$ | $\langle 0_1^+ \|\|E2\|\| 2_1^+ \rangle \langle 2_1^+ \|\|E2\|\| 2_1^+ \rangle \langle 2_1^+ \|\|E2\|\| 0_1^+ \rangle$ | -0.154 |
| | $\langle 0_1^+ \|\|E2\|\| 2_1^+ \rangle \langle 2_1^+ \|\|E2\|\| 2_2^+ \rangle \langle 2_2^+ \|\|E2\|\| 0_1^+ \rangle$ | 0.132 |
| | $\langle 0_1^+ \|\|E2\|\| 2_1^+ \rangle \langle 2_1^+ \|\|E2\|\| 2_3^+ \rangle \langle 2_3^+ \|\|E2\|\| 0_1^+ \rangle$ | 0.002 |
| | $\langle 0_1^+ \|\|E2\|\| 2_2^+ \rangle \langle 2_2^+ \|\|E2\|\| 2_2^+ \rangle \langle 2_2^+ \|\|E2\|\| 0_1^+ \rangle$ | 0.013 |
| | $\langle 0_1^+ \|\|E2\|\| 2_2^+ \rangle \langle 2_2^+ \|\|E2\|\| 2_3^+ \rangle \langle 2_3^+ \|\|E2\|\| 0_1^+ \rangle$ | -0.001 |
| | $\langle 0_1^+ \|\|E2\|\| 2_3^+ \rangle \langle 2_3^+ \|\|E2\|\| 2_3^+ \rangle \langle 2_3^+ \|\|E2\|\| 0_1^+ \rangle$ | -0.0001 |
| | Total | -0.008 |
| $0_2^+$ | $\langle 0_2^+ \|\|E2\|\| 2_1^+ \rangle \langle 2_1^+ \|\|E2\|\| 2_1^+ \rangle \langle 2_1^+ \|\|E2\|\| 0_2^+ \rangle$ | -0.09 |
| | $\langle 0_2^+ \|\|E2\|\| 2_1^+ \rangle \langle 2_1^+ \|\|E2\|\| 2_2^+ \rangle \langle 2_2^+ \|\|E2\|\| 0_2^+ \rangle$ | -0.31 |
| | $\langle 0_2^+ \|\|E2\|\| 2_1^+ \rangle \langle 2_1^+ \|\|E2\|\| 2_3^+ \rangle \langle 2_3^+ \|\|E2\|\| 0_2^+ \rangle$ | -0.04 |
| | $\langle 0_2^+ \|\|E2\|\| 2_2^+ \rangle \langle 2_2^+ \|\|E2\|\| 2_2^+ \rangle \langle 2_2^+ \|\|E2\|\| 0_2^+ \rangle$ | 0.12 |
| | $\langle 0_2^+ \|\|E2\|\| 2_2^+ \rangle \langle 2_2^+ \|\|E2\|\| 2_3^+ \rangle \langle 2_3^+ \|\|E2\|\| 0_2^+ \rangle$ | -0.13 |
| | $\langle 0_2^+ \|\|E2\|\| 2_3^+ \rangle \langle 2_3^+ \|\|E2\|\| 2_3^+ \rangle \langle 2_3^+ \|\|E2\|\| 0_2^+ \rangle$ | -0.06 |
| | Total | -0.51 |

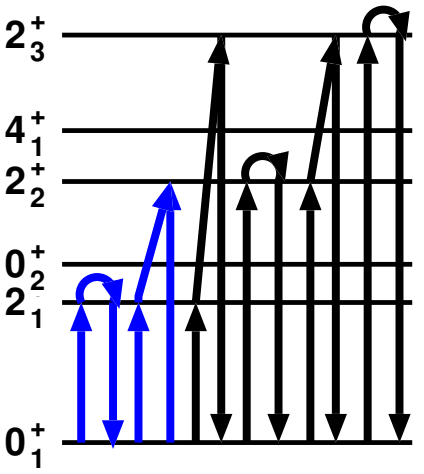


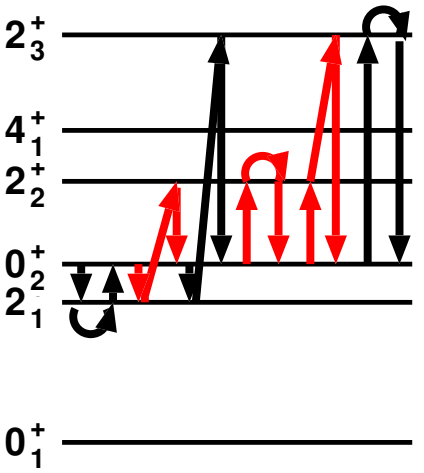

# Shape evolution of $^{96-100}$Mo

MZ *et al.*, Nucl. Phys. A 712 (2002) 3

K. Wrzosek-Lipska *et al.*, PRC 86 (2012) 064305

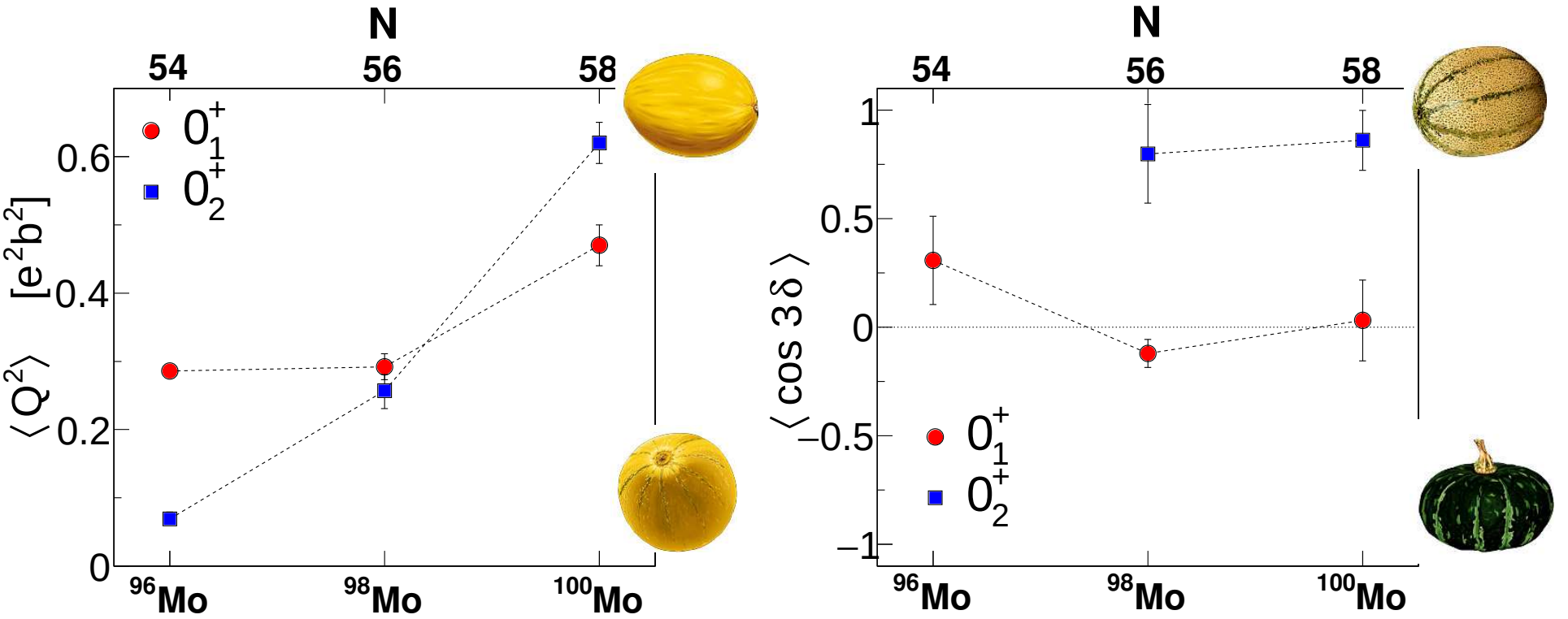


- $^{96}$Mo: coexistence of the deformed ground state with a spherical $0_2^+$
- ground states of the Mo isotopes triaxial (average shape, may result from dynamic effects), deformation of $0_2^+$ increasing with N
- shape coexistence in $^{98}$Mo manifested in a different triaxiality of $0_1^+$ and $0_2^+$

# Higher-order quadrupole invariants, convergence – examples of $^{72,76}$Ge

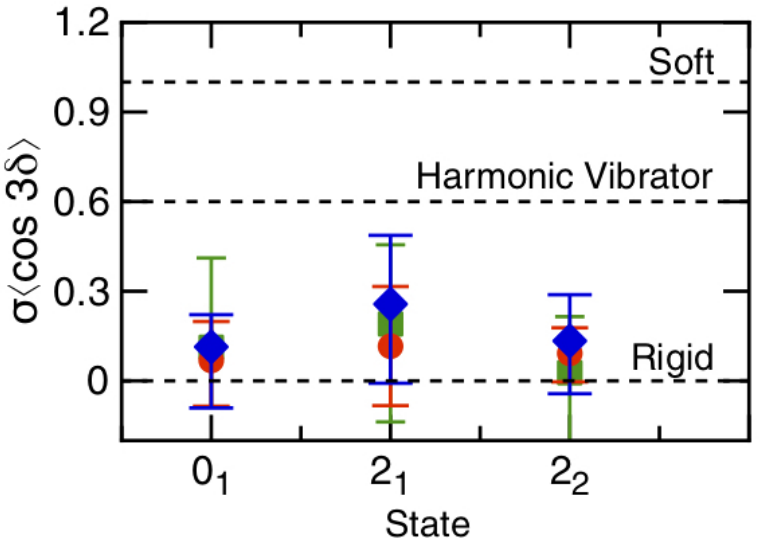


A.D. Ayangeakaa *et al.*,
PRL 123, 102501 (2019), PLB 754, 254 (2016)

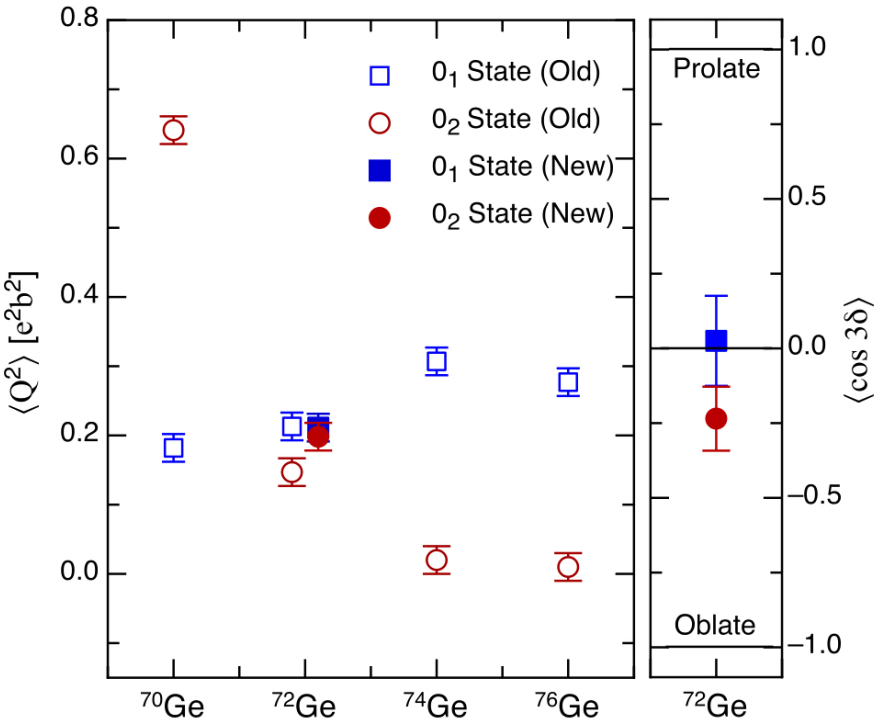


- $^{76}$Ge: unique example of determination of softness in $\gamma$ from experimental data

$$\sigma(\cos 3\delta) = \sqrt{\frac{\langle Q^6 \cos^2 3\delta\rangle}{\langle Q^6\rangle} - \left(\frac{\langle Q^3 \cos 3\delta\rangle}{\langle Q^3\rangle}\right)^2}$$

- $^{72}$Ge: much higher number of transitions observed in a new measurement

$\rightarrow$ slight change of the deduced invariants due to extra states entering the sum

# Do we know all states that should enter the sum?

- especially for the (E2 x E2 x E2), where terms can cancel out – can we say that terms involving higher lying levels (the $2_4^+$ state etc) do not significantly influence the rotational invariant?
  - if such state was coupled to the state in question via a large E2 matrix element, it would be populated in the experiment
  - comparison with GBH calculations for $^{100}$Mo: $Q^2$, $Q^3\cos(3\,\delta)$ calculated directly from probability density distributions and from theoretical values of matrix elements, limited to the same three intermediate states

$\Rightarrow$ difference below 3% for both $0^+$ states

| | GBH | | exp |
|---|---|---|---|
| $0_1^+ : \overline{\beta}$ | 0.20 | 0.20 | 0.22 $\pm$0.01 |
| $0_1^+ : \overline{\gamma}$ | 27° | 27° | 29°$\pm$3° |
| $0_2^+ : \overline{\beta}$ | 0.24 | 0.24 | 0.25 $\pm$0.01 |
| $0_2^+ : \overline{\gamma}$ | 18° | 17° | 10°$\pm$3° |

K. Wrzosek-Lipska, PRC 86 (2012) 064305

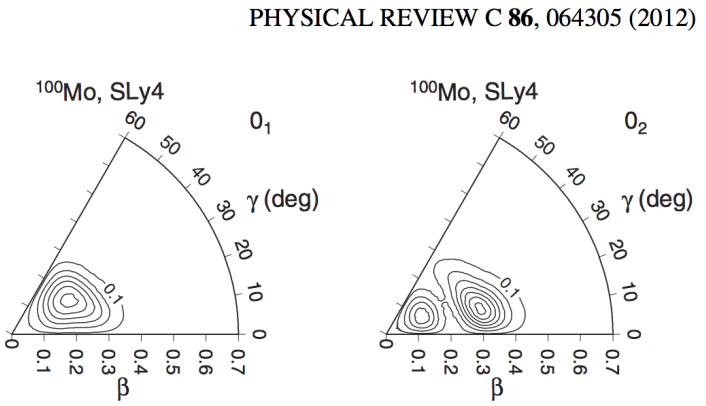


FIG. 15. Probability density [Eq. (26)] for the $0_1^+$ and $0_2^+$ states for the Skyrme SLy4 interaction. The contour interval is 0.3.

# Shape coexistence

# Landscape of shape coexistence

- appearance of states characterised by different shapes closely lying in energy
- a widespread phenomenon in areas close to proton and neutron shell closures

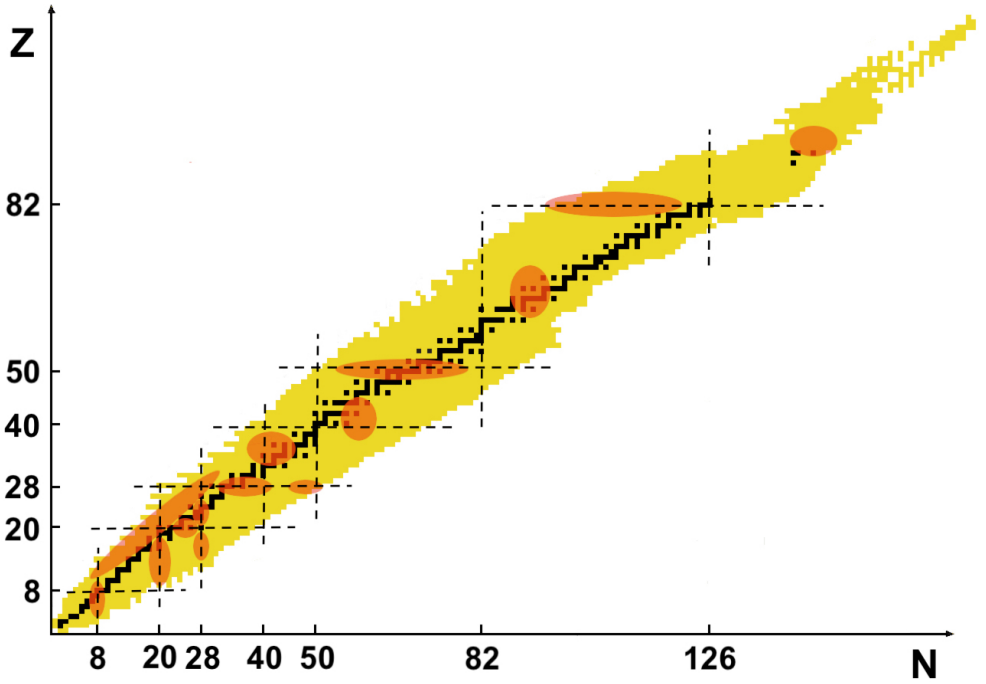


- difficult to establish experimentally as nuclear shape is not an observable
- depends on a delicate balance of macroscopic, liquid-drop-like properties of the nuclear matter and microscopic shell effects – provides stringent tests of modern nuclear structure models

# Proposed mechanism behind shape coexistence

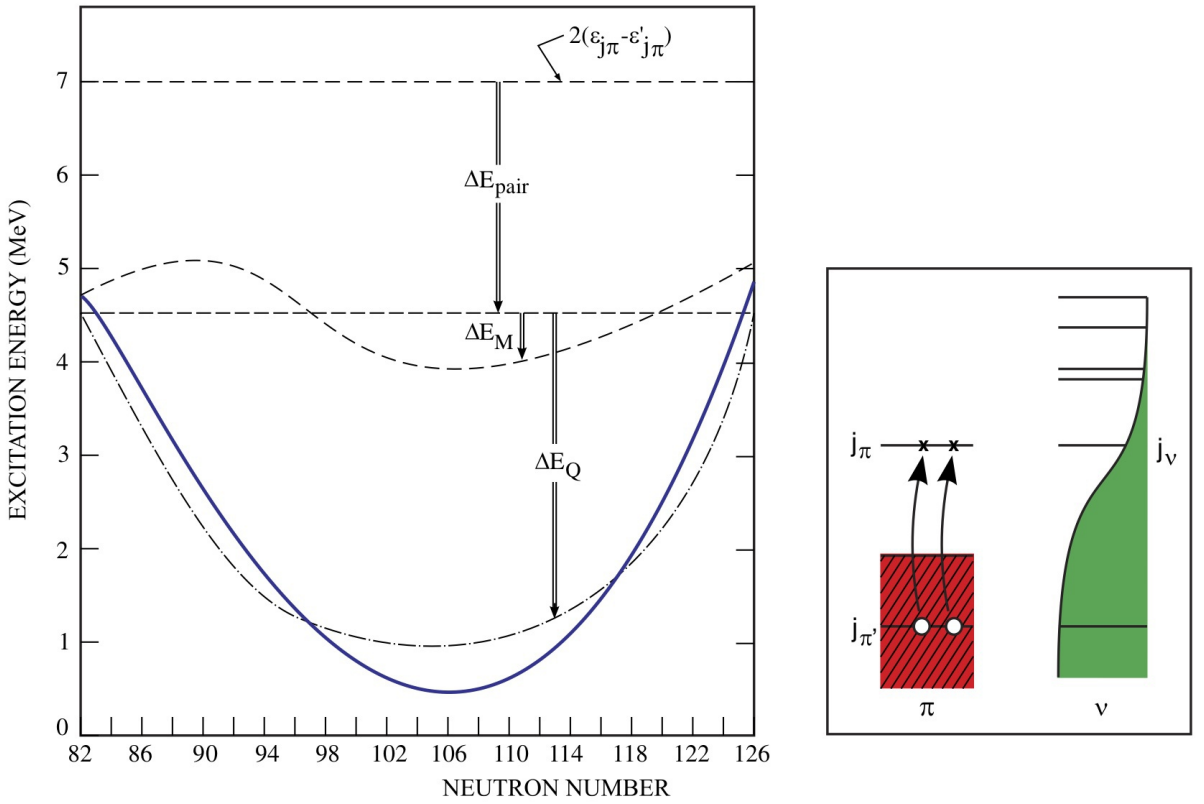


K. Heyde and J. Wood, Rev. Mod. Phys. 83, 1467 (2011)

- gain from correlations offsets the shell gap and multiparticle-multihole excitations go down in excitation energy

- characteristic parabolic behaviour of intruder states energies

# Experimental studies of shape coexistence

What observables can be used to conclude on shape coexistence?

- level energies (but they need to be put in context of systematics: neighbouring nuclei, other bands in the nucleus under study...)
- transition probabilities
- transfer-reaction cross sections
- quadrupole moments
- charge radii
- quadrupole invariants
- monopole transition strengths

How can we deduce level mixing from experimental data?

# Level energies – systematics of isotopic chains

- parabolic behaviour experimentally observed for nuclei with A>100, less evident in lighter nuclei

Hg isotopes, Z=80

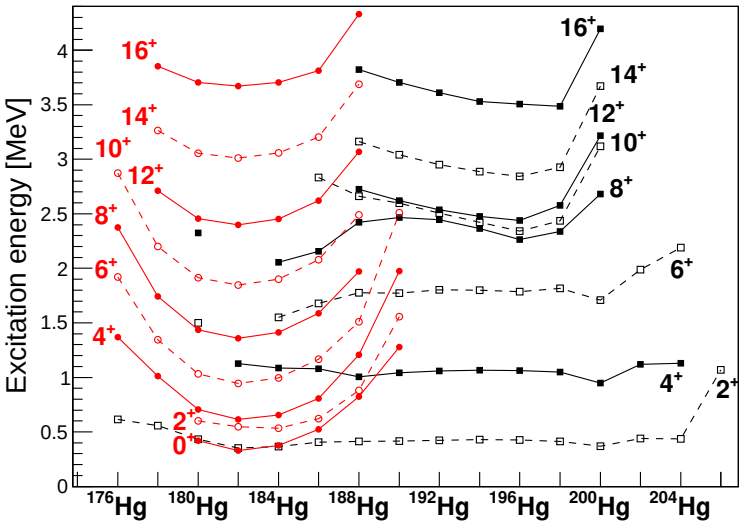


Sn isotopes, Z=50

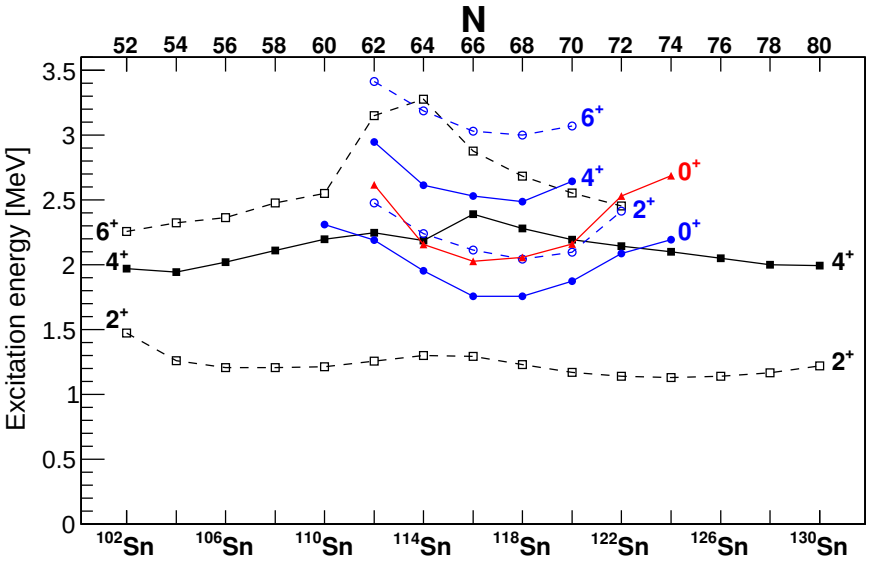


data compilation: P. Garrett, MZ, E. Clément, Prog. Part. Nucl. Phys. 124, 103931 (2022)

# Level energies – moments of inertia

- $^{72,74,76}$Se: presence of bands built on low-lying $0^+$ states
- $^{76}$Se: different transition strengths in the gsb and the band built on the $0_2^+$ state:

$B(E2; 2_3^+ \rightarrow 0_2^+)$ = 31(5) W.u. versus $B(E2; 2_1^+ \rightarrow 0_1^+)$) = 44(1) W.u.;
(S. Mukhopadhyay *et al.*, PRC 99, 014313 (2019))

- $^{72,76}$Se: negative quadrupole moments of $2_1^+$ states

(J. Henderson *et al.*, PRL 121, 082502 (2018); A.E. Kavka, NPA 593, 177 (1995))

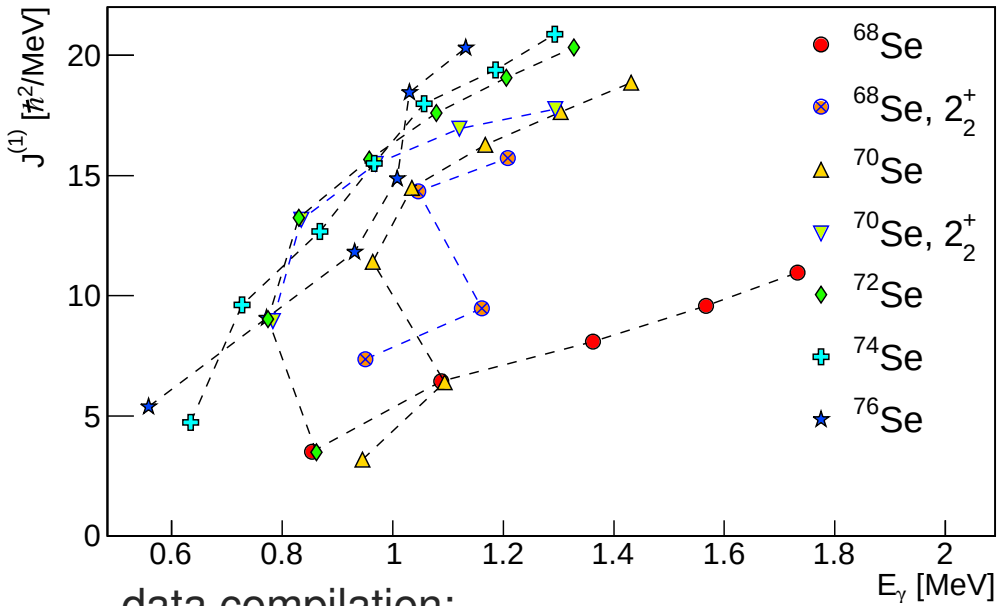


data compilation:
P. Garrett, MZ, E. Clément,
Prog. Part. Nucl. Phys. 124, 103931 (2022)

- $^{68,70}$Se: no excited $0^+$ states known, but in particular for $^{68}$Se very different moment of inertia in the ground state band (S.M. Fischer *et al.*, PRL 84, 4064 (2000))

→ conclusion on shape coexistence in $^{68,70}$Se and different shapes of their ground states with respect to heavier Se

# Level energies – rotational bands in less deformed nuclei

- it is much easier to find deformed configurations in nuclei with nearly spherical ground states, than vice versa!

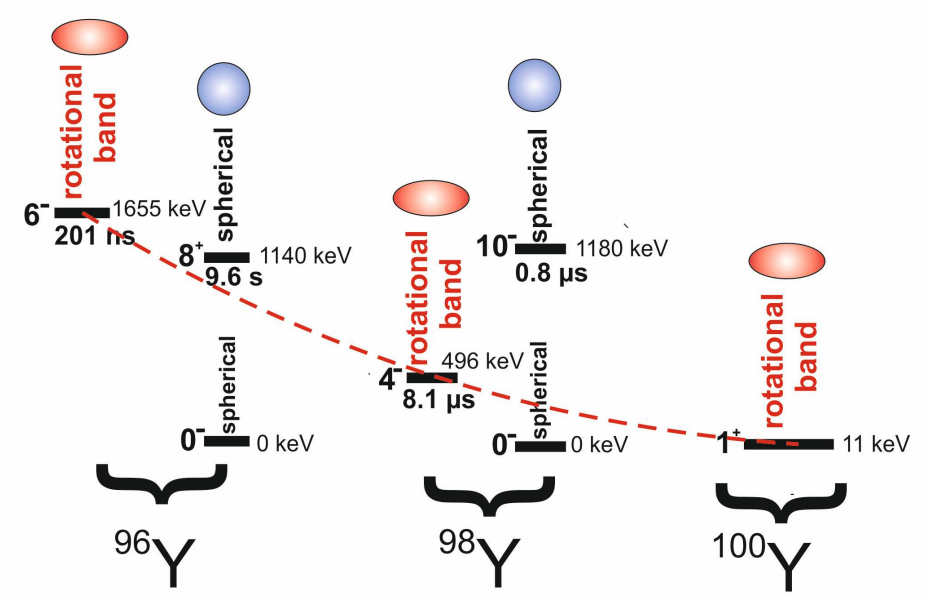


L. Iskra *et al.*, EPL 117, 12001 (2017)

# Level energies – rotational bands in less deformed nuclei

- it is much easier to find deformed configurations in nuclei with nearly spherical ground states, than vice versa!

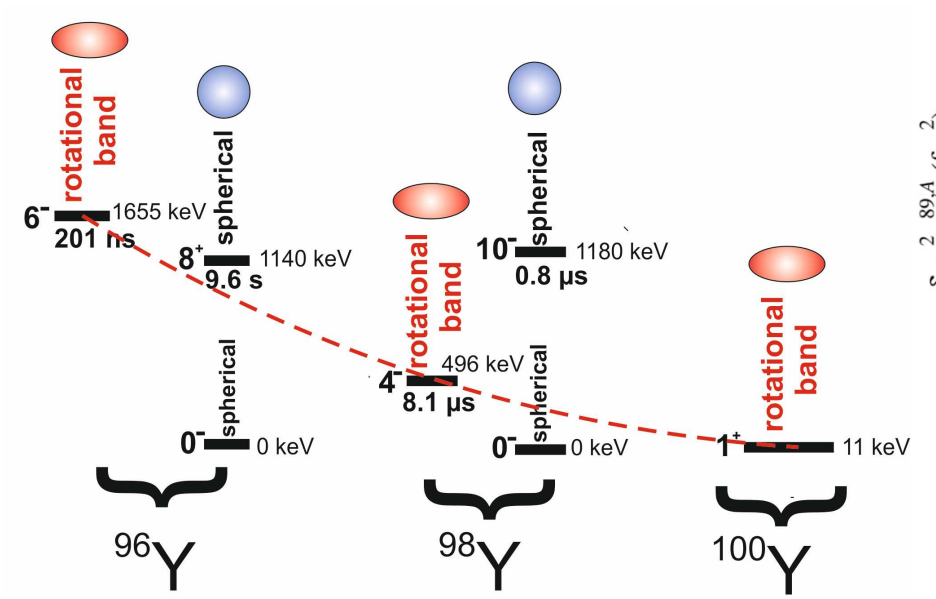


L. Iskra *et al.*, EPL 117, 12001 (2017)

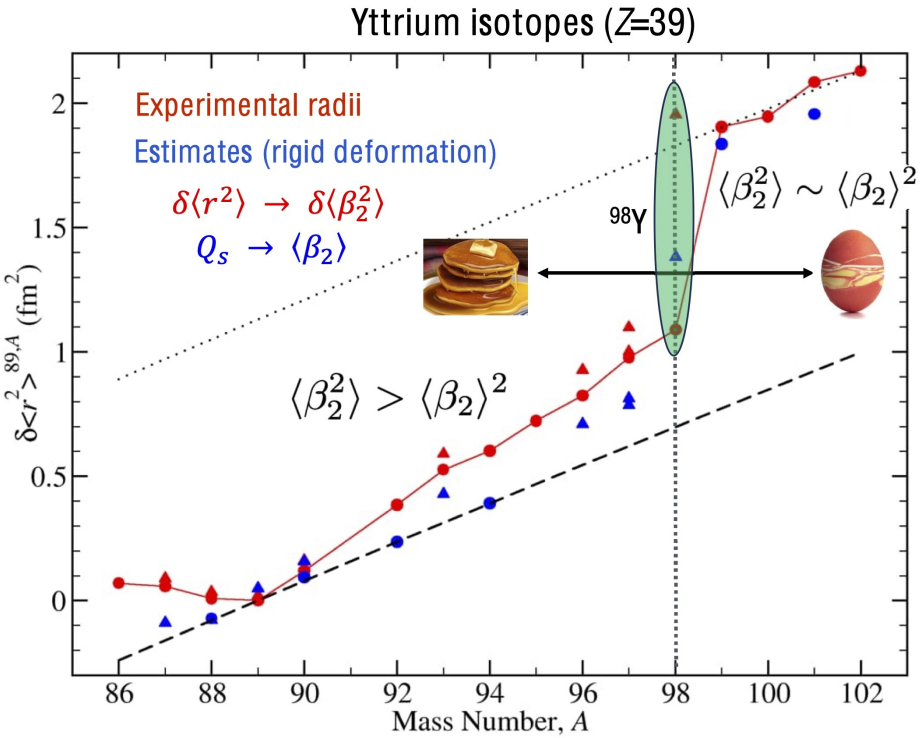


Iain's lecture on Tuesday

# Level energies – rotational bands in less deformed nuclei

- it is much easier to find deformed configurations in nuclei with nearly spherical ground states, than vice versa!

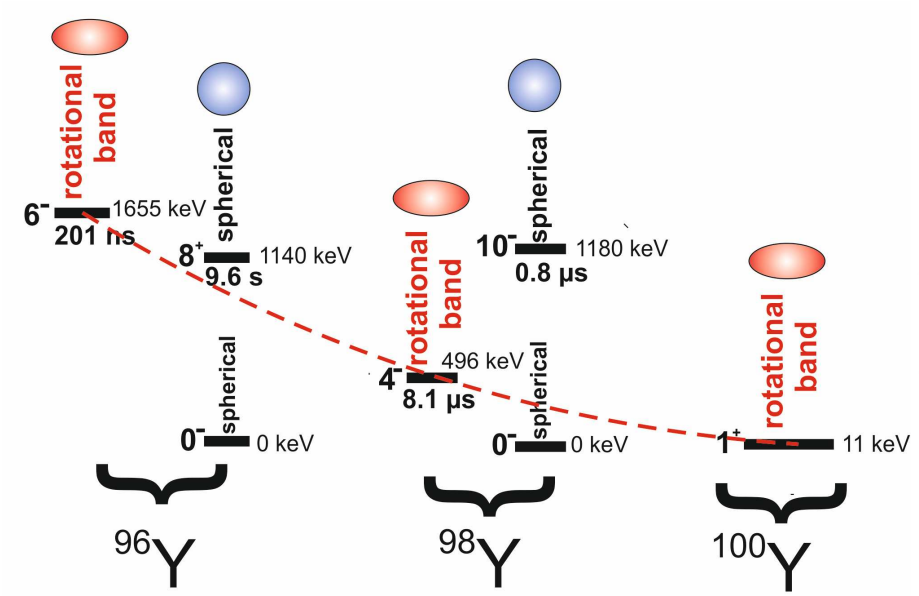


L. Iskra *et al.*, EPL 117, 12001 (2017)

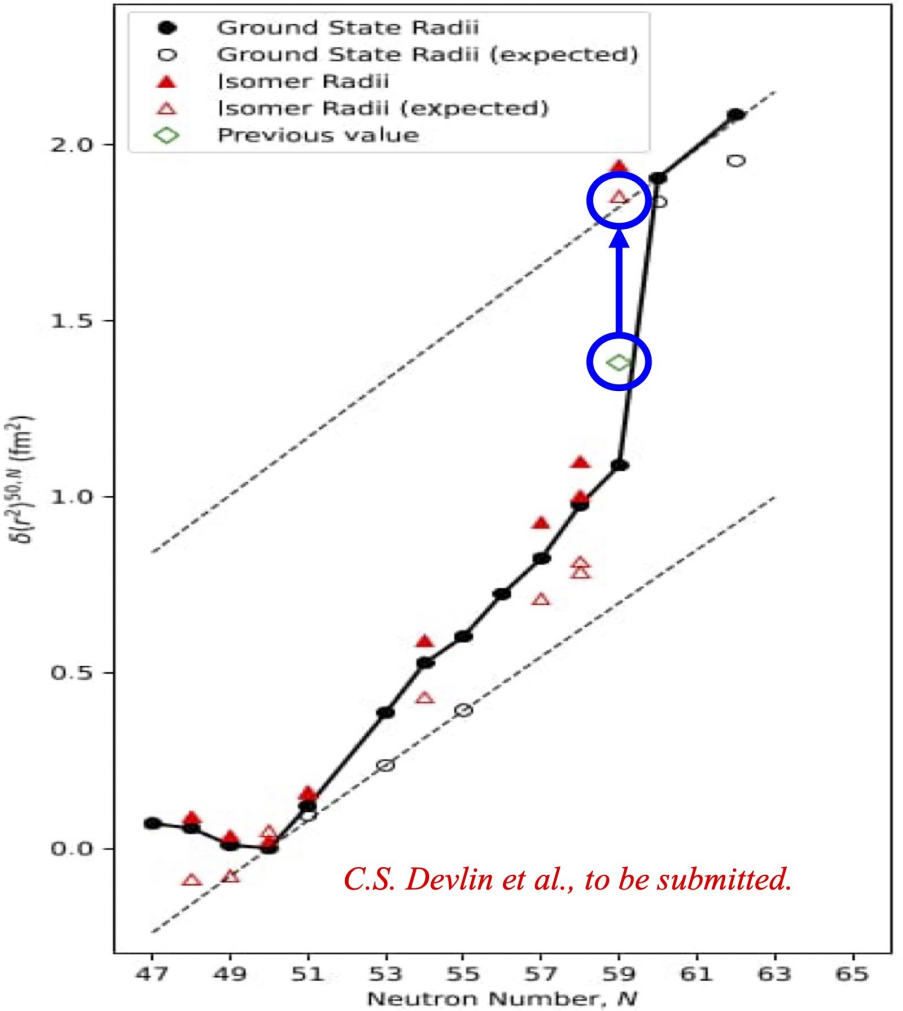


Iain's lecture on Tuesday

# Finding spherical states in deformed nuclei – example of $^{32}$Mg

K. Wimmer *et al.*, PRL 105, 252501 (2010)

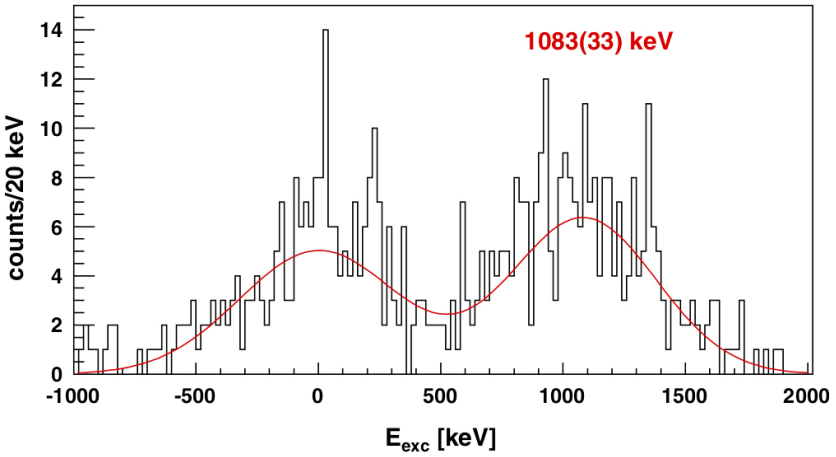


- 2*n* transfer from spherical normal-order configuration in $^{30}$Mg g.s. populates preferentially the spherical normal-order excited state in $^{32}$Mg

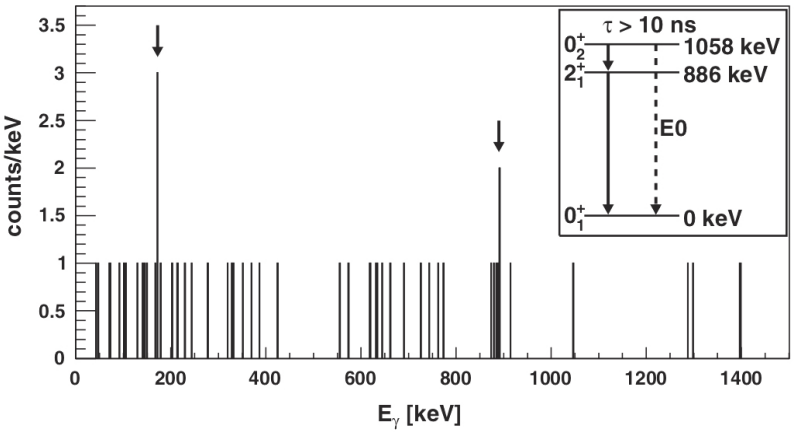


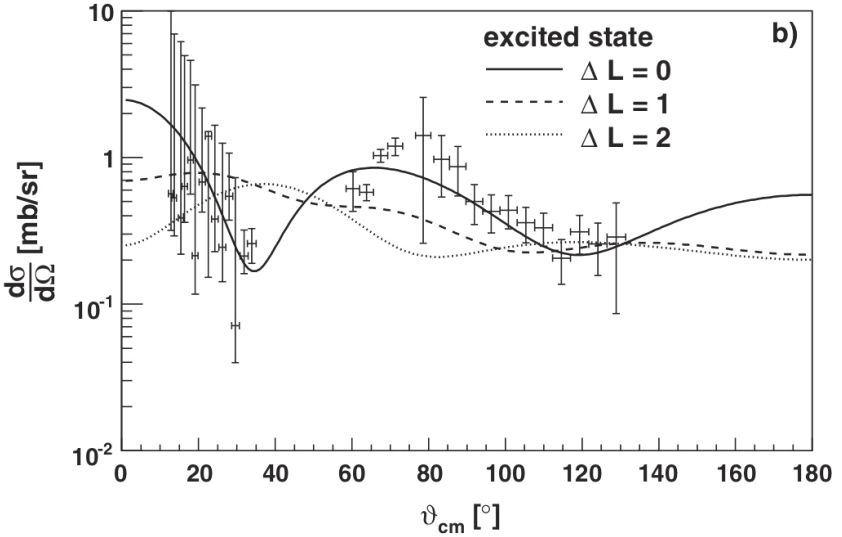


- level spin confirmed by proton angular distributions
- excitation energy precisely measured from $\gamma$-ray decay in coincidence with protons

# Information from transfer reactions

- identfication of 4p-4h and 8p-8h structures in $^{40}$Ca ($\alpha$-particle transfer); admixture of the 4p-4h configuration to 8p-8h states

- proton domination in the wave functions of the excited $0^+$ states in $^{112,114,116,118}$Sn

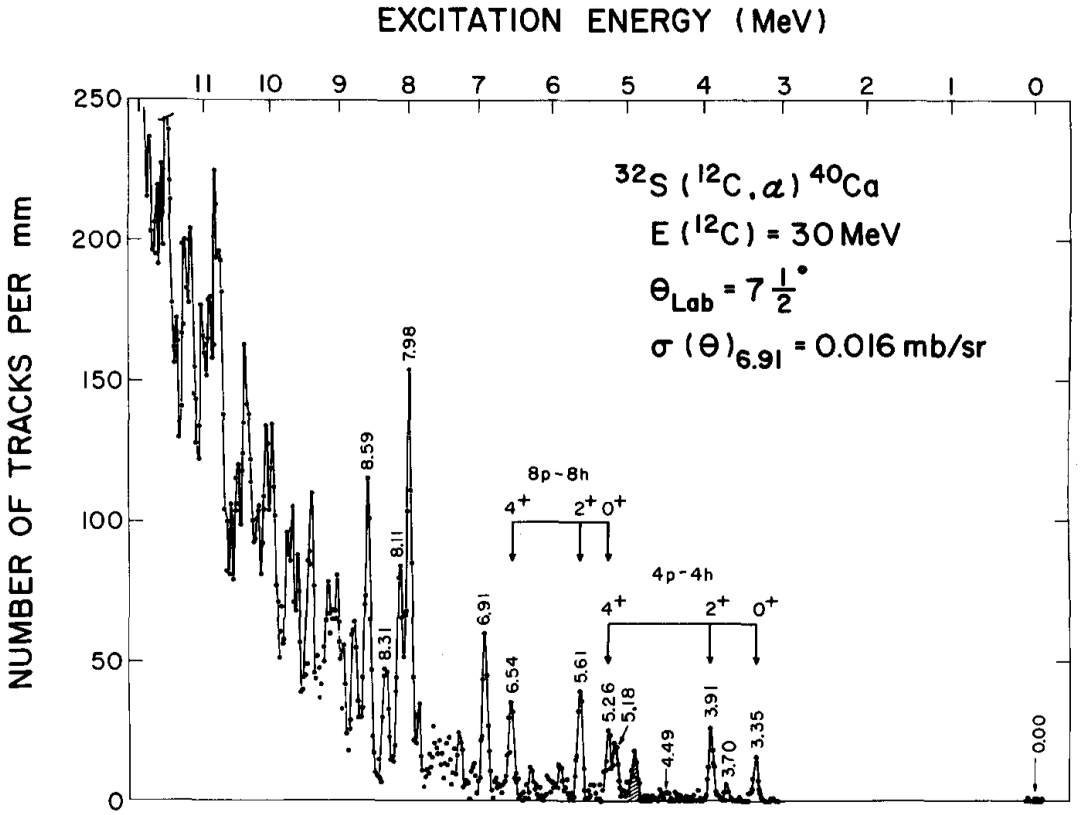


R. Middleton *et al.*, Phys. Lett. 39B, 339 (1972)

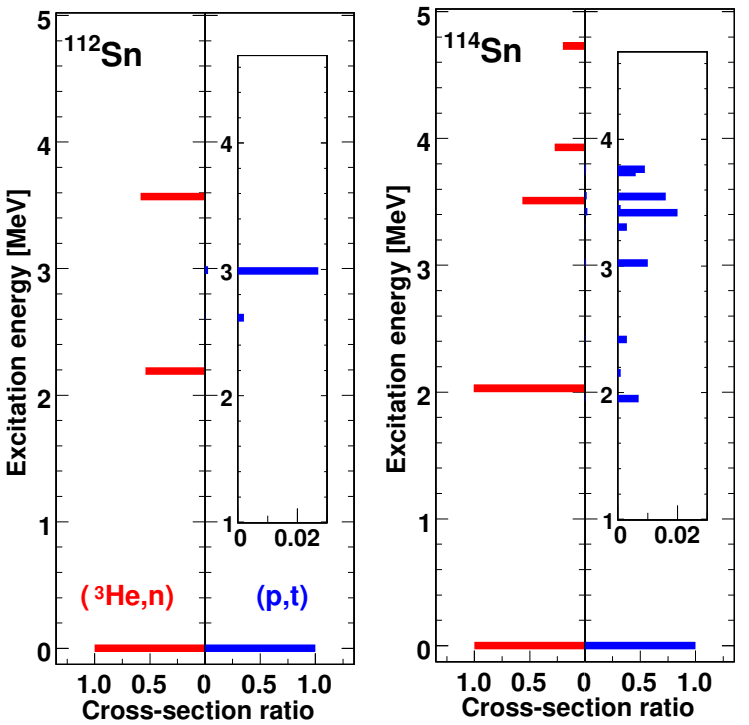


P. Guazzoni *et al.*, PRC 85, 054609 (2012), PRC 69, 024619 (2004)

# Alpha-decay hindrance

- similar type of information as from transfer reactions in lighter nuclei

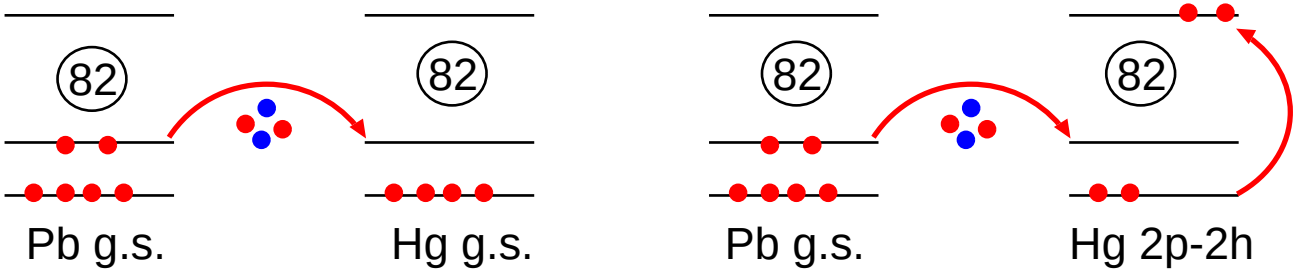


- ground states of Pb nuclei are spherical (experimentally confirmed by charge radii measurements) → the same is true for ground states of Hg nuclei, while their excited states are dominated by the 2p-2h configuration

- triple shape coexistence in $^{186}$Pb was deduced using this method

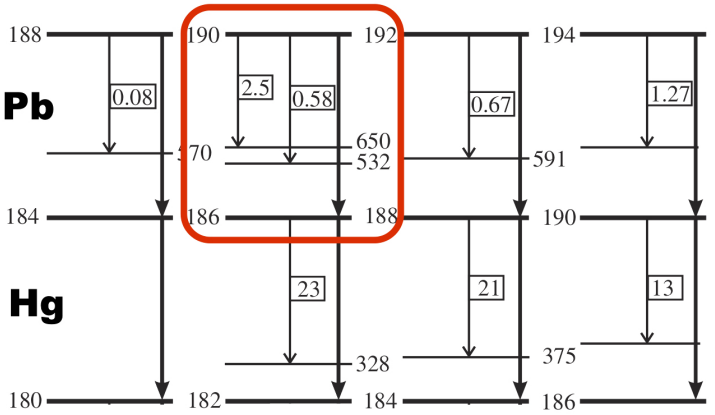


compilation: K. Heyde and J.L. Wood, RMP 83, 1467 (2011)

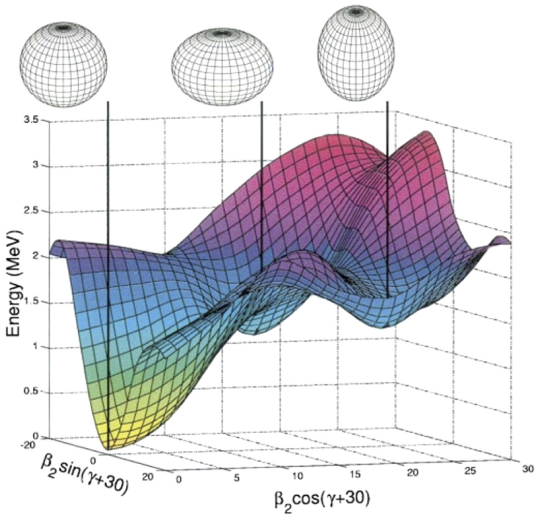


A. Andreyev *et al.*, Nature 405, 431 (2000)

# Reinterpretation of the $^{186}$Pb level scheme

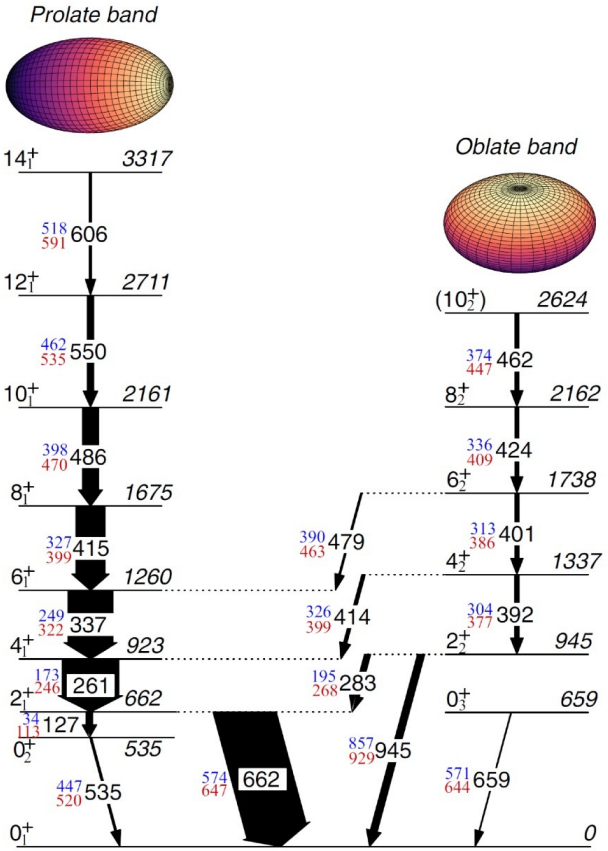


J. Ojala *et al*, Nature Communications 5, 213 (2022)

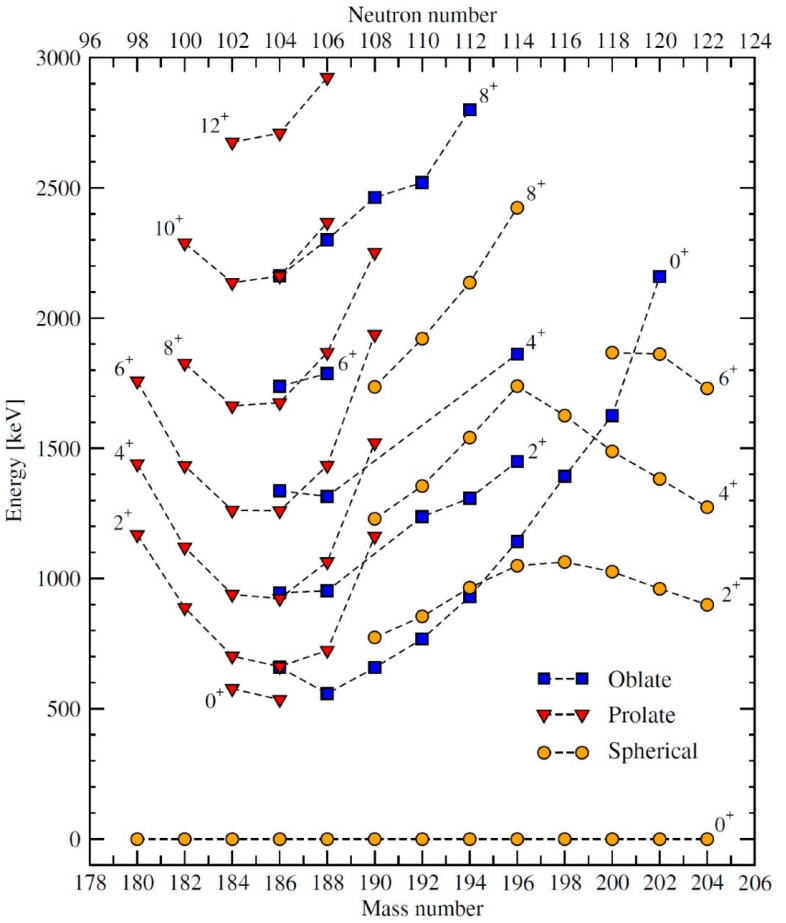


first observation of the weak in-band $2_1^+ \rightarrow 0_2^+$ transition establishing the $0_2^+$ state as the head of the prolate band with B(E2; $2_1^+ \rightarrow 0_2^+$) = 190(80) W.u.
(from $\gamma$-$\gamma$ and $\gamma$-electron spectroscopy with recoil decay tagging, Jyväskylä)

# Laser spectroscopy data

• precise measurements of charge radii, spectroscopic quadrupole moments, g factors for long-lived states

Example of $^{79}$Zn:

• large isomer shift for the $1/2^+$, 1-MeV isomer in $^{79}$Zn

• combined with $\beta_2 \approx 0.14$ deduced from B(E2) values in $^{78,80}$Zn, results in $\beta_2 \approx 0.22$ for the isomer

• 1p-2h neutron configuration determined from the measured g factor

• first evidence for shape coexistence in the immediate vicinity of $^{78}$Ni

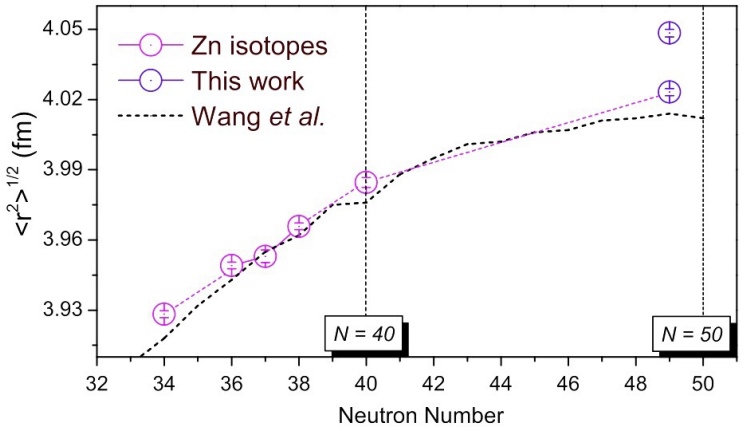


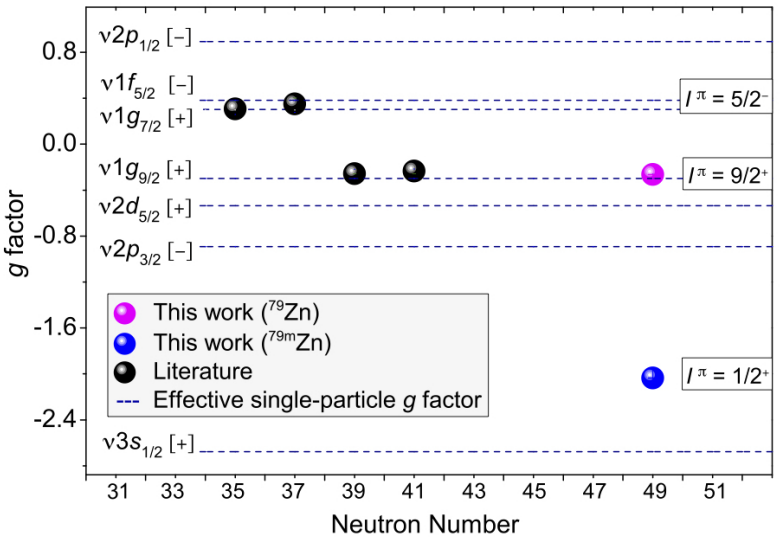


X.F. Yang *et al.*, PRL 116, 182502 (2016)

# Quadrupole moments of excited states

E. Clément *et al.*
Phys. Rev. C75, 054313 (2007)

- prolate-oblate shape coexistence in $^{74,76}$Kr

- first Coulomb-excitation measurement of spectroscopic quadrupole moments using a radioactive beam

$$\langle 2_1^+ \| E2 \| 2_1^+ \rangle = -\,0.70^{-0.33}_{-0.30}$$
$$\langle 4_1^+ \| E2 \| 4_1^+ \rangle = -\,1.02^{+0.59}_{-0.21}$$

$$\langle 2_2^+ \| E2 \| 2_2^+ \rangle = +\,0.33^{+0.28}_{-0.23}$$

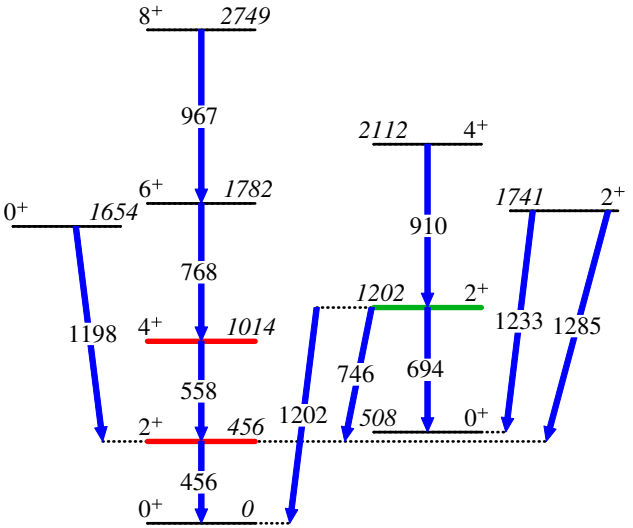


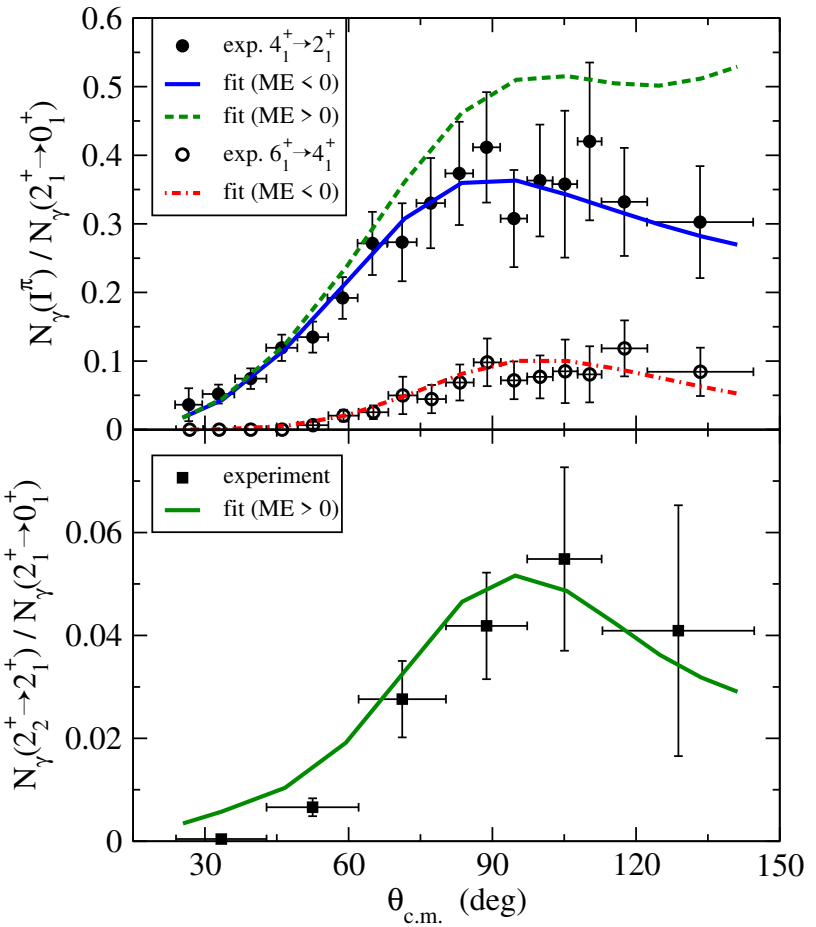


- spectroscopic quadrupole moments are zero for J=0,1/2 – complication for even-even nuclei

# Two-state mixing model

• we assume that physical states are linear combinations of pure spherical and deformed configurations:

$| I_1^+ \rangle = +\cos\theta_I \times | I_d^+ \rangle + \sin\theta_I \times | I_s^+ \rangle$
$| I_2^+ \rangle = -\sin\theta_I \times | I_d^+ \rangle + \cos\theta_I \times | I_s^+ \rangle$

with transitions between the pure spherical and deformed states forbidden:
$\langle 2_d^+ \| E2 \| 0_s^+ \rangle = \langle 2_d^+ \| E2 \| 2_s^+ \rangle = \langle 2_s^+ \| E2 \| 0_d^+ \rangle = 0$

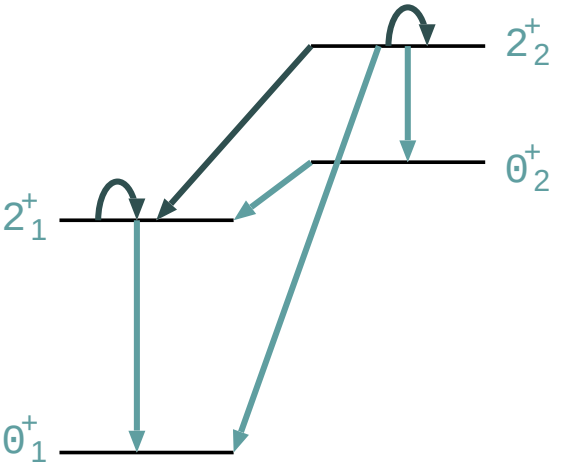


• the measured matrix elements can be expressed in terms of the "pure" matrix elements and the mixing angles:

$\langle 2_1^+ \| E2 \| 0_1^+ \rangle =$
$\sin\theta_0 \sin\theta_2 \langle 2_s^+ \| E2 \| 0_s^+ \rangle + \cos\theta_0 \cos\theta_2 \langle 2_d^+ \| E2 \| 0_d^+ \rangle$

$\langle 2_1^+ \| E2 \| 0_2^+ \rangle =$
$\cos\theta_0 \sin\theta_2 \langle 2_s^+ \| E2 \| 0_s^+ \rangle - \sin\theta_0 \cos\theta_2 \langle 2_d^+ \| E2 \| 0_d^+ \rangle$

$\langle 2_2^+ \| E2 \| 0_1^+ \rangle =$
$\sin\theta_0 \cos\theta_2 \langle 2_s^+ \| E2 \| 0_s^+ \rangle - \cos\theta_0 \sin\theta_2 \langle 2_d^+ \| E2 \| 0_d^+ \rangle$

$\langle 2_2^+ \| E2 \| 0_2^+ \rangle =$
$\cos\theta_0 \cos\theta_2 \langle 2_s^+ \| E2 \| 0_s^+ \rangle + \sin\theta_0 \sin\theta_2 \langle 2_d^+ \| E2 \| 0_d^+ \rangle$

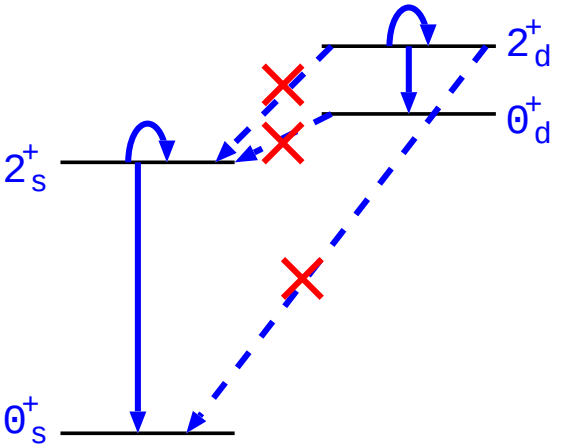

# Dependence on additional assumptions

• two-state mixing parameters for $^{180,182,184,186,188}$Hg derived under three different assumptions:

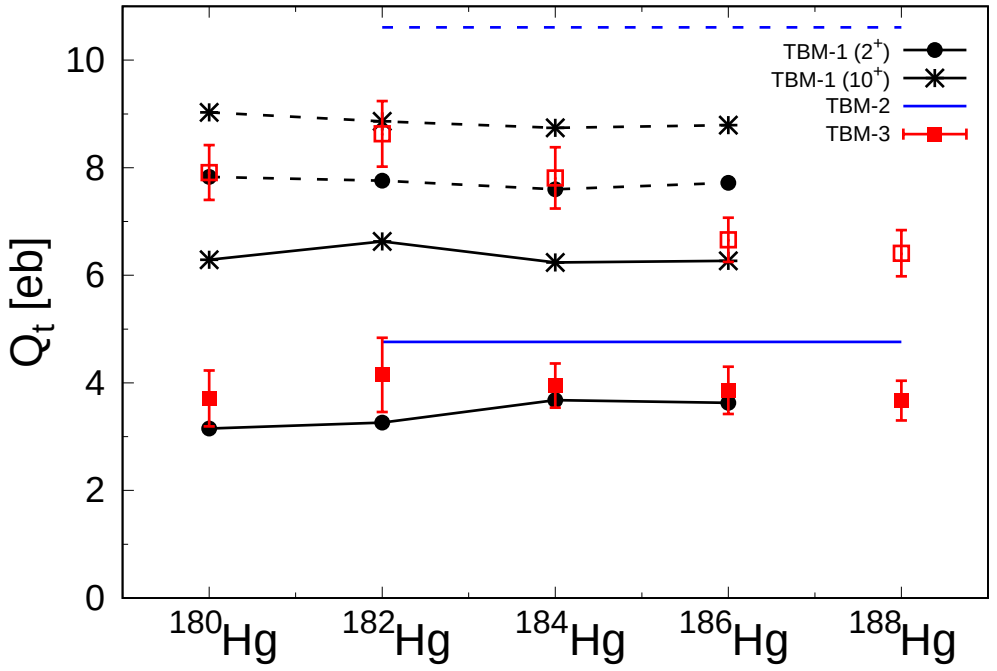


M. Siciliano *et al.*, PRC 102, 014318 (2020)

A) $Q_t$ values the same for all four Hg isotopes and constant within bands

B) $Q_t$ evolve within bands according to moments of inertia

C) $Q_t$ calculated independently for each mass and spin

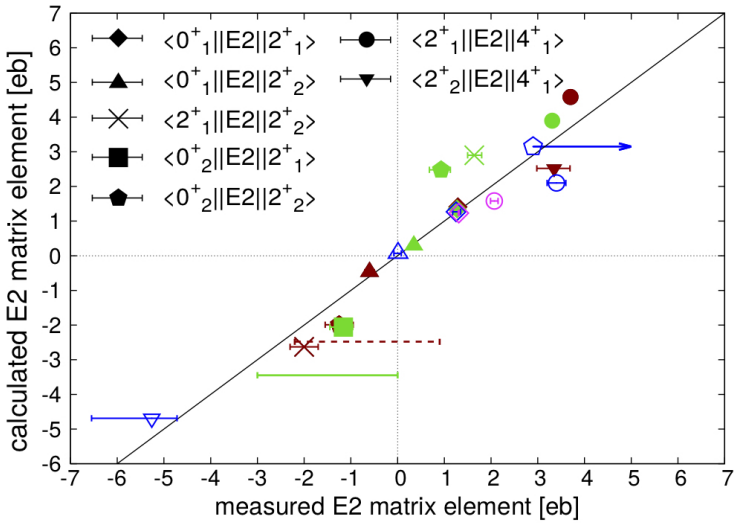


K. Wrzosek-Lipska *et al.*, EPJA 55, 130 (2019) (variant A)

• large difference in resulting $Q_t$ values; $Q_t$ for the less deformed configuration in variant B approaches values for the more deformed one in variant C

# E0 strengths, shape coexistence and mixing

- E0 transitions are sensitive to the changes in the nuclear charge-squared radii
- their strengths depends on the mixing of configurations that have different mean-square charge radii:

$$\rho^2(E0) = \frac{Z^2}{R^4}\cos^2\theta_0\,\sin^2\theta_0\,\left(\langle r^2\rangle_A - \langle r^2\rangle_B\right)^2$$

$$= \left(\frac{3Z}{4\pi}\right)^2 \cos^2(\theta_0)\sin^2(\theta_0)\cdot\left[\left(\beta_1^2-\beta_2^2\right)+\frac{5\sqrt{5}}{21\sqrt{\pi}}\left(\beta_1^3\cos(\gamma_1)-\beta_2^3\cos(\gamma_2)\right)\right]^2$$

J.L. Wood *et al.*, NPA 651, 323 (1999)

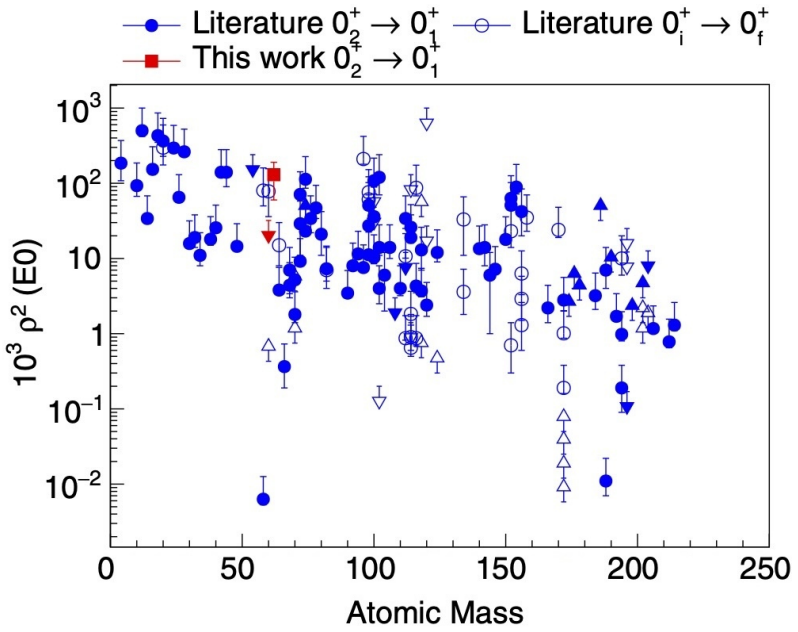


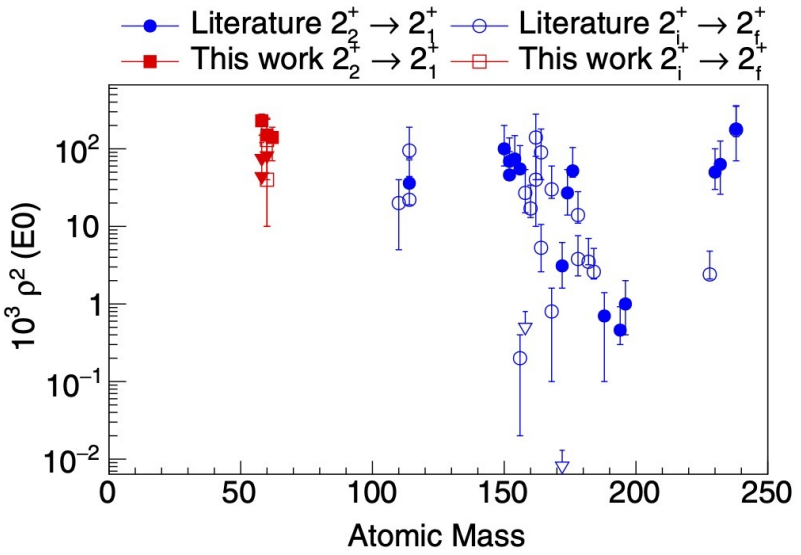


L.J. Evitts *et al.*, PRC 99, 024306 (2019)

- we do not understand the origin of strong $2^+ \to 2^+$ transitions in Ni isotopes

# Mixing in Hg – data compatibility

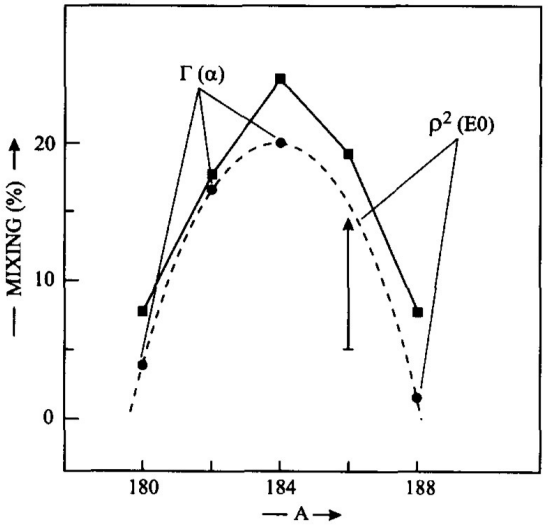


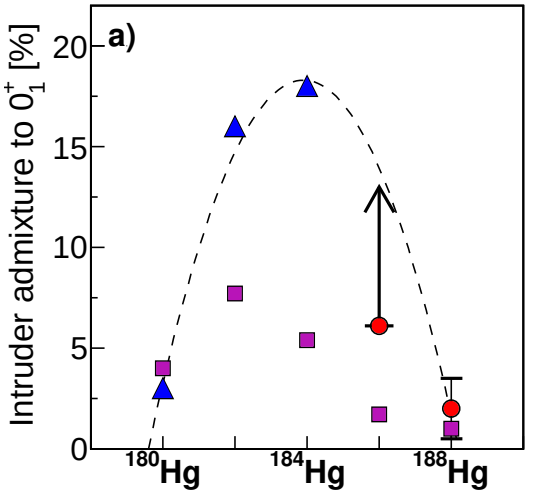


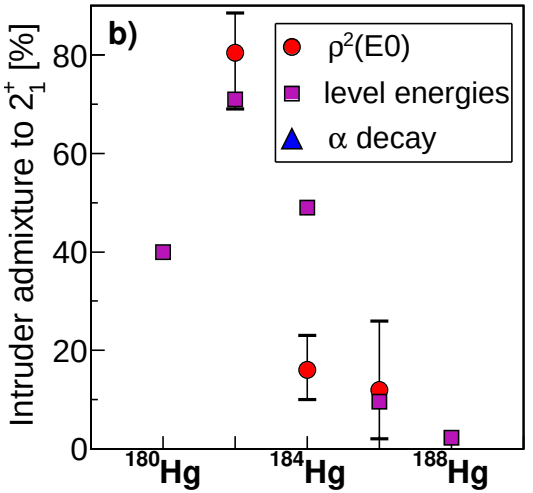


data compilation:

J. Wood et al, Nucl. Phys. A 651, 323 (1999)

P. Garrett, MZ, E. Clément, Prog. Part. Nucl. Phys. 124, 103931 (2022)

# Three-state mixing

• three-state mixing provides good reproduction of B(E2) values and transfer cross sections for $^{30,32}$Mg (A. Machiavelli, Phys. Scr. 92, 064001 (2017))

• future challenge: identification of the predominantly 0p-0h $0^+$ state in $^{32}$Mg that would confirm this scenario (two $(0,2)^+$ states observed recently in a knockout study, N. Kitamura *et al.*, PLB 221, 136682 (2021))

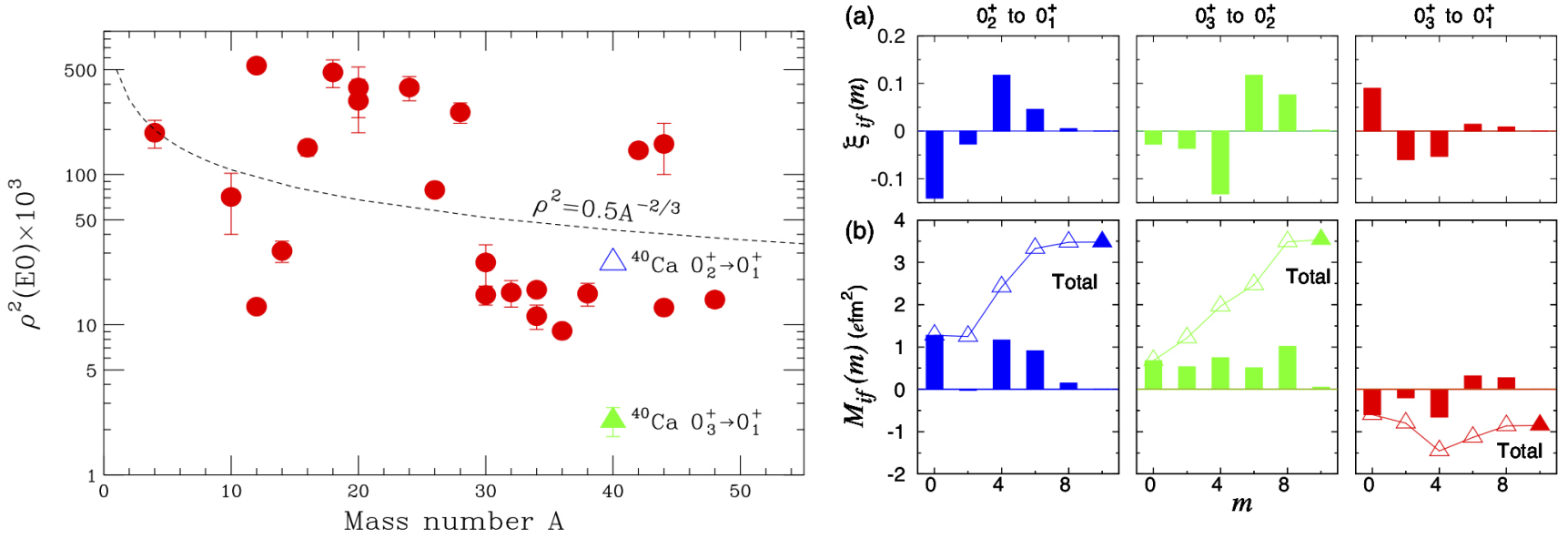


E. Ideguchi *et al.*, PRL 128, 252501 (2022)

• destructive interference in three-state mixing proposed as the reason for an anomalously low $\rho^2(E0; 0_3^+ \to 0_1^+)$ value

# Octupole collectivity

# Experimental information on octupole collectivity in even-even nuclei

- energy of the first $3^-$ state (first hint)
- $B(E3; 3_1^- \rightarrow 0_1^+)$ value; $B(E3; I_i \rightarrow I_f) = \frac{7}{16\pi}(I_f 030|I_i 0)^2 Q_3^2$
  $Q_3 = \frac{3}{\sqrt{7\pi}} Z\, e\, R_0^3 \beta_3$
- negative-parity states decay predominantly by fast E1 transitions; large B(E1) values usually correlate with octupole collectivity, but the inverse is not true
- lifetime of a negative-parity state is a very poor indicator of octupole collectivity
- direct E3 decay is rarely observed
- Coulomb excitation and inelastic scattering are the methods of choice to determine E3 strength

# Rigid octupole deformation versus octupole vibration

- apart from actinides, E3 collectivity is usually attributed to surface vibrations
- rigid octupole deformation can be claimed on the basis of B(E3) values between the ground-state band and the negative-parity band, or identical rotational alignments in these bands ($\rightarrow$ interleaving of positive and negative-parity states)

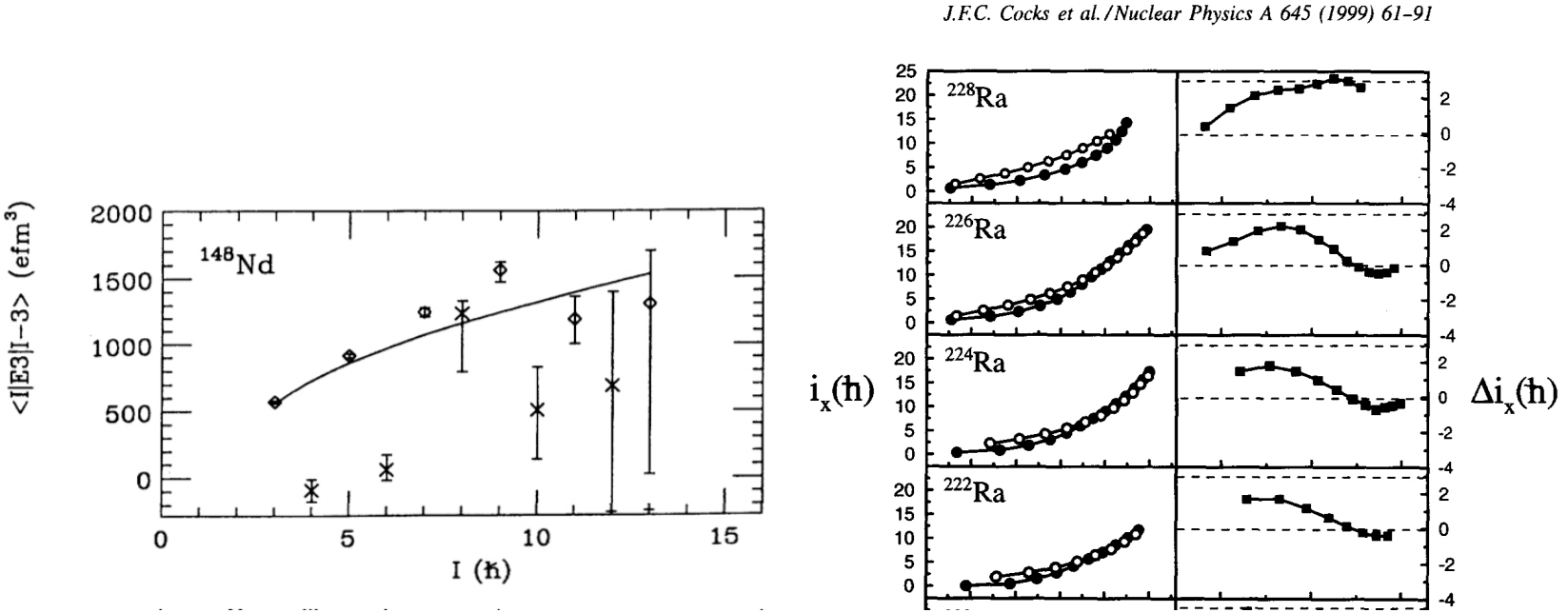


R. Ibbotson et al, PRL 71, 27 (1993)

More details: P. A. Butler and W. Nazarewicz, Rev. Mod. Phys. 68, 349 (1996); P. Butler, Proc. R. Soc. A 476, 202 (2020)

# Octupole collectivity in Zr isotopes: anomalous value for $^{96}$Zr

- evaluated B(E3; $3^-_1 \rightarrow 0^+_1$) strength for $^{96}$Zr strikingly high (53(6) W.u.), comparable with those known for nuclei with rigid pear shapes
- observed trend of B(E3; $3^-_1 \rightarrow 0^+_1$) values in Zr isotopes inconsistent with $3^-_1$ energies and hard to explain

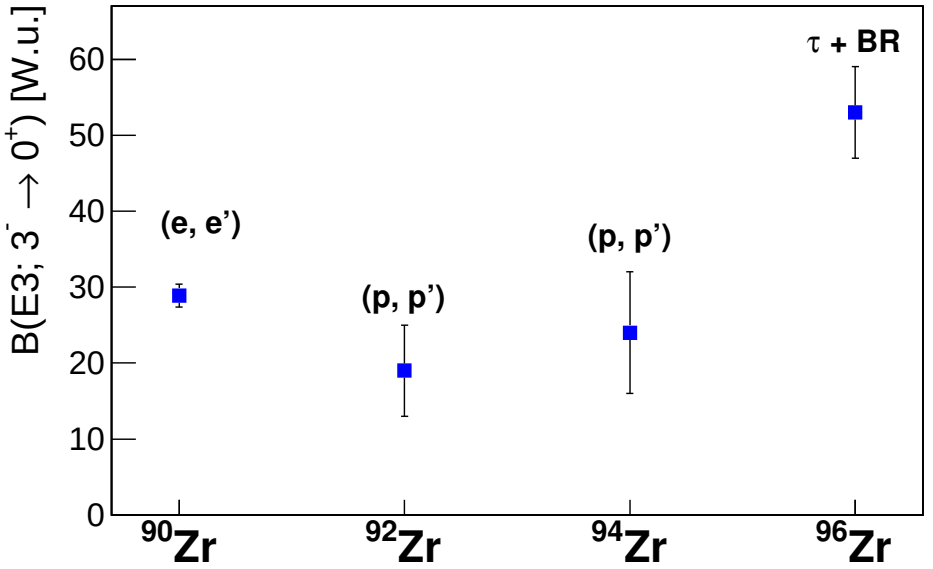


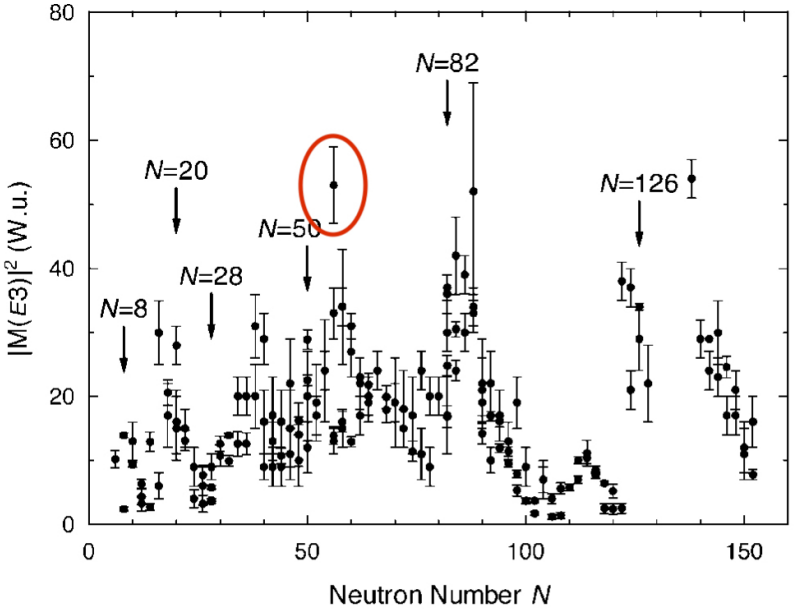


T. Kibédi and R.H. Spear, At. Data Nucl. Data Tables 80, 35 (2002)

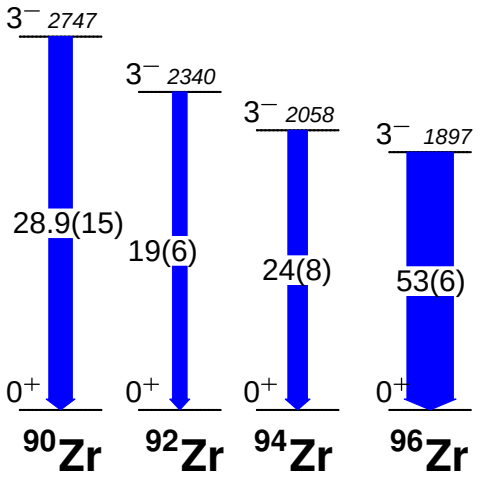

# Revision of the E3 strength in $^{96}$Zr

- determination of E3 strength in $^{96}$Zr using gamma-ray spectroscopy requires two measurements:
  - lifetime ($\approx$ 70ps – plunger measurements)
  - branching ratio E3/E1
- if the 147 keV / 1897 keV intensity ratio is directly measured, the efficiency must be known precisely
  - walk effect, conversion at 147 keV

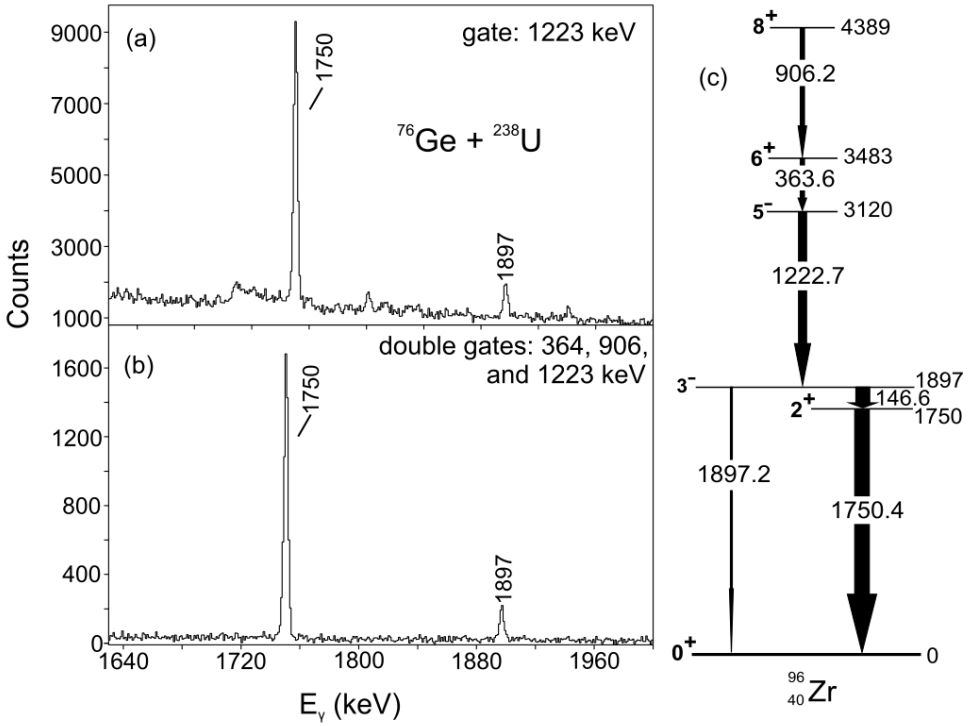


- new measurement – gating from above and comparison of 1750 keV and 1897 keV intensities

Ł. Iskra et al, Phys. Lett. B 788 (2019) 396

# Octupole collectivity in Zr isotopes: new BR measurement for $^{96}$Zr

- new measurement of E1/E3 branching ratio in $^{96}$Zr (Ł. Iskra et al, Phys. Lett. B 788 (2019) 396) points to lower octupole collectivity, but the overall trend remains puzzling

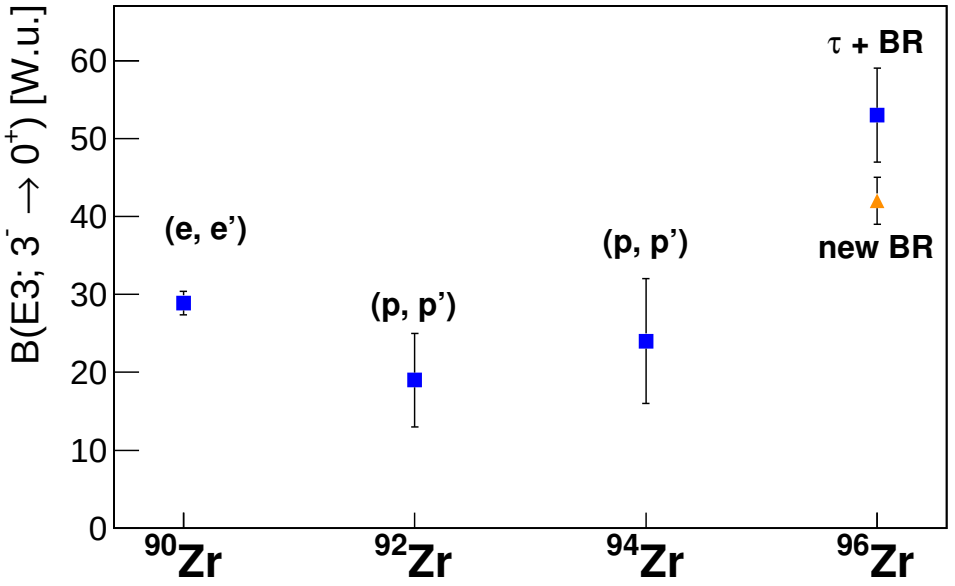


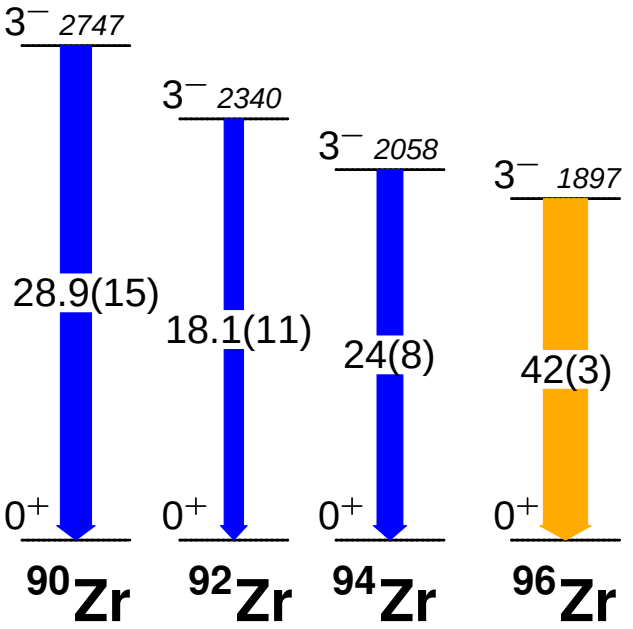

# Octupole deformation: E3 moments measured in Coulomb excitation

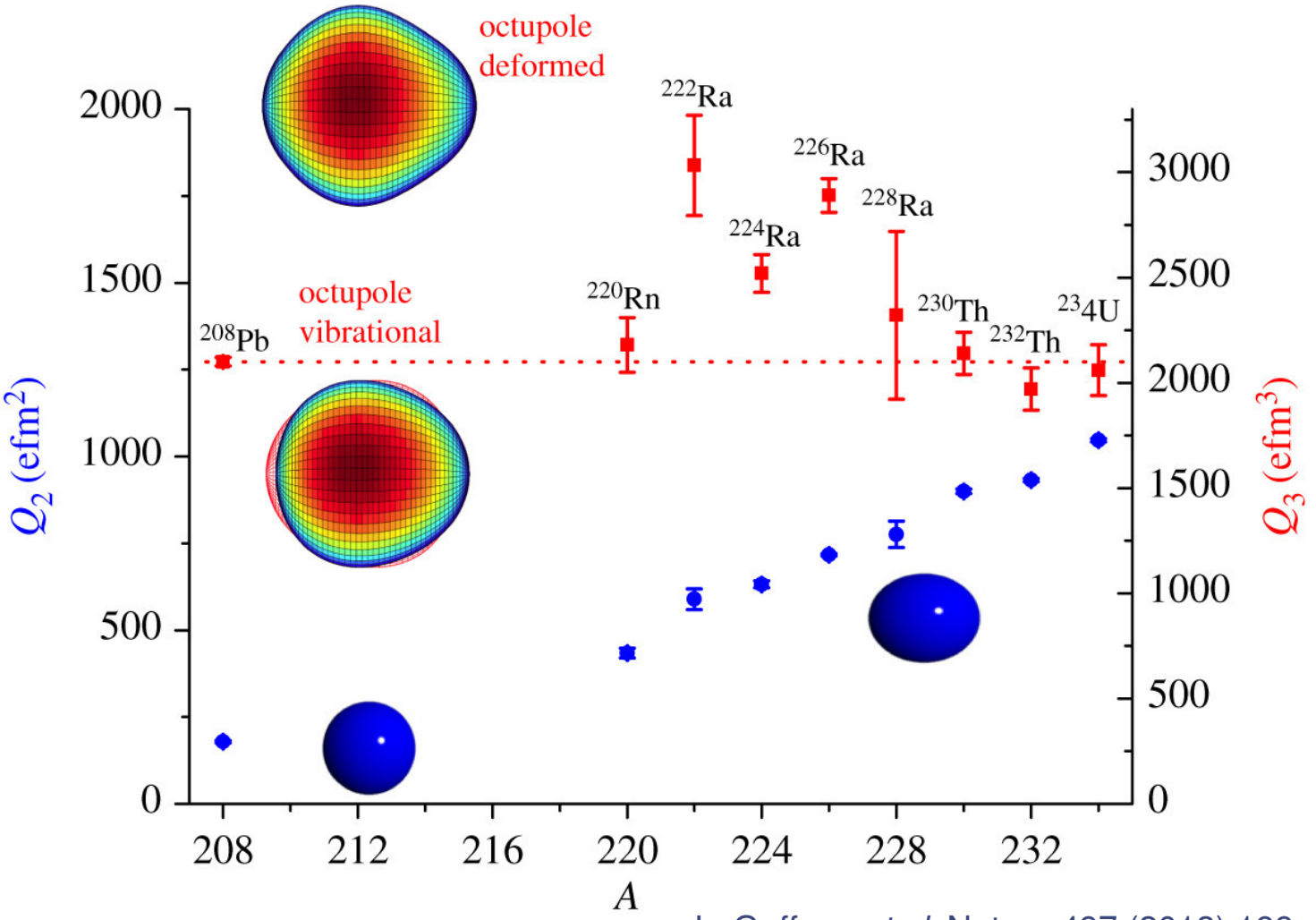


L. Gaffney *et al*, Nature 497 (2013) 199

P. Butler, Proc. R. Soc. A 476, 202 (2020)

# Example: superdeformation in $^{42}$Ca

# Highly-deformed structures in the A ∼ 40 region

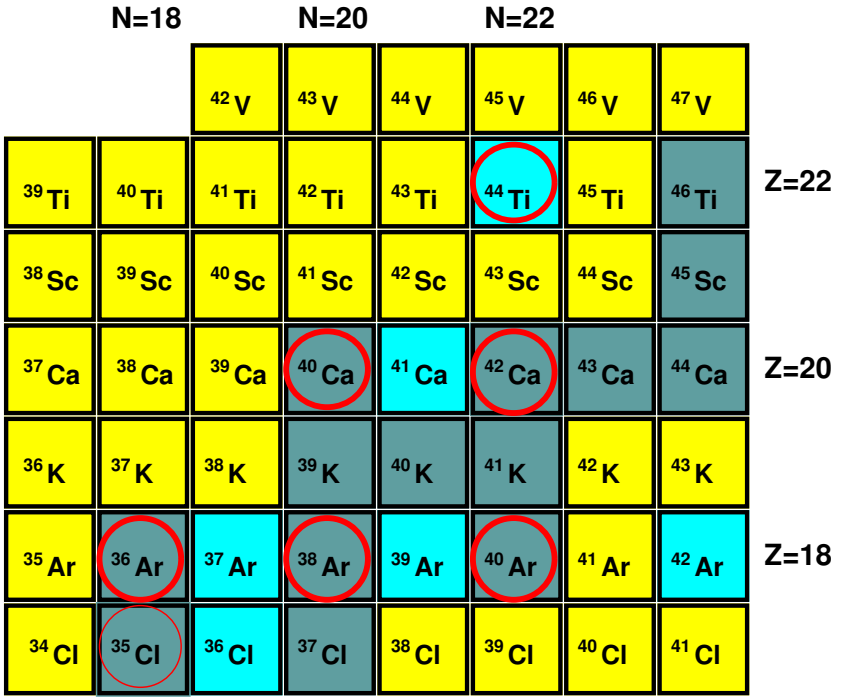


E. Ideguchi et al., PRL 81 (2001) 222501

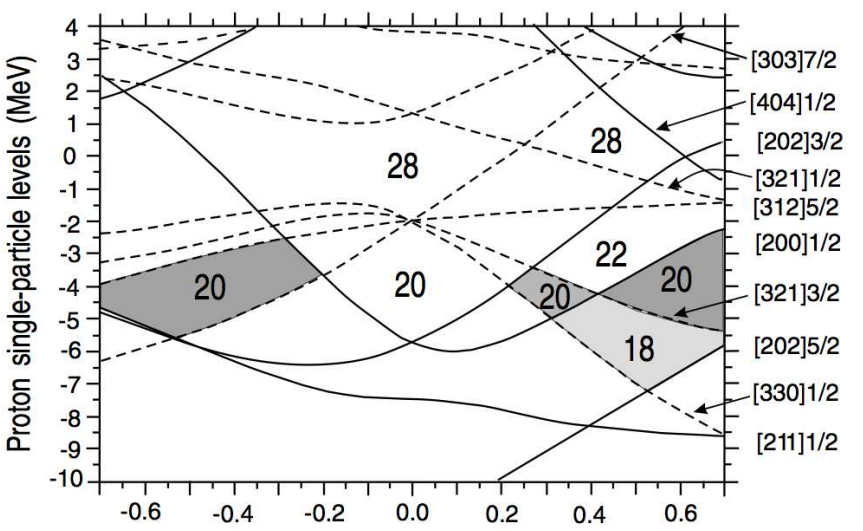


- spherical and highly-deformed magic numbers appear at similar particle numbers – dramatic shape coexistence
- first identification of deformed structures via particle transfer in 1970s (see example of $^{40}$Ca in an earlier lecture)

# High-spin spectroscopy around $^{40}$Ca

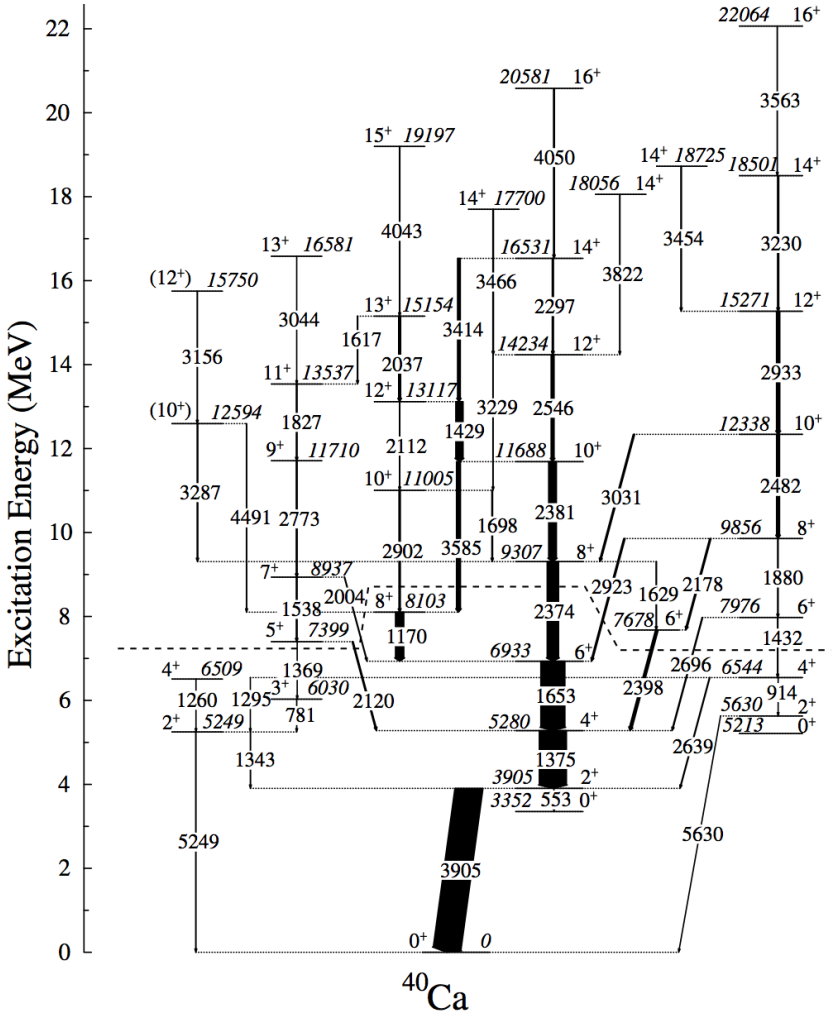


- regular rotational bands built on $0^+$ states observed up to spin $14^+$ – $16^+$ in $^{40}$Ca, $^{36,38,40}$Ar, ...

E. Ideguchi et al., PRL 81 (2001) 222501

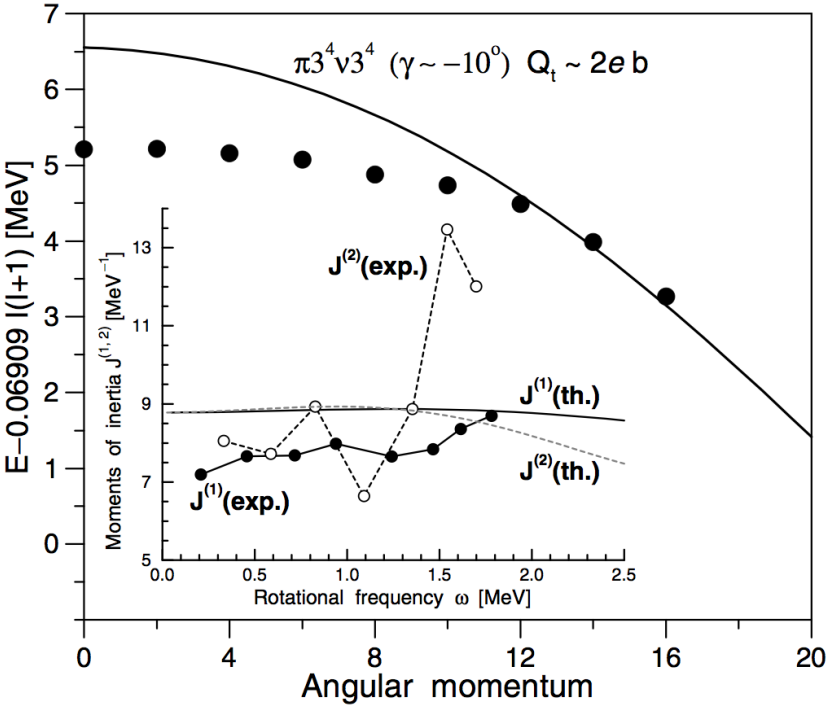


- intense transitions linking very deformed structures to ground-state bands – mixing of configurations

# Coulomb excitation of $^{42}$Ca at LNL

- Targets: $^{208}$Pb, $^{197}$Au, 1mg/cm$^2$
- AGATA: 3 triple clusters
- DANTE: 3 MCP detectors, $\theta$ range: 100-144°

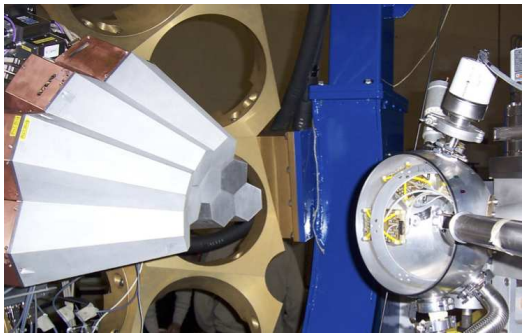

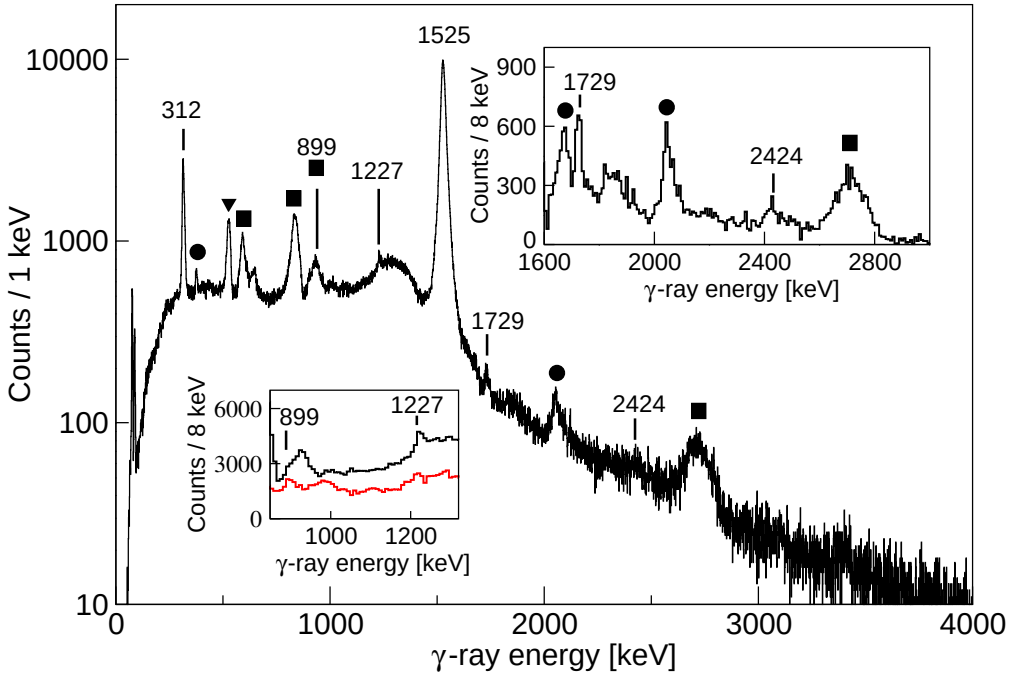


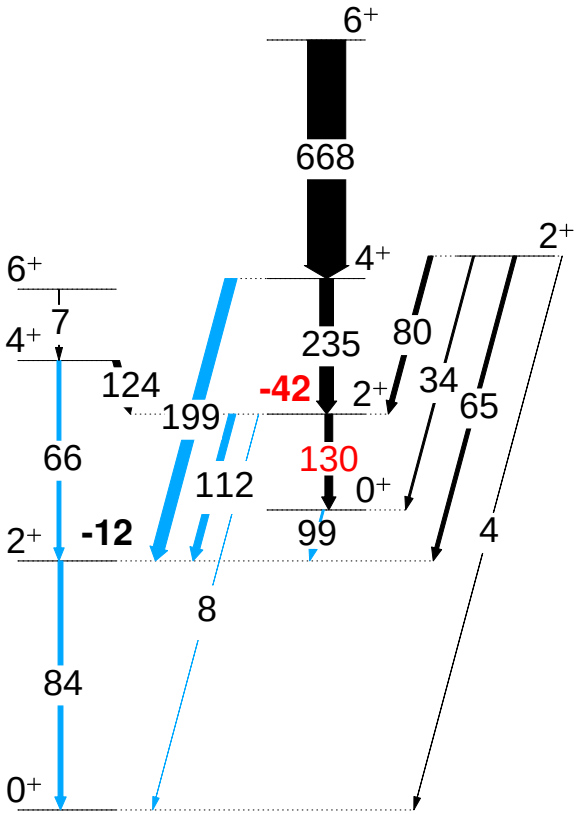


- first population of a superdeformed band in Coulomb excitation
- measured quadrupole moment of $2_2^+$ corresponds to $\beta = 0.48(14)$

K. Hadyńska-Klęk et al, PRL 117 (2016) 062501

# Shape parameters of $0^+$ and $2^+$ states in $^{42}$Ca

K. Hadyńska-Klęk, PRC 97 (2018) 024326

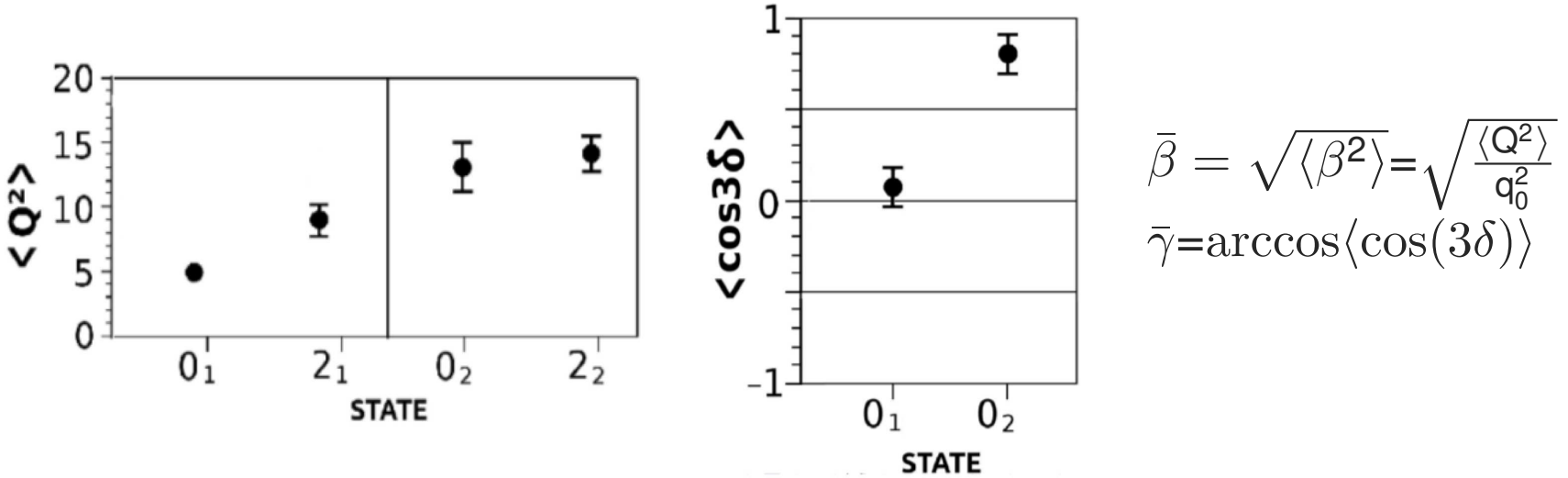


$$\bar{\beta} = \sqrt{\langle\beta^2\rangle} = \sqrt{\frac{\langle Q^2\rangle}{q_0^2}}$$

$$\bar{\gamma} = \arccos\langle\cos(3\delta)\rangle$$

- deformation parameters:
  - side band: $\bar{\beta}$=0.43(4), $\bar{\gamma}$=13(6)°
  - ground-state band: $\bar{\beta}$=0.26(2), $\bar{\gamma}$=29(2)° (?)
- are these static deformations, or fluctuations?
  - what about softness in $\beta$: $\sigma(Q^2) = \sqrt{\langle Q^4\rangle - \langle Q^2\rangle^2}$ ?

# Shape parameters of $0^+$ and $2^+$ states in $^{42}$Ca

K. Hadyńska-Klęk, PRC 97 (2018) 024326

red rectangles: $\sigma(Q^2)$

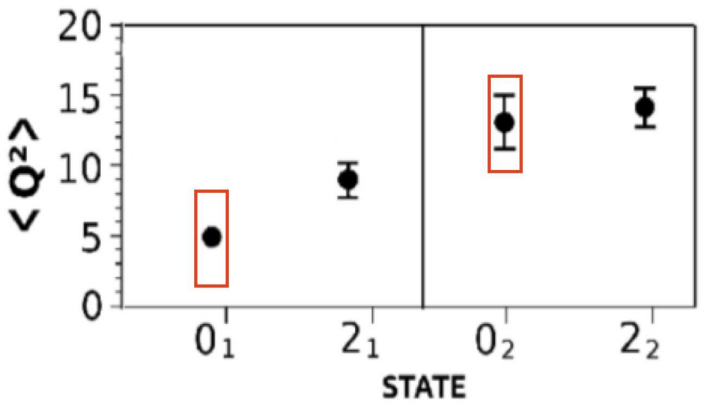


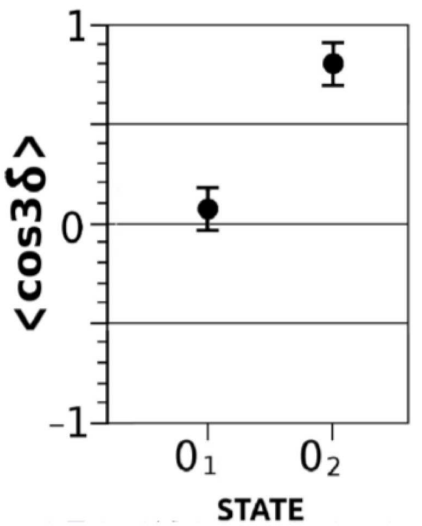


$$\bar{\beta} = \sqrt{\langle \beta^2 \rangle} = \sqrt{\frac{\langle Q^2 \rangle}{q_0^2}}$$

$$\bar{\gamma} = \arccos \langle \cos(3\delta) \rangle$$

$\sigma(Q^2)$ comparable with $\langle Q^2 \rangle$ for the ground-state band

$\rightarrow$ fluctuations about a spherical shape; $\langle \cos(3\delta) \rangle$=0 resulting from averaging over all possible quadrupole shapes ranging from prolate to oblate

excited band: $\sigma(Q^2)$ few times lower than $\langle Q^2 \rangle$

$\rightarrow$ static deformation

# Level mixing from E2 and E0 strengths

• E0 transition strength can be linked to the mixing of configurations that have different mean-square charge radii:

$$\rho^2(E0) = \frac{Z^2}{R^4}\cos^2\theta_0\,\sin^2\theta_0\,\left(\langle r^2\rangle_A - \langle r^2\rangle_B\right)^2$$
$$= \left(\frac{3Z}{4\pi}\right)^2 \cos^2(\theta_0)\sin^2(\theta_0)\cdot\left[\left(\beta_1^2-\beta_2^2\right)+\frac{5\sqrt{5}}{21\sqrt{\pi}}\left(\beta_1^3\cos\gamma_1-\beta_2^3\cos\gamma_2\right)\right]^2$$

J.L. Wood *et al.*, NPA 651, 323 (1999)

Example of $^{42}$Ca: K. Hadyńska-Klęk *et al.*, PRC 97 (2018) 024326 (Coulomb excitation), J.L. Wood *et al.*, NPA 651, 323 (1999) (E0)

| | from E2 matrix elements [KHK] | from $\rho^2(E0)$ [JLW] + sum rules results [KHK] |
|---|---|---|
| $\cos^2(\theta_0)$ | 0.88(4) | 0.84(4) |
| $\cos^2(\theta_2)$ | 0.39(8) | - |

- good agreement of the $\cos^2(\theta_0)$ values obtained with the two methods
- $\cos^2(\theta_2)<0.5$: two-state mixing model cannot be applied to $2^+$ states in $^{42}$Ca

# Population of the deformed structure in one-neutron transfer

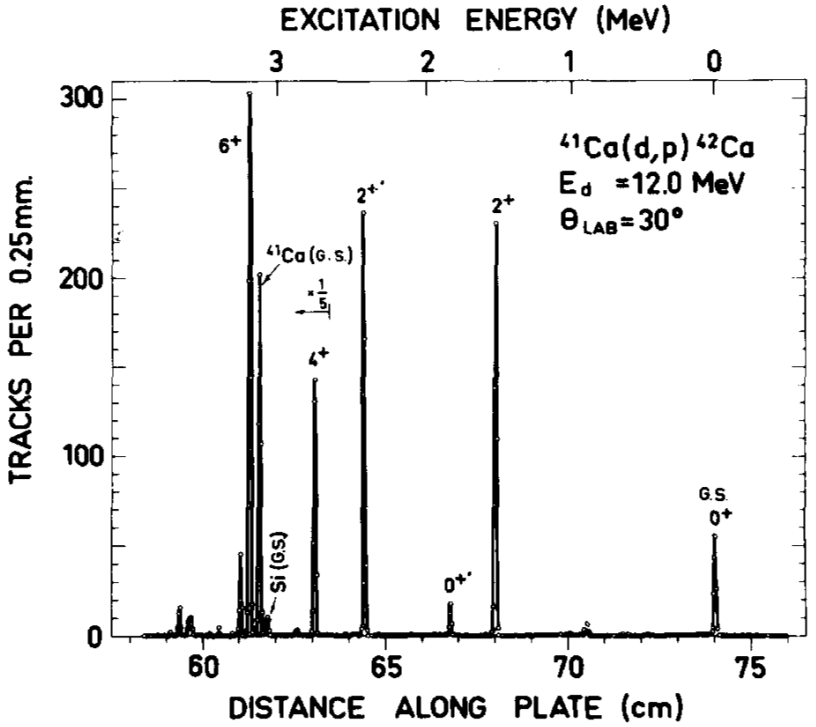


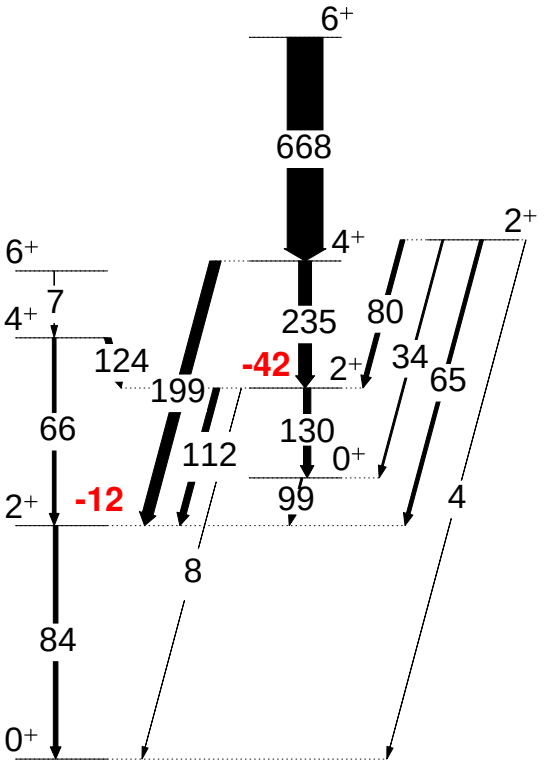


C. Ellegaard *et al.*, Phys. Lett. 40B (1972) 641

- equal population of $2_1^+$ and $2_2^+$ in $^{41}$Ca(d,p)$^{42}$Ca – the same admixture of $(f_{7/2})^2$, while the quadrupole moments are very different!

$\rightarrow$ the remaining admixtures to the $2_1^+$ and $2_2^+$ wave functions must be different $\rightarrow$ another configuration must enter the mixing

## Take-away message

- multiple observables can be used to infer nuclear shapes and collectivity
- they can be measured using various experimental techniques, each of them having different limitations
- use of complementary probes improves our understanding and provides necessary consistency checks

# Bonus: nuclear shapes from high-energy collisions?

# Nuclear shapes from high-energy collisions?

- the collision takes place on a time scale of order $10^{-24}$ s (0.1 fm/c), much faster than any internal nuclear dynamics
- the shape of the produced QGP droplet reflects the shape of the distribution of nucleons in the region of interaction
- data from RHIC (STAR collaboration) and LHC have been collected for several combinations of heavy ions

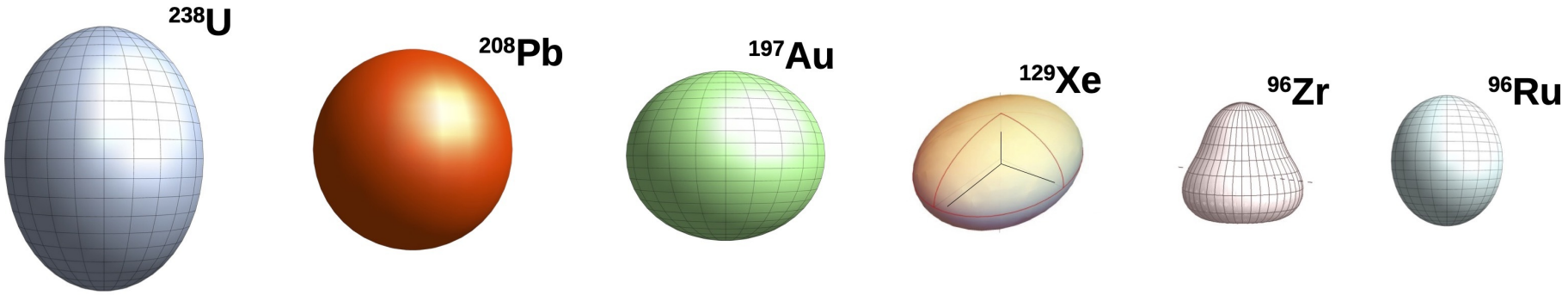


G. Giacalone, PhD thesis, Université Paris-Saclay, 2020
(2018-2021 PhD Prize of the EPS Nuclear Physics Division)

B. Bally et al, PRL 128, 082301 (2022)

C. Zhang and J. Jia, PRL 128, 022301 (2022)

G. Giacalone, EPJA 59, 297 (2023)

# Observables related to nuclear shape (slide courtesy G. Giacalone)

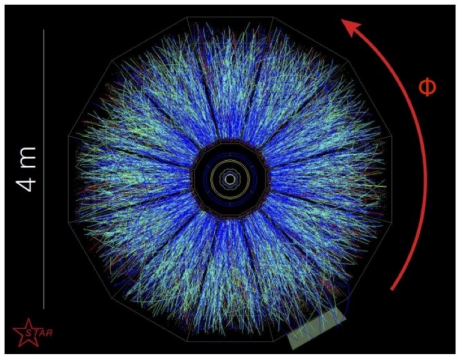


## The art of event-by-event analysis

**SPECTRUM**

$$\frac{dN_{\rm ch}}{d\phi p_t dp_t}$$

**CHARGED MULTIPLICITY**

$$N_{\rm ch} = \int d\phi p_t dp_t \, \frac{dN_{\rm ch}}{d\phi p_t dp_t}$$

**MEAN MOMENTUM**

$$[p_t] = \frac{1}{N_{\rm ch}} \sum_{i=1}^{N_{\rm ch}} p_{t,i}$$

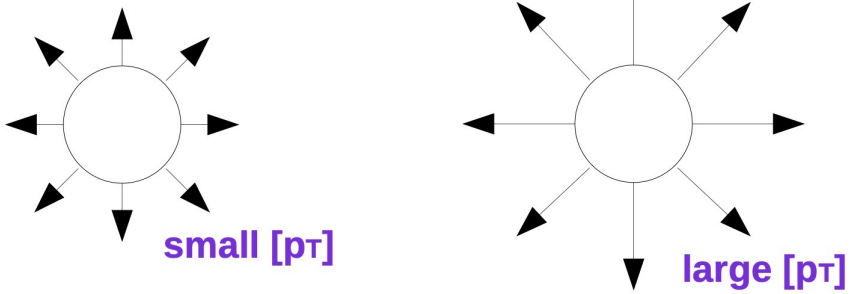


**FOURIER HARMONICS**

$$V_n = \frac{1}{N_{\rm ch}} \sum_{i=1}^{N_{\rm ch}} e^{-in\phi_i}$$

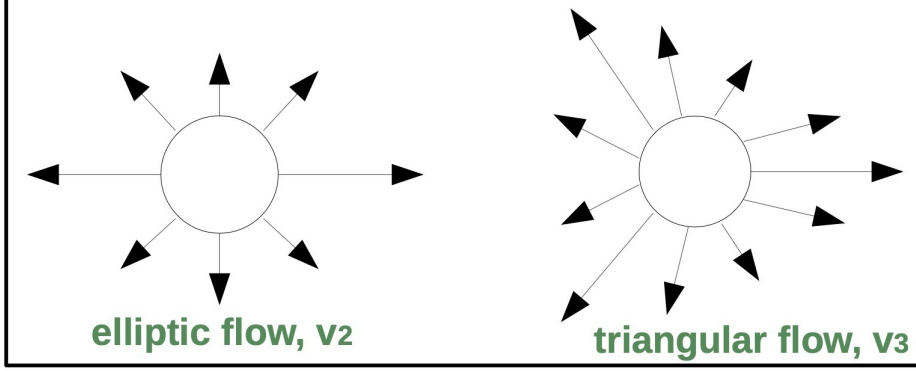

# Isobar collisions at RHIC (slide courtesy G. Giacalone)

[STAR collaboration, PRC **105** (2022) 1, 014901]

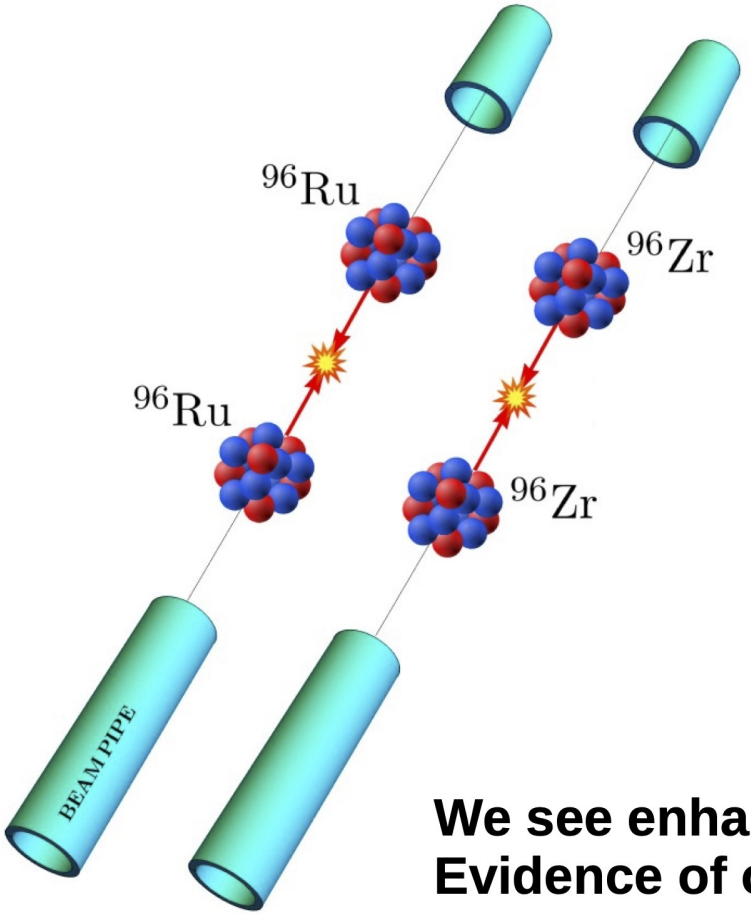


[courtesy Chunjian Zhang]

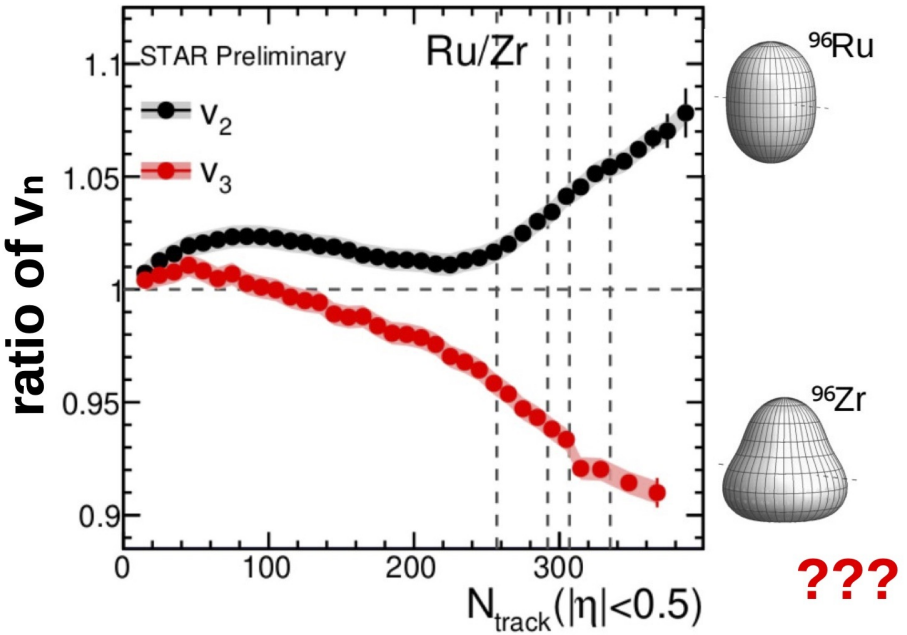


???

**We see enhanced triangular flow in Zr+Zr collisions**
**Evidence of octupole deformation in Zirconium-96**

[Zhang, Jia, PRL **128** (2022) 2, 022301]
[Nijs, van der Schee, SciPost Phys. **15** (2023) 041]

# Example: shape transition at N=60 in Zr and Sr nuclei

# Shape transition at N=60

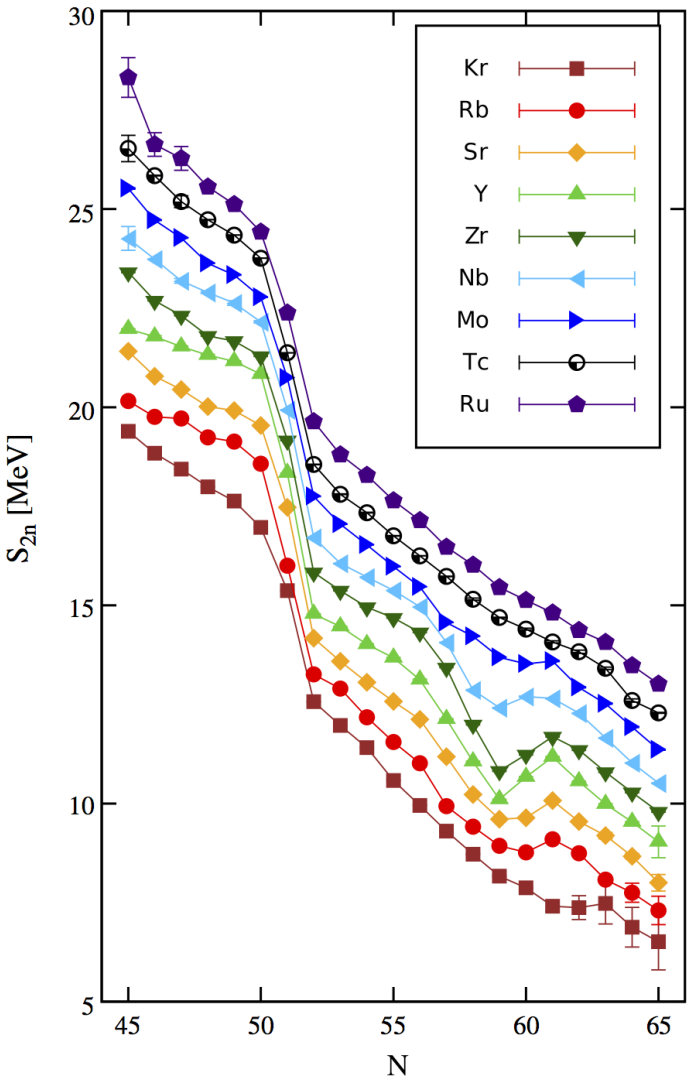


- dramatic change of the ground-state structure observed at N = 58, 60 for Rb, Sr, Y, Zr
- considerable theoretical and experimental effort in this mass region

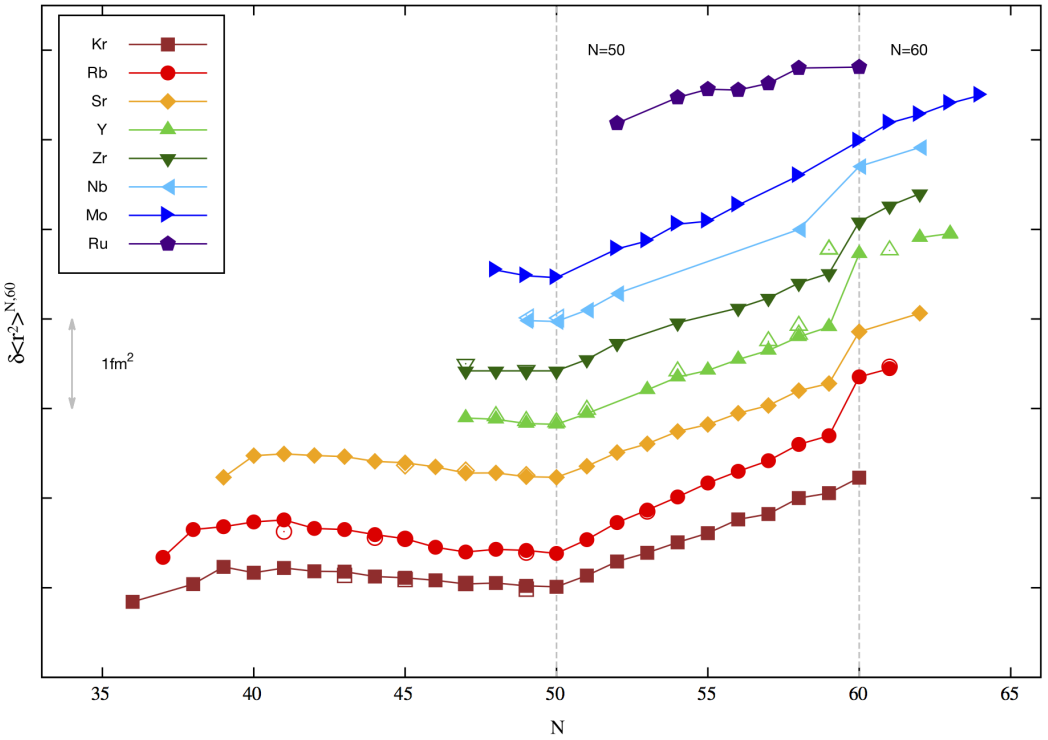


P. Campbell *et al.*, Prog. Part. Nucl. Phys. 86 (2016) 127

# Shape transition at N=60

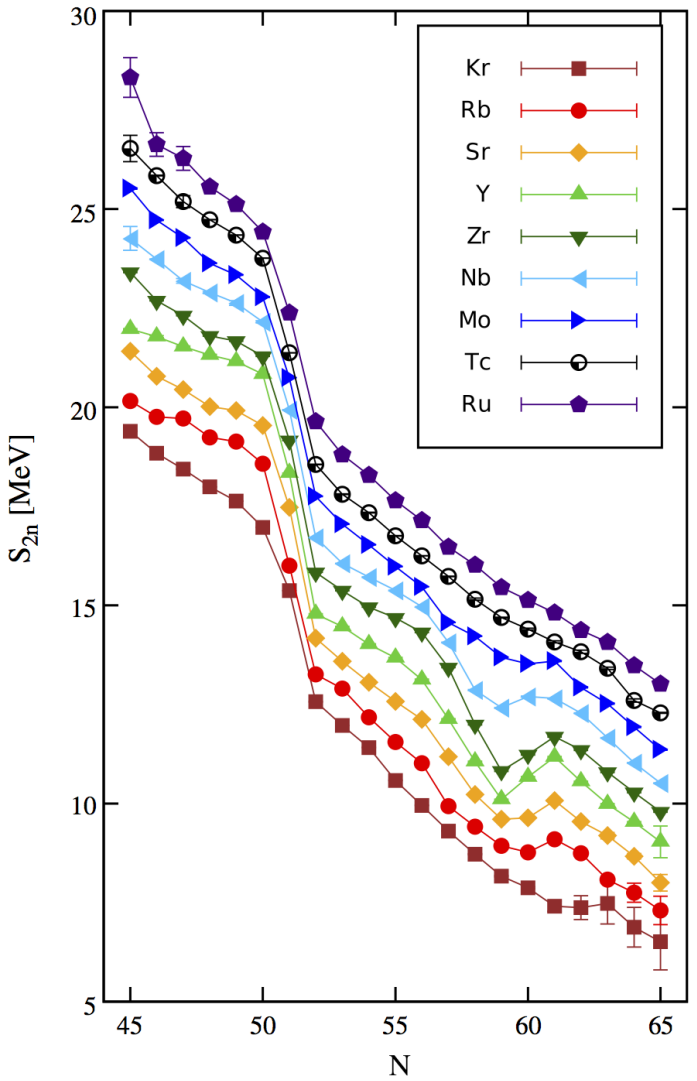


- dramatic change of the ground-state structure observed at N = 58, 60 for Rb, Sr, Y, Zr
- onset of deformation at N=60 confirmed by $2_1^+$ energies and transition probabilities

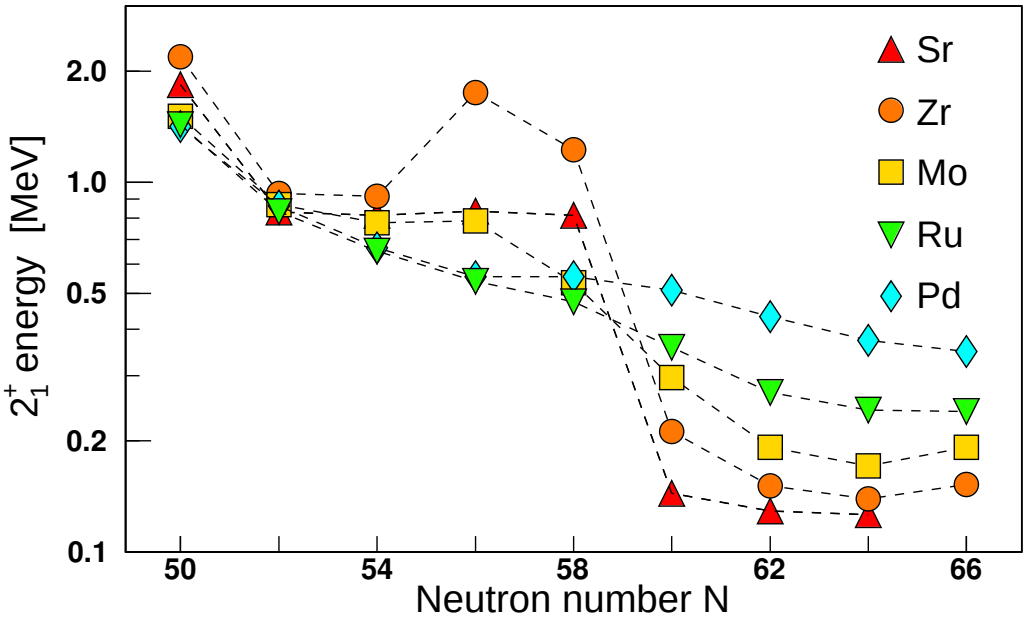


P. Campbell *et al.*, Prog. Part. Nucl. Phys. 86 (2016) 127

# Shape transition at N=60

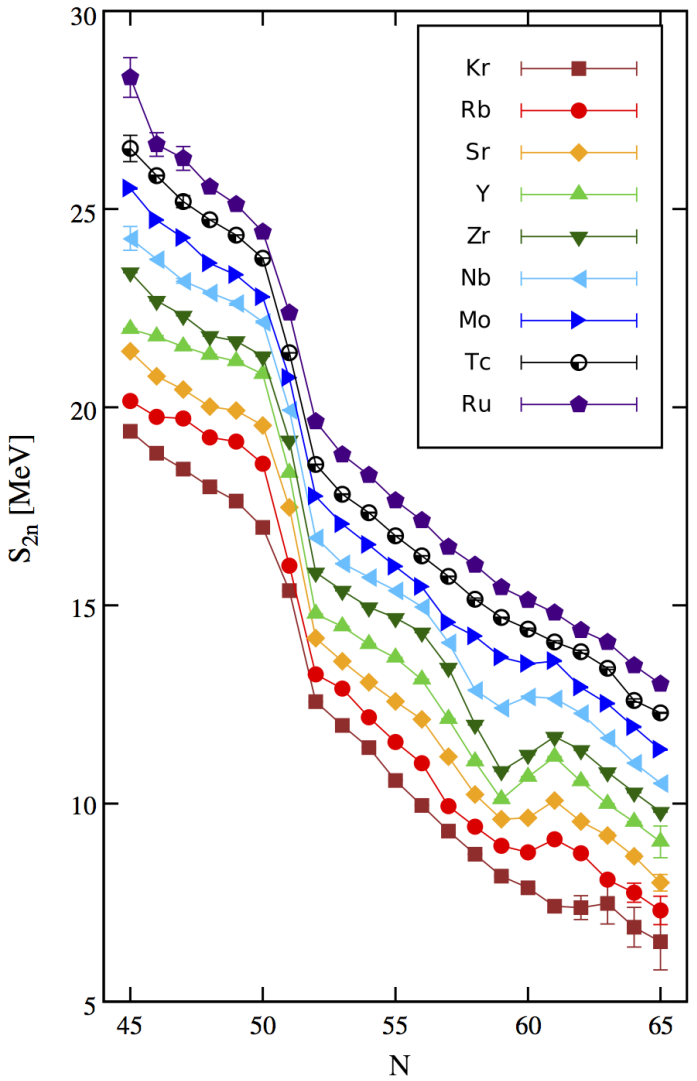


- dramatic change of the ground-state structure observed at N = 58, 60 for Rb, Sr, Y, Zr
- onset of deformation at N=60 confirmed by $2_1^+$ energies and transition probabilities

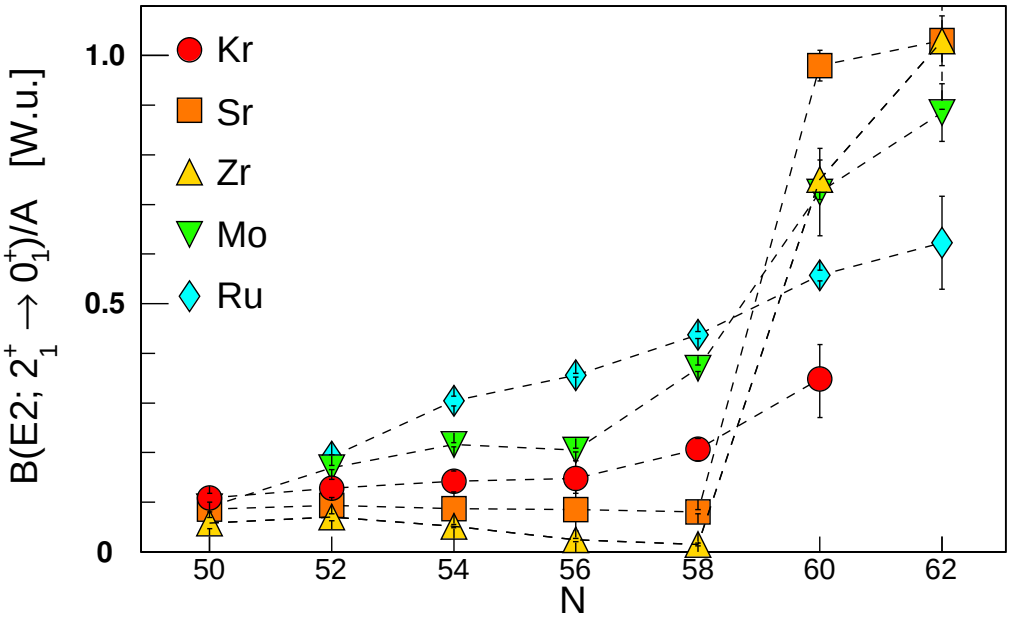


P. Campbell *et al.*, Prog. Part. Nucl. Phys. 86 (2016) 127

# Southern border of the deformed region: N=60,62 $^{97,99}$Rb

C. Sotty, MZ *et al.*, Phys. Rev. Lett. 115, 172501 (2015)

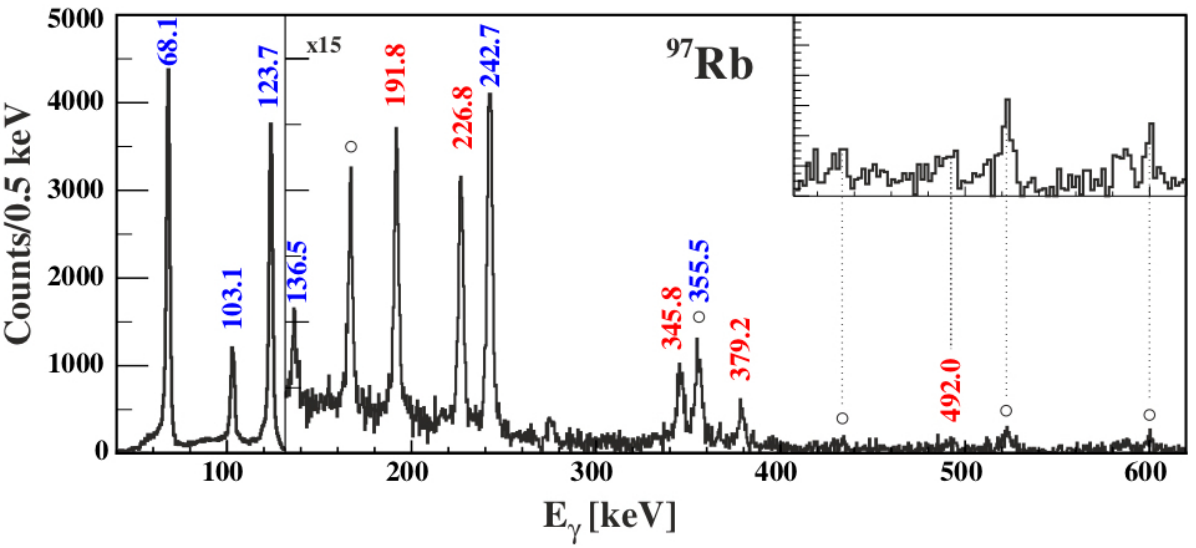


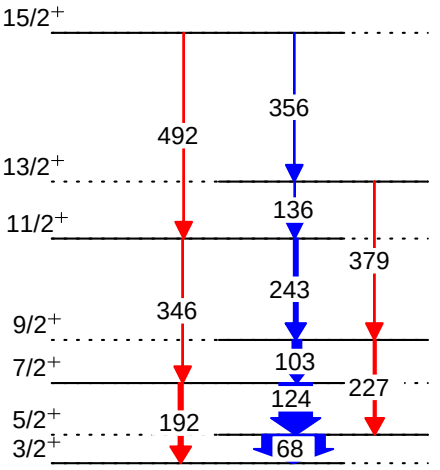


- identification of rotational bands in $^{97,99}$Rb via Coulomb excitation at REX-ISOLDE
- extracted B(E2) values confirm strong constant deformation in $^{97,99}$Rb ground-state bands
- full consistency with the quadrupole moment of the $^{97}$Rb ground state from laser spectroscopy

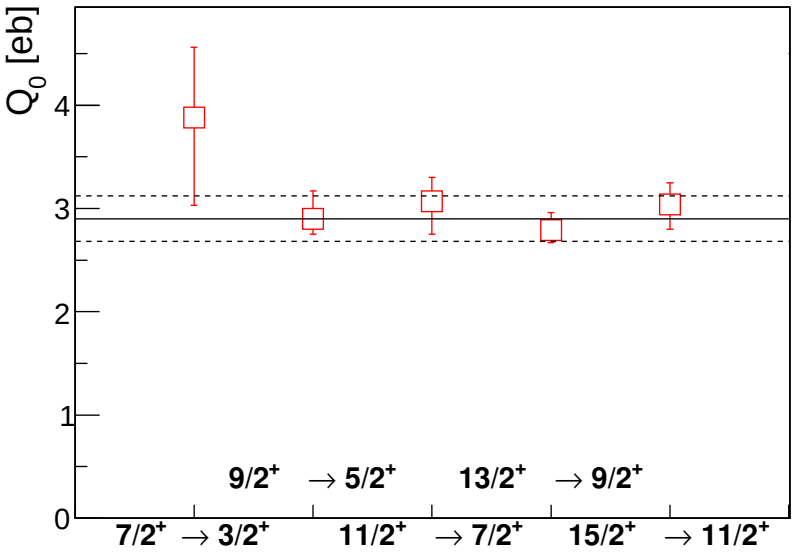

# Shape transition at N=60 and shape coexistence around $^{100}$Zr

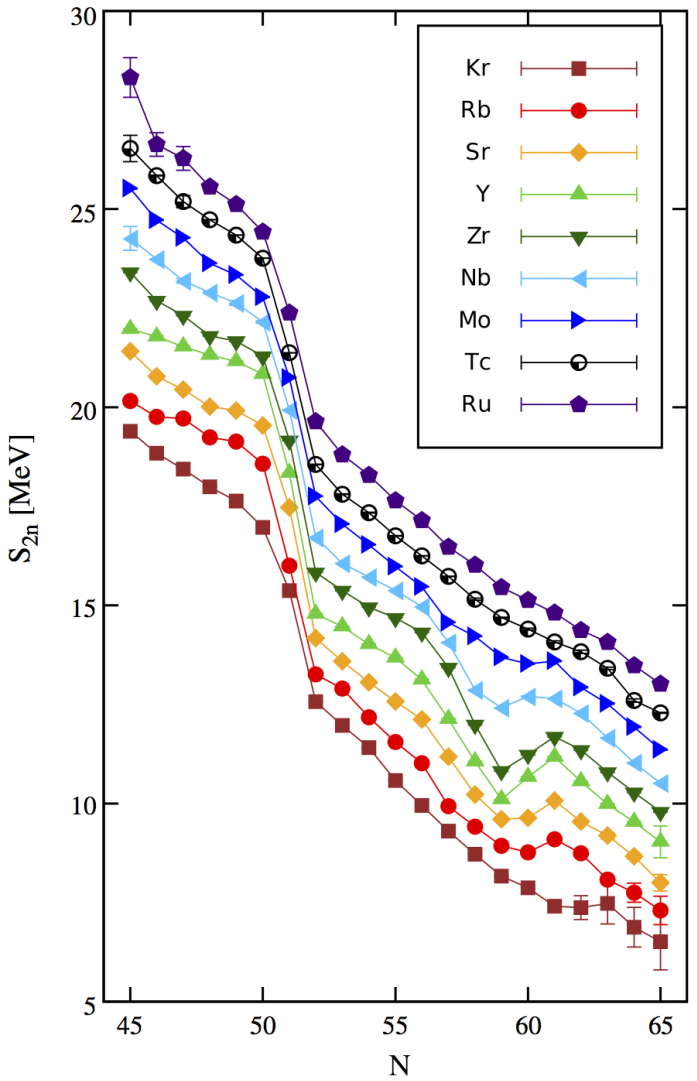


- dramatic change of the ground-state structure observed at N = 58, 60 for Rb, Sr, Y, Zr
- onset of deformation at N=60 confirmed by $2_1^+$ energies and transition probabilities
- low-lying $0_2^+$ states observed in the Sr, Zr, Mo, Ru isotopes

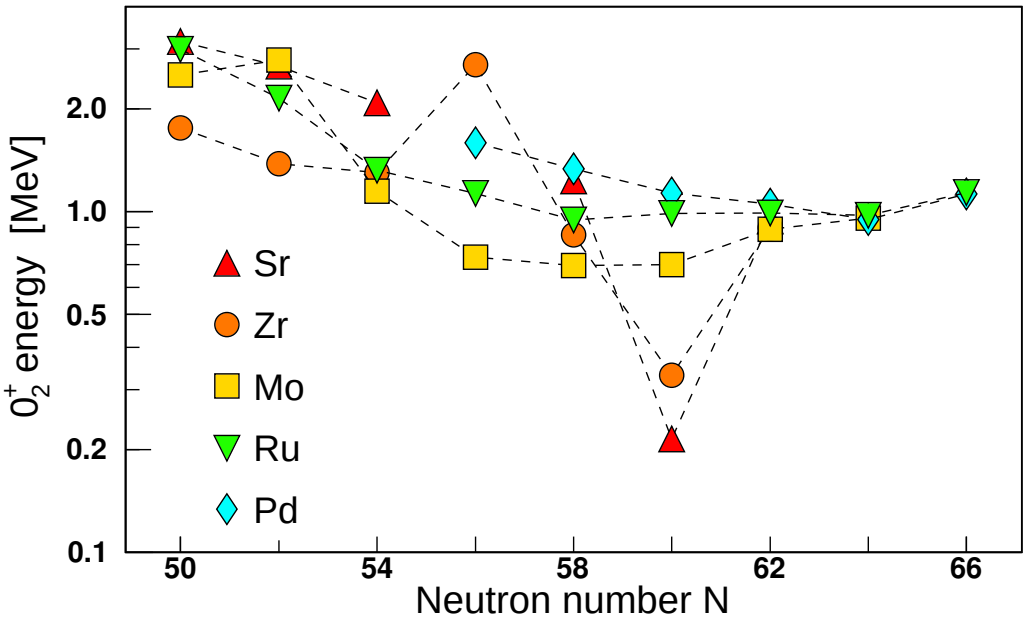


P. Campbell *et al.*, Prog. Part. Nucl. Phys. 86 (2016) 127

# Shape coexistence in $^{96}$Zr – experimental information

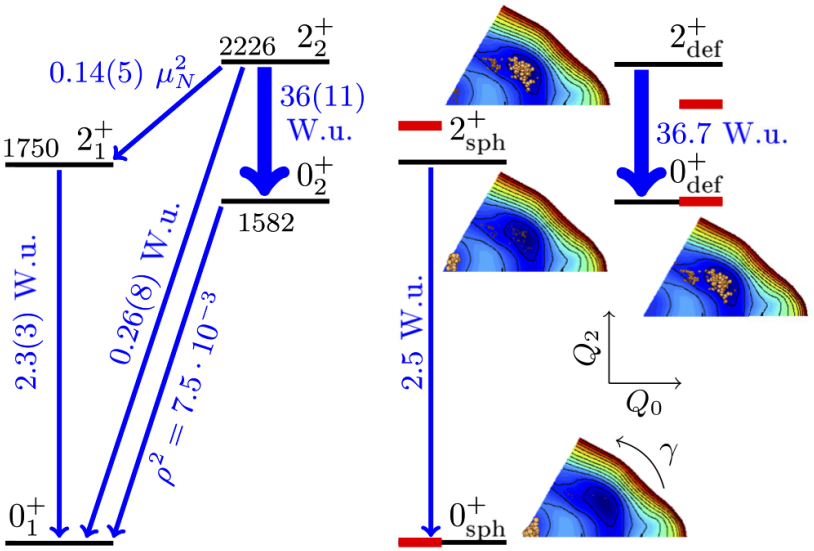


S. Kremer et al, Phys. Rev. Lett. 117 (2017) 172503

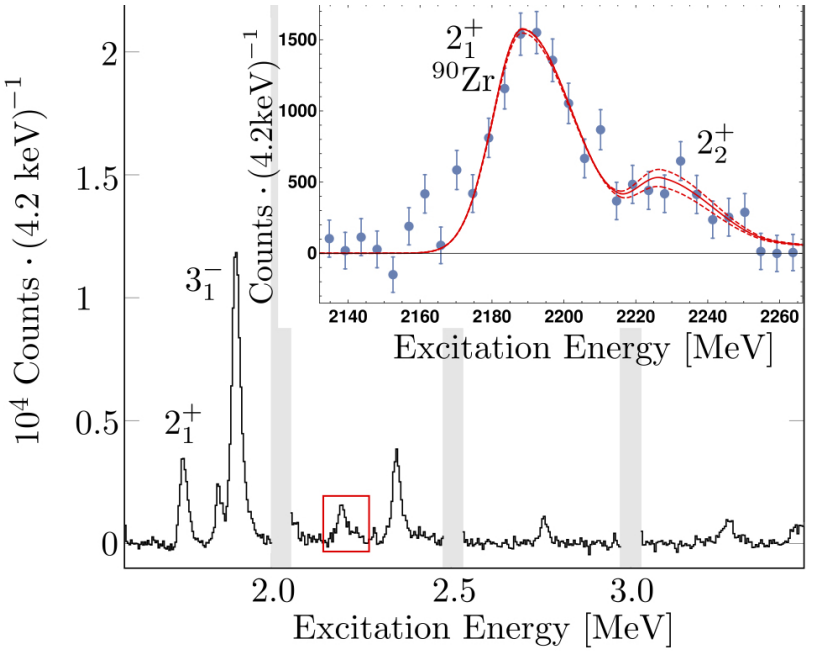


- B(E2; $2_2^+ \rightarrow 0_1^+$) measured using electron scattering, combined with known branching and mixing ratios:
  $\rightarrow$transition strengths from the $2_2^+$ state
- B(E2; $2_1^+ \rightarrow 0_1^+$) = 2.3(3) Wu vs B(E2; $2_2^+ \rightarrow 0_2^+$) = 36(11) Wu: nearly spherical and a well-deformed structure ($\beta \approx 0.24$)
- very low mixing of coexisting structures: $\cos^2\theta_0$=99.8%, $\cos^2\theta_2$=97.5%

# Shape coexistence and type-II shell evolution in Zr isotopes

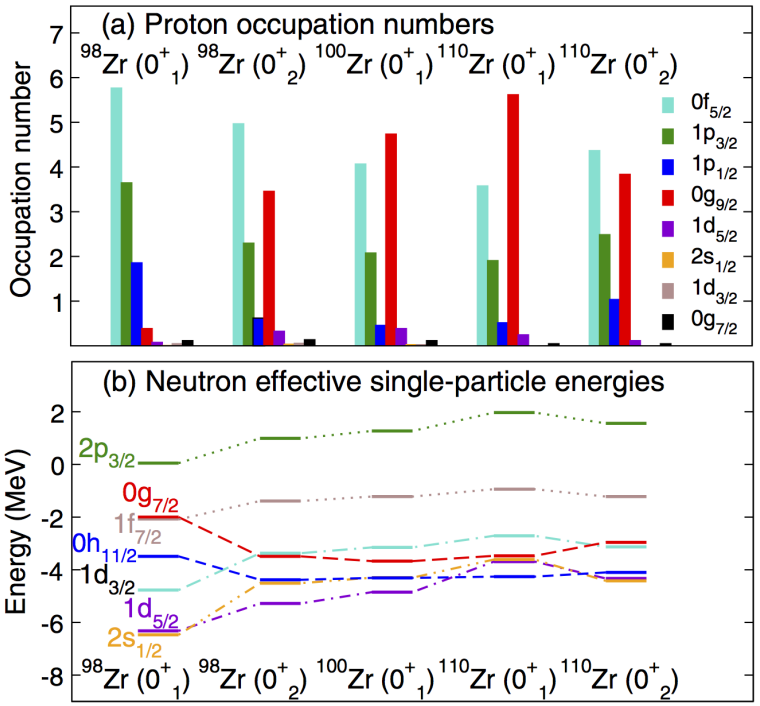


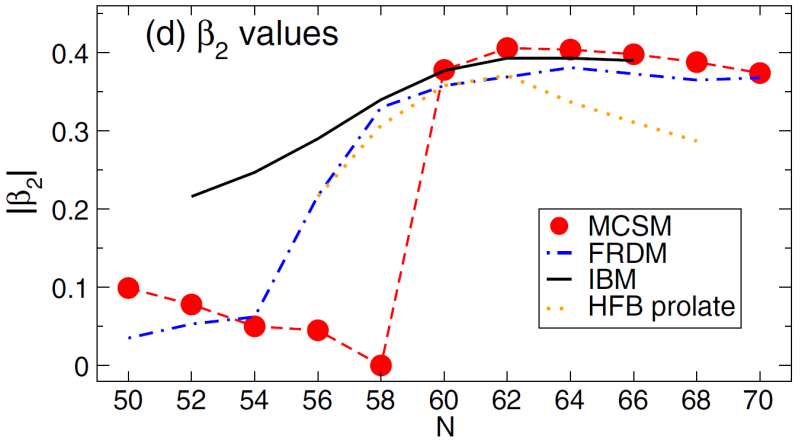


T. Togashi *et al.*, PRL 117, 172502 (2016)

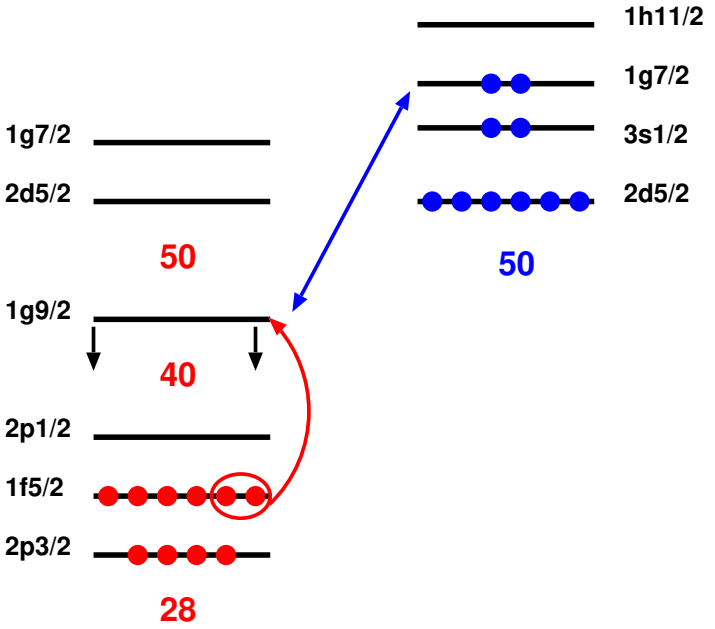


- p-n tensor interaction reduces the Z=40 gap when $\nu g_{7/2}$ is being filled
- $0^+_2$ states created by 2p-2h (+ 4p-4h...) excitation across Z=40
- very different configurations and small mixing of $0^+_1$ and $0^+_2$

# Shape coexistence in $^{94}$Zr

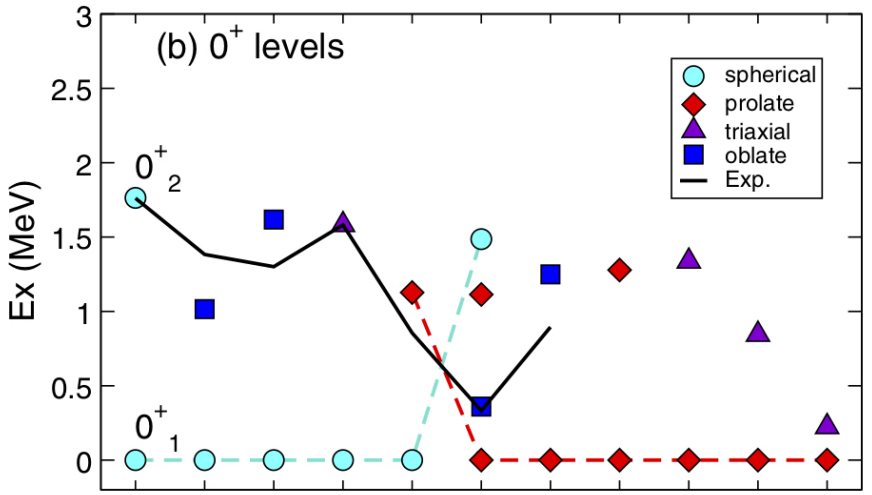


T. Togashi et al, PRL 117, 172502 (2016)

- MCSM calculations suggest a variety of shapes appearing at low excitation energy in Zr nuclei
- $^{94}$Zr selected as the first candidate for a detailed experimental investigation
- oblate deformed structure predicted to be built on the $0_2^+$ state

A. Chakraborty et al, PRL 110, 022504 (2013)

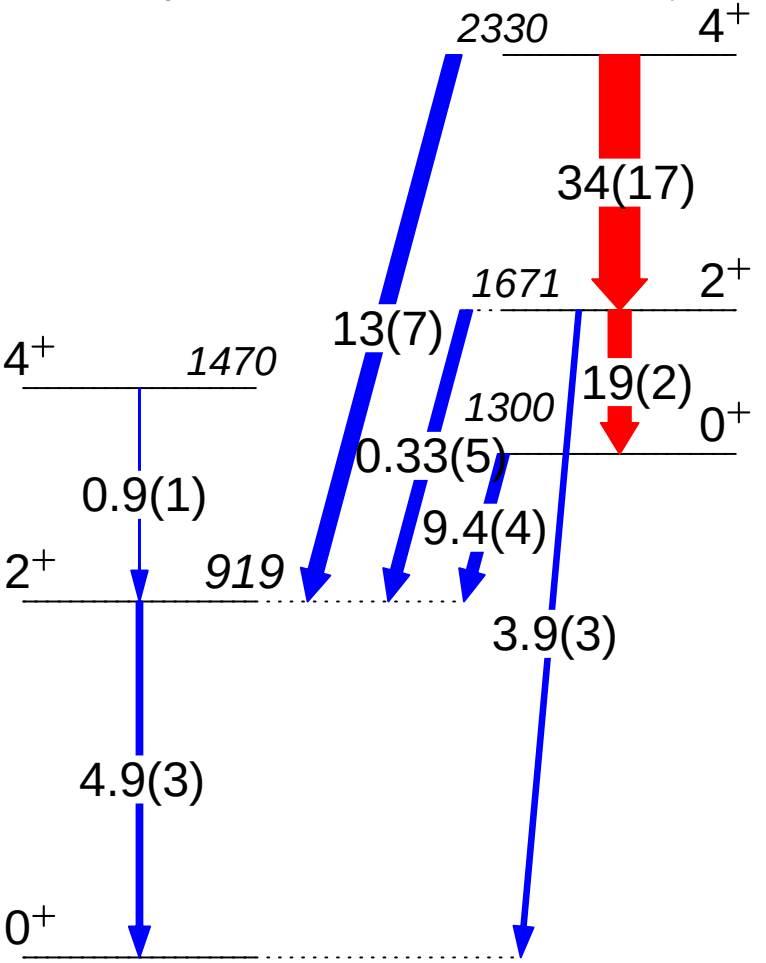


- high-statistics $\beta$-decay study at TRIUMF: observation of a strong $2_2^+ \rightarrow 0_2^+$ transition (19 W.u.) – a deformed band built on $0_2^+$

# Quadrupole invariants for $^{94}$Zr

N. Marchini et al, submitted to PRL

- experiment performed at LNL Legnaro: $^{94}$Zr beam on $^{208}$Pb target
- GALILEO + SPIDER + $LaBr_3$

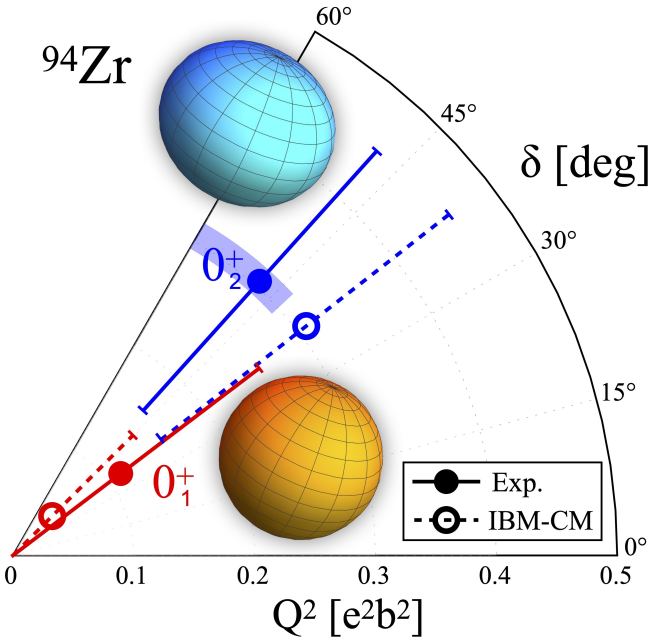


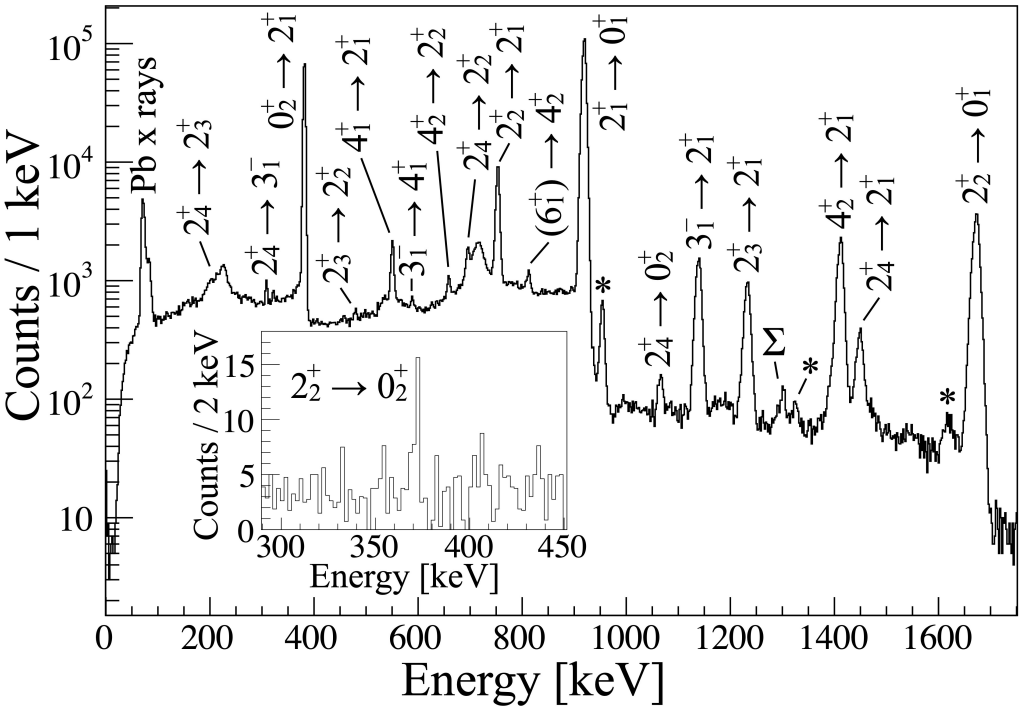


Quadrupole invariants for $0^+_{1,2}$ states:

- spherical shape and softness of the $0^+_1$ state
- more rigid, oblate deformed $0^+_2$ state

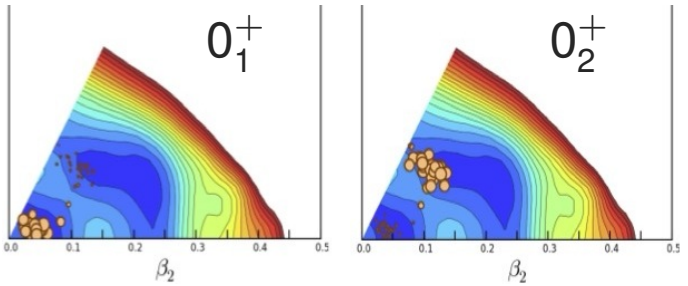


IBM-CM calculations: Noam Gavrielov, GANIL

MCSM calculations: T. Otsuka, in: S. Leoni et al, Prog. Nucl. Part. Phys. 104119 (in press)

# Coulomb-excitation at ISOLDE: deformation of $^{96}$Sr

E. Clément, MZ *et al.*, Phys. Rev. Lett. 116, 022701 (2016)

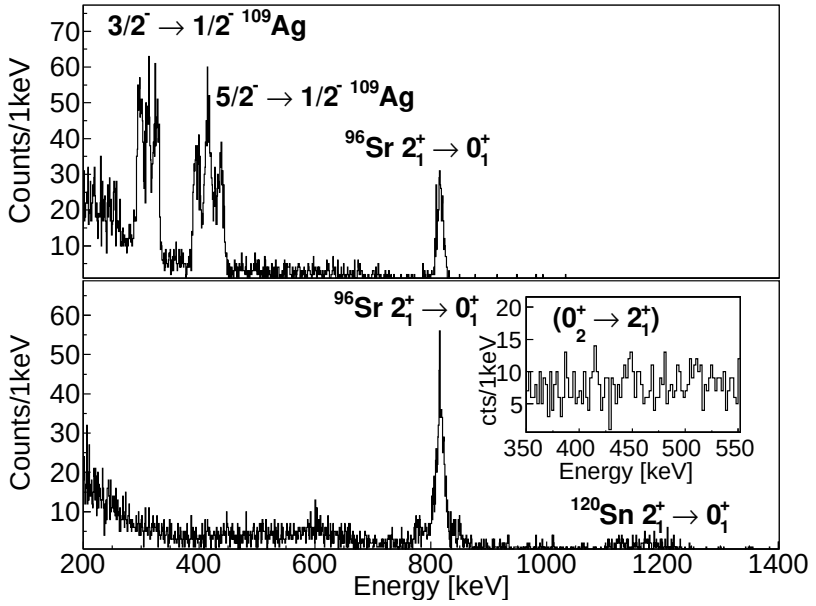


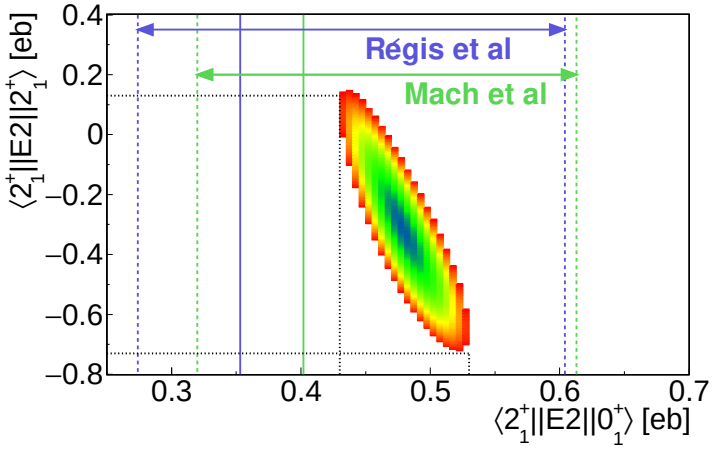


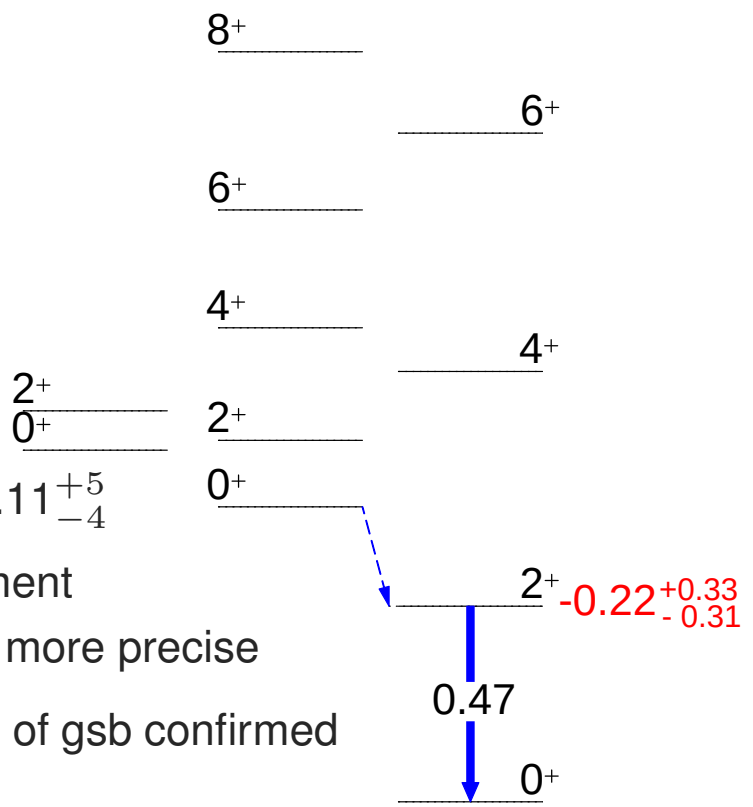


$\beta$ (from $Q_s$) = $0.11^{+5}_{-4}$

B(E2) in agreement with lifetime but more precise

low deformation of gsb confirmed

# $^{98}$Sr: quadrupole moments and transition probabilities

E. Clément, MZ *et al.*, Phys. Rev. Lett. 116, 022701 (2016)

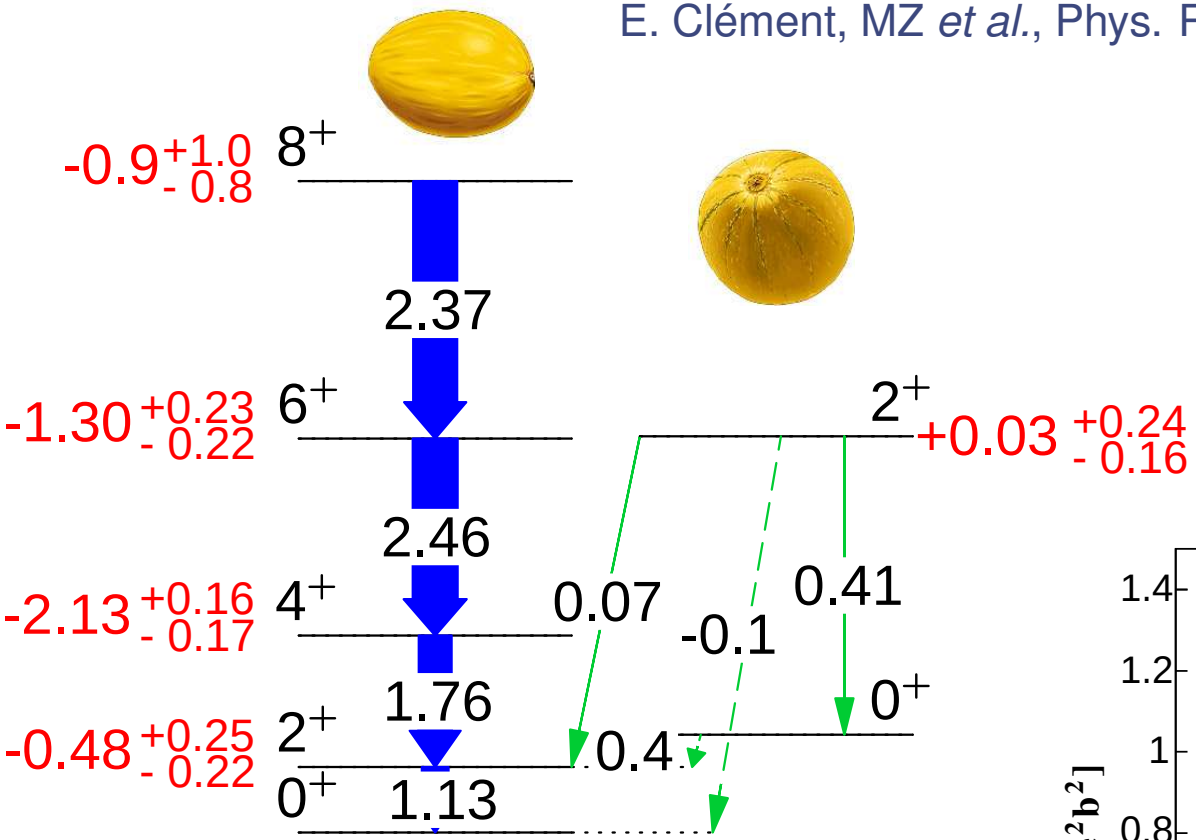


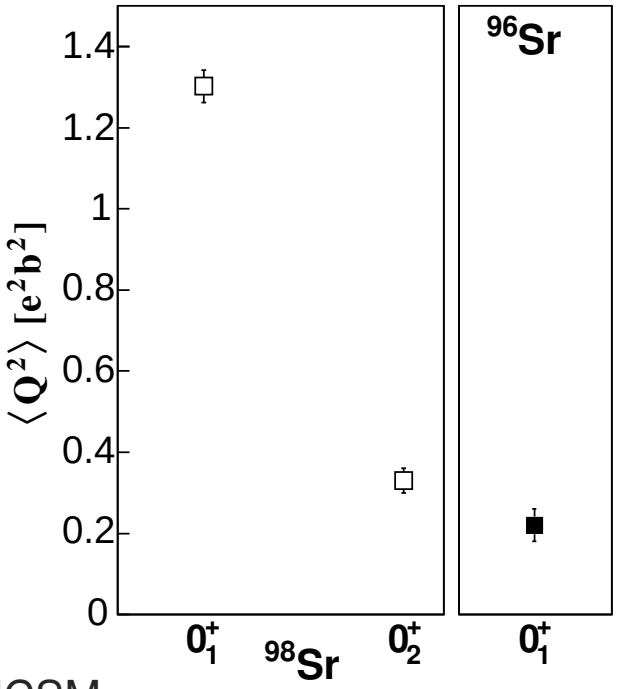


- well deformed prolate band ($\beta \geq 0.3$)
- low deformation of the excited band ($\beta < 0.1$)
- similar deformation of $0_1^+$ in $^{96}$Sr and $0_2^+$ in $^{98}$Sr
- low mixing of the two configurations in agreement with MCSM